The properties of gas-phase multiply-charged ions

A Thesis submitted for the Degree of Doctor of Philosophy

by

Karl Adrian Newson

University College London

1999

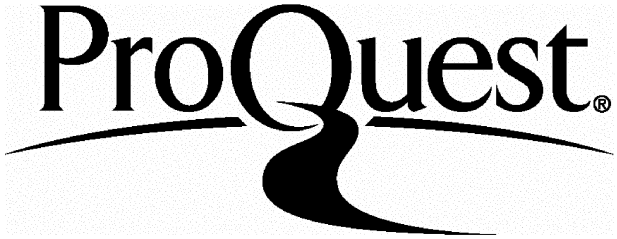

Abstract

This thesis presents the results of a series of experiments investigating the reactivity of gas-phase molecular dications with various neutral collision partners, at collision energies between 3 and 13 eV in the laboratory frame, using a crossed-beam apparatus. The experiment involves the measurement of product ion intensities, which are determined by means of time-of-flight mass spectrometry. The experimental apparatus and methodology, together with the areas of theory important to ion chemistry, are described in the thesis.

The product ions of greatest interest are those ions formed by bond-forming (chemical) reactivity. The relative intensities of such product ions, and those ions formed as a result of electron-transfer reactions, are, when recorded as a function of the collision energy, a powerful probe of the reaction mechanism. Additionally, where appropriate, the reactions are examined for isotope effects by using the isotopic analogue of the neutral collision partner.

The results of the experiments indicate that no intermolecular isotope effects are present in the reactions of CF_2^{2+} and CF_3^{2+} with H_2 and D_2 neutral targets. In addition, the observed collision energy dependence is symptomatic of the absence of a barrier to reaction. These observations suggest that the reactions proceed via an impulsive direct reaction mechanism. Such a conclusion casts doubt on the applicability of the Landau-Zener model of H^-/D^- transfer reactivity. Other results presented in this thesis include the first reported observation of a bond-forming reaction between a molecular dication (CF_2^{2+}) and a polyatomic neutral species (NH_3). Finally, the branching ratio of the products of bond-forming reactions between CF_2^{2+} with HD indicates the operation of a strong intramolecular isotope effect, favouring the formation of the deuterated product. This observation points to a reaction mechanism in which the bond-formation is preceded by electron-transfer.

Table of contents

Acknowledgements

I would like to acknowledge the unstinting support and assistance given to me by my supervisor, Stephen Price. His patient help and advice have been invaluable, both in an academic and personal capacity, particularly so in the summer of 1996 during my son's illness. In addition to being a supervisor of the highest quality, Steve's attention to detail and methodical approach to all aspects of scientific research have been a real inspiration.

I would also like to express my gratitude to the other members of the Price group research team, together with the numerous technical and workshop staff at UCL for all their efforts over the past four years. The financial support given to me by the EPSRC is gratefully acknowledged, without this help the research would not have been possible.

Finally, I would like to thank my good friend Damian Royal, my son Alexander, my wife Debbie and our parents for their staunch support and unfaltering patience over the past four years.

Chapter 1

Introduction

1.1 Gas-phase molecular dications

This thesis discusses the gas-phase reactions of doubly-charged molecular ions (molecular dications) with neutral targets. A molecular dication is a molecular species that has undergone a double ionization event, such double ionization is usually brought about by means of electron-impact ionization [1-16] or photoionization [17-29]

The first detection of a gas-phase atomic dication was made by means of mass spectrometry in the early part of this century [30], this was followed by the observation of carbon monoxide molecular dications in 1931 [31]. Despite these early observations, the volume of research work involving gas-phase molecular dications has been relatively low. However, the past two decades have seen many developments in experimental techniques which have brought about a revival of interest in the study of molecular dications. Since 1980, the properties of these species have been the subject of an increasing number of investigations [3-29, 32-43].

At first glance, the study of molecular dications may be considered as esoteric and of little relevance outside the specialized field of ion chemistry. However, the properties of these species may influence many areas of physical science. For example, the double photoionization of molecular species has been proposed as a source of energetic ions in planetary atmospheres including the Earth's ionosphere [44]. In such situations a thorough knowledge of the chemical and physical properties of molecular dications is essential for the successful modelling of their role in atmospheric chemistry. Other areas of research with an interest in the study of molecular dications include astrochemistry where, following the observations of IR emission, doubly-charged polycyclic aromatic hydrocarbons (PAH) have been proposed as existing in the interstellar medium [45-47]. Molecular dications are also thought to be a potentially important species in combustion chemistry [16]. In addition to the practical applications, the modelling of molecular dications and their spectroscopic properties is also a serious theoretical challenge [48-53]. Consequently, comparative experimental data is an essential requirement in assessing the applicability of new theoretical methodologies.

This thesis presents the first results from an investigation of the collision-induced reactivity of gas-phase molecular dications with neutral collision partners at laboratory frame collision energies between 3 and 13 eV. The investigation is carried out using a purpose-built crossed-beam apparatus that incorporates a time-of-flight mass spectrometer. A full description of the experimental apparatus and the operational methodology is given in Chapter 2. The procedure used in the subsequent analysis of the experimental data is explained in detail in Chapter 3.

This investigation of dication-neutral reactivity is based on experimentation. This is reflected in the content of this thesis which concentrates on the experimental aspects of the subject. However, in order to fully appreciate the results of this investigation, and to draw the appropriate conclusions, a comprehensive understanding of areas of the theory underpinning ion chemistry is an essential prerequisite. Relevant theoretical topics are discussed in detail in Chapter 4. The bulk of this thesis involves the presentation of the results of the experimental work. Such results are displayed in graphical and tabular form, together with a discussion of the results and the appropriate conclusions gained from the experimental data. Finally, in the light of this general examination of molecular dication-neutral reactivity, the thesis examines the direction further investigations should take.

As stated above, this thesis presents the first results from a new experiment to study the gas-phase reactivity of doubly-charged molecular ions with neutral target species. Therefore, in order to understand the motivation for this new experiment, and to appreciate the value of the results obtained, it is necessary first to examine the nature, formation, stability and reactivity of gas-phase molecular dications.

1.2 The stability of gas-phase molecular dications

The stability of any molecular species depends upon the form of its potential energy surface. In the case of a prototypical diatomic molecule XY, that is able to undergo unimolecular dissociation (Equation 1.1), there are three possible situations.

$$XY \rightarrow X+Y \qquad (1.1)$$

Firstly, if the potential energy curve of XY (Figure 1.1a) has a minimum at an internuclear separation of R_e, where the energy corresponding to the minimum, $E(R_e)$, is lower than the energy corresponding to the dissociation asymptote E(X+Y), that is:

$$E(R_e) < E(X+Y) \qquad (1.2)$$

then molecule XY is considered to be in a *stable* electronic state. The second possibility is, as illustrated in Figure 1.1b, characterised by the absence of a minimum in the potential energy curve. Such electronic states of XY are dissociative in nature. In such cases molecule XY is said to be in an *unstable* electronic state. The third situation describes the case where the potential energy curve contains both a localised minimum and a maximum, occurring at internuclear distances of R_e and R_m respectively. As illustrated in Figure 1.1c, the presence of a local minimum and maximum means there is a barrier to dissociation. For molecular dications, owing to the fact that the energy corresponding to the local minimum lies above the dissociation asymptote, the electronic states of molecules trapped in the potential well are considered to be *metastable*.

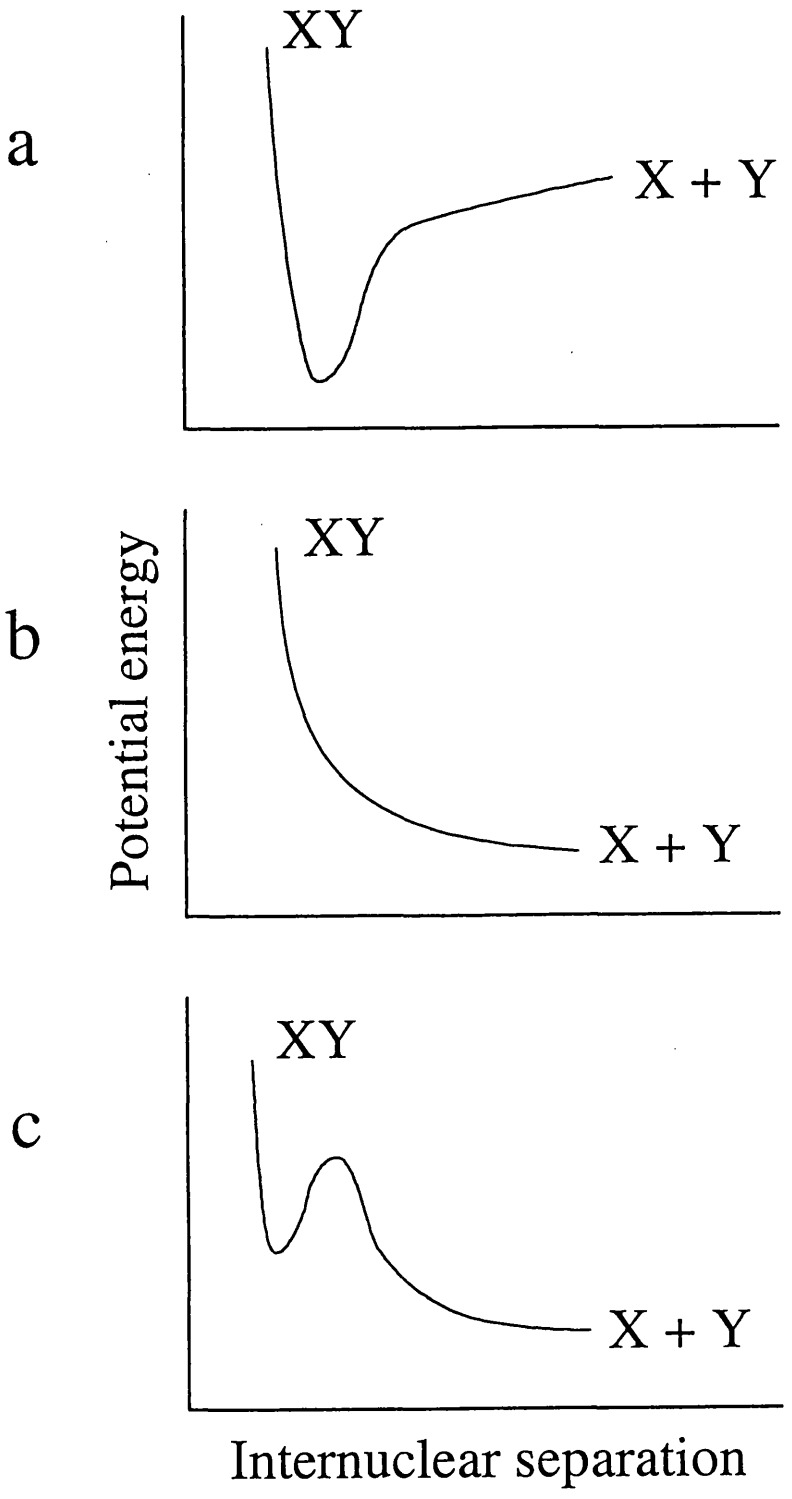

Figure 1.1. Schematic representation of the potential energy curves for molecule XY in (**a**) a stable electronic state, (**b**) an unstable electronic state, and (**c**) a metastable electronic state.

The electronic states of doubly-charged molecular ions are usually unstable due to the Coulombic repulsion between the two positive charges. The lifetimes of such unstable molecular dications are short [19,54], typically of the order of 10^{-13} s. A further effect is that, upon the dication's fragmentation, there is a considerable release of kinetic energy, usually between 4-8 eV, although values as high as 18 eV have been reported [12,18,37,55]. Consequently, these fragmentations are sometimes referred to as Coulomb explosions. The majority of molecular dications, being energetically unstable with respect to dissociation, undergo fragmentation to give two singly-charged ions [56,57] and, in some cases, additional neutral fragments [23]. Prototypical dissociations of these types are given in Equations 1.3 and 1.4.

$$XY^{2+} \rightarrow X^+ + Y^+ \tag{1.3}$$

$$XY_2^{2+} \rightarrow X^+ + Y^+ + Y \tag{1.4}$$

Some molecular dications may fragment without charge separation. Such behaviour is predominantly observed in larger doubly-charged molecular species such as the naphthalene molecular dication [25]. Prototypically:

$$X_mY_n^{2+} \rightarrow X_mY_{n-1}^{2+} + Y \tag{1.5}$$

In some cases the daughter dication may also undergo further fragmentation by means of charge-separation (Equation 1.6) or additional neutral-loss (Equation 1.7).

$$X_mY_{n-1}^{2+} \rightarrow X_mY_{n-2}^{+} + Y^+ \tag{1.6}$$

$$X_mY_{n-1}^{2+} \rightarrow X_mY_{n-2}^{2+} + Y \tag{1.7}$$

Although the majority of electronic states of molecular dications are repulsive, many molecular dications possess at least one electronic state that has a barrier to charge-separation. In common with neutral molecules, the presence of the barrier arises because of a localised minimum in the potential energy surface. As can be seen in Figure 1.2, the energy of the localised minimum is higher than the asymptote for charge separating dissociation. Consequently, the dications trapped in the potential well formed by the minimum are energetically unstable with respect to dissociation and are termed as *metastable*.

In certain cases the potential well of the molecular dication may be deep enough to support many vibrational levels [58]. Therefore, as dissociation can occur by the dication tunnelling through the potential energy barrier, the lifetimes of these metastable electronic states are strongly dependent on such factors as the depth of the well (E_2 - E_1) with respect to the barrier, and the width of the barrier itself. In addition, the lifetime of a molecular dication will also depend upon its degree of vibrational excitation, as a molecular dication in a higher-lying vibrational level will tunnel through the barrier with greater ease than a molecular dication in a low-lying vibrational level. Consequently, molecular dications in low-lying vibrational levels are

expected to be relatively long-lived. For molecular dications in such low-lying vibrational levels the most important mechanism of decay involves predissociation via curve crossings to unbound electronic states [59]. As stated above, molecular dications were first identified by means of mass spectrometry. Consequently, their lifetimes must be of at least microsecond order for them to be detectable [16,19,60]. In fact, in the case of the CO^{2+} molecular dication, lifetimes in excess of 1 s have been reported [61].

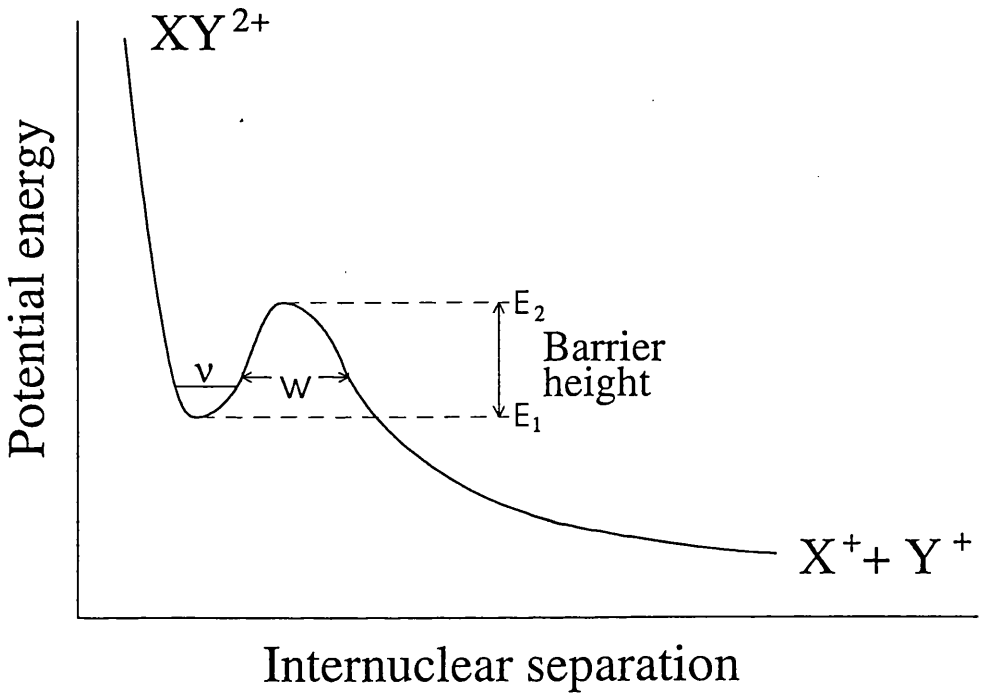

Figure 1.2 Schematic potential energy curve for a diatomic molecular dication in a metastable electronic state. The main features of the potential energy curve are the localizsed minimum and barrier of width *w* which form a well of depth E_2 - E_1.

Two competing physical interpretations are available to account for the existence of long-lived electronic states of molecular dications in the presence of the large intramolecular Coulombic repulsion. Firstly, the local minimum and maximum in the potential energy surface of a hypothetical molecular dication XY^{2+} can be shown (Figure 1.3) to arise from an avoided crossing between the potential energy curves corresponding to the neutral-dication fragmentation ($X+Y^{2+}$), and the repulsive charge-separating dissociation ($X^{+}+Y^{+}$) [39]. In the former case, at large internuclear distances, charge polarization effects cause the curve for $X+Y^{2+}$ to be weakly attractive; the form of the potential is given by:

$$V_{X+Y^{2+}} = -CR^{-4} \qquad (1.8)$$

whereas at large internuclear distances, the potential energy curve for the charge-separating dissociation $X^{+}+Y^{+}$ is dominated by the Coulombic repulsion, given by:

$$V_{X^+ + Y^+} = +BR^{-1} \tag{1.9}$$

where B and C are constants, and R is the internuclear separation. Avoided crossings between these curves may, as shown in Figure 1.3, give rise to potential wells whose depth and width support at least one vibrational level, thus allowing the existence of metastable molecular dications.

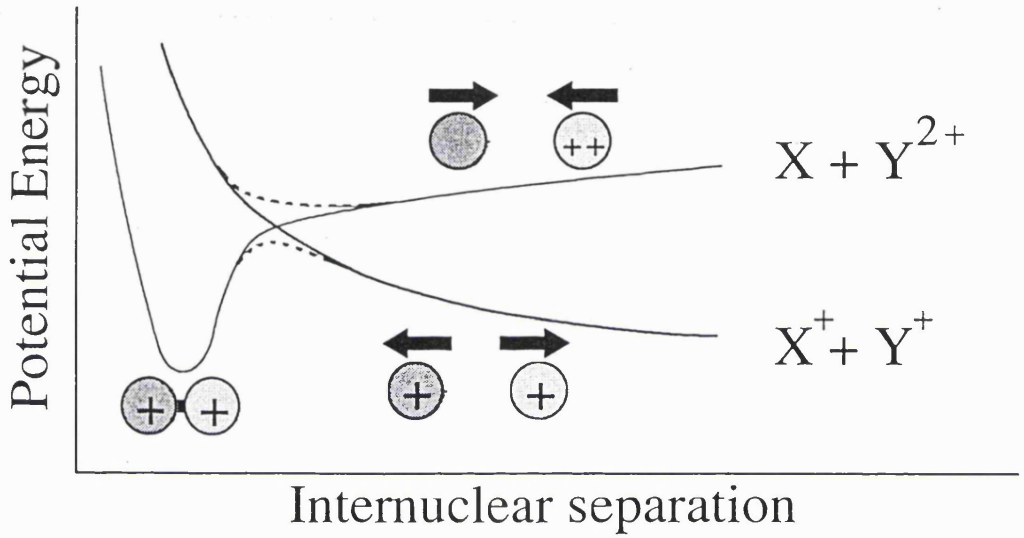

Figure 1.3 Schematic potential energy curves of molecular dication XY^{2+} illustrating the avoided crossing (dashed lines) between the potential energy curves, corresponding to charge-separating ($X^+ + Y^+$) and neutral-dication fragmentation ($X + Y^{2+}$), that give rise to metastable electronic states.

An alternative explanation for the existence of molecular dications, has been proposed by O'Neil *et al* [62] following their theoretical investigation of the electronic states of the fluorine molecular dication. In their hypothesis, the potential energy curve of the F_2^{2+} molecular dication may be closely approximated by superimposing a Coulombic repulsion potential term onto the potential energy curve of the isoelectronic neutral O_2. Hence, in general, the potential energy curves of a molecular dication can be thought of as the combination of the chemical binding potential of the isoelectronic neutral and the repulsive Coulombic potential between the like-charged constituent ions. The form of such a combination of potentials is given by:

$$V_{XY^{2+}} = V_{\text{bond}} + \frac{e^2}{R} \tag{1.10}$$

where V_{bond} is the binding potential of a neutral molecule isoelectronic with the molecular dication. In the model the metastable state of the molecular dication will exist when the attractive

bonding potential is greater than the repulsive potential. One problem with this additive model is its inability to account for the existence of certain heteronuclear diatomic dications such as HCl^{2+}, where at small internuclear separations the two positive charges are located on the same atom [63].

1.3 The formation of gas-phase molecular dications

As stated in section 1.1, reactant molecular dications may be formed by the double ionization of a suitable neutral precursor molecule. For example, CF_4 in the case of CF_2^{2+}. This double ionization may be achieved by means of either electron-impact or photon-impact.

1.3.1 Electron-impact ionization

Electron-impact ionization, as illustrated by Equation 1.11, is a long established method of ion generation. The principal advantage of ionization by means of electron-impact is the relative simplicity and robustness of the apparatus required to produce ions in usable quantities. A schematic illustration of a typical electron-impact ion source is given in the next chapter in Figure 2.2. The essential feature of this method of ionization is the generation of electrons by means of thermionic emission from a hot cathodic filament. Prior to encountering the neutral precursor, the electron flux may be collimated and, if required, accelerated to the desired collision energy.

$$M_2 + e^- \rightarrow M_2^{2+} + 3e^- \qquad (1.11)$$

For the majority of neutral species the electron-impact double ionization cross-section is not usually greater than 5% of the single ionization cross-section, although a few molecules such as CS_2 [64] and larger molecules [65] have significantly larger double ionization cross-sections. Consequently, the majority of ions formed by this method are the singly-charged parent ions and singly-charged products of the dissociative single ionization of the neutral precursor. Hence, the generation of usable quantities of doubly-charged molecular ions necessitates the generation of large numbers of the singly-charged species, making the efficient mass selection of the reactant beam a vitally important procedure.

1.3.2 Photon-impact ionization (photoionization)

In contrast to electron-impact, the widespread use of photoionization as a means of generating ions is a comparatively recent phenomenon. The double ionization of a neutral molecule M using photon-impact may be achieved by three distinct methods, either by means of a discharge lamp [17-23], synchrotron radiation [24-27] or laser [28,29] (Equation 1.12).

$$M_2 + h\nu \rightarrow M_2^{2+} + 2e^- \qquad (1.12)$$

Despite the relative complexity of the equipment required to use photon-impact as a means of double ionization, the use of this method does offer two significant advantages over electron-impact. Firstly, an investigation of the ionization of various molecules by means of a He discharge has revealed that photon-impact ionization produces significantly greater numbers of doubly-charged species than the impact of electrons of corresponding energies [17]. The second advantage of photoionization is that the energy deposited to the molecule upon ionization is known. This contrasts sharply with electron-impact ionization where the energy deposition is not only variable, but is very difficult to determine in the environment of a typical electron-impact ion source.

1.4 The bimolecular reactivity of molecular dications

The bimolecular reactivity of a doubly-charged molecular ion with a neutral collision partner is dependent upon the collision energy and the identity of the two reactants. However, the results of the few experiments performed to investigate the reactivity of molecular dications with neutral collision partners at collision energies ranging from thermal to high (keV) energies [3-11,13-15,32-34,66,67], have indicated that four main types of reaction have been observed.

The first and most prolific category of reaction between molecular dications and neutral species is electron-transfer. As indicated in Table 1.1, this reaction involves the transfer of an electron from the neutral species to the reactant dication. Following the transfer of the electron, the ionic products may be formed in stable electronic states (non-dissociative electron-transfer) [4-7,32]. Alternatively, the reaction may result in either or both of the two singly-charged product ions being formed in a dissociative electronic state, whereupon the ion in this excited state fragments (dissociative electron-transfer) [4-7,32,67].

Two further categories of reaction may be observed following collisions between molecular dications and neutral collision partners. Firstly, collision-induced charge-separation (CICS) [4-7,11,32], and, secondly, collision-induced neutral-loss (CINL) [8,32,38]. These reactions are characterized by the transfer of some of the kinetic energy of the collision to the dication, thus leaving the dication in a dissociative electronic state, which then either fragments to give two singly-charged ions (CICS) or simply divides with the double charge intact on one of the fragments (CINL).

The final category of reactive process involves the chemical rearrangement of the reactants with the formation of new chemical bonds. The investigation of this category of reactive process is the primary objective of this thesis. Owing to the greater number of possible channels of reaction, it is difficult to give a prototypical equation for this class of reactive process. In addition,

the research performed to date on this particular class of dication/neutral reactivity has been extremely limited. However, the results of an investigation of the bond-forming reactivity of molecular dications with neutral species, reported in this thesis, indicate that the prototypical equation for this category of reaction given in Table 1.1 is common to many dication/neutral collision systems [3,4,9,13,32,68].

Table 1.1 Categories of gas-phase reactions observed between molecular dications (XY_2^{2+}) and neutral reactants (M_2).

Category of reaction	Prototypical equation
Electron-transfer (non-dissociative)	$XY_2^{2+} + M_2 \rightarrow XY_2^{+} + M_2^{+}$
Electron-transfer (dissociative)	$XY_2^{2+} + M_2 \rightarrow \left[XY_2^{+}\right]^{*} + M_2^{+} \rightarrow XY^{+} + Y + M_2^{+}$
Collision-induced charge-separation	$XY_2^{2+} + M_2 \rightarrow XY^{+} + Y^{+} + M_2$
Collision-induced neutral-loss	$XY_2^{2+} + M_2 \rightarrow XY^{2+} + Y + M_2$
Bond-forming[a] (chemical)	$XY_2^{2+} + M_2 \rightarrow MXY_2^{+} + M^{+}$

[a] The equation for this category of reactive process is the prototypical form of the bond-forming reaction between CF_2^{2+} and X_2 [3,4], between CF_3^{2+} and X_2, where X is H or D, and between CF_2^{2+} and HD [68].

1.5 Experimental investigations of the properties of molecular dications: Coincidence techniques

1.5.1 Basic methodology

The first experimental evidence for the existence of molecular dications came from mass spectrometric studies of carbon monoxide [31] ionized by means of electron-impact. This work concentrated on the analysis of the ionic products of electron-impact ionization, and resulted in the determination of the single and double ionization potentials of carbon monoxide. To investigate in more detail the properties of molecular dications, such as the kinetic energy release upon dissociation, dicationic lifetime and fragmentation branching ratios, a new experimental technique is required. One suitable method involves coincidence techniques.

There are many different types of coincidence experiments, but all rely on the same fundamental methodology. Namely, the detection of two or more charged dissociation products, electrons and/or fragment ions, that originate from the same ionization event. This subsection will look at the main types of coincidence techniques and their features.

1.5.2 Electron-impact ion-ion coincidence spectrometry

The earliest experiments to study molecular dications [69] employed a time-of-flight mass spectrometer utilizing electron impact ionization to instigate the ionization and fragmentation process:

$$e^- + AB \rightarrow \left[AB^{2+} + 3e^-\right] \rightarrow A^+ + B^+ + 3e^- \qquad (1.13)$$

The above equation demonstrates electron-impact ion-ion coincidence. Here A^+ and B^+ are the fragment ions formed by the fragmentation of the parent molecular dication AB^{2+}. As both A^+ and B^+ originate from the same dissociation event, and are thus formed at the same time, a measurement of the time-of-flight difference between detected ion pairs will show a predominance of the correlated time-of-flight difference of the ion pair A^+ and B^+. These true coincidence signals are seen as one or more peaks on a background of detected pairs of uncorrelated ions (false coincidences). A representative ion-ion coincidence spectrum of the dissociation products of the ozone dication is shown in Figure 1.4. The observation of these ion-ion coincidence peaks for benzene [69,70] confirmed the existence of fast charge separating dication decay:

$$C_6H_6^{2+} \rightarrow CH_3^+ + C_5H_3^+ \qquad (1.14)$$

The position of the peak centre ($\Delta\tau_{tof}$) is the characteristic time-of-flight difference between the two thermal product ions. The shape and width of the coincidence peaks are determined by the following factors: the kinetic energy release, the angular distribution of the dissociation, and apparatus parameters, the most important of which are the size of the ion detector, and the magnitude of the repeller (source) potential [18].

As mentioned above, the ion-ion coincidence method uses a time-of-flight mass spectrometer to measure the differences in the fragment ions flight times. Consequently, the arrangement of electronics used in the measurement of time-of-flight differences is different to that of conventional time-of-flight mass spectrometry. Instead of a pulsed potential, the source electric field is static. Therefore, the ions themselves are utilized to deliver the START/STOP signals to the timing electronics. The arrival of the first ion of an ion pair at the detector triggers a START signal and the subsequent arrival of the second (slower) ion provides the STOP signal. Therefore, the resulting signal sent to the computer from the electronic timing components is the difference in the flight times of successive ions.

The flight time τ_{tof} of an ion in a time-of-flight mass spectrometer conforming to the Wiley-McLaren focusing conditions [71], described in Appendix 2, may be expressed as a linear sum [18]:

$$\tau_{tof} = \tau_0 - \frac{v}{a} \qquad (1.15)$$

Where τ_0 is the time-of-flight for a thermal ion, v is the ions initial velocity component along the spectrometers axis in the direction of the ion detector and a is the acceleration of the ion in the spectrometers source region. The v/a term in Equation 1.15 represents the *braking time*, that is the change in the ion's time-of-flight caused by the ion's initial velocity. Clearly, ions with large kinetic energies will, if their trajectories are close to parallel with the spectrometer's axis, have significantly reduced or increased flight times. The effect of this is to cause a widening of the coincidence peak away from τ_0.

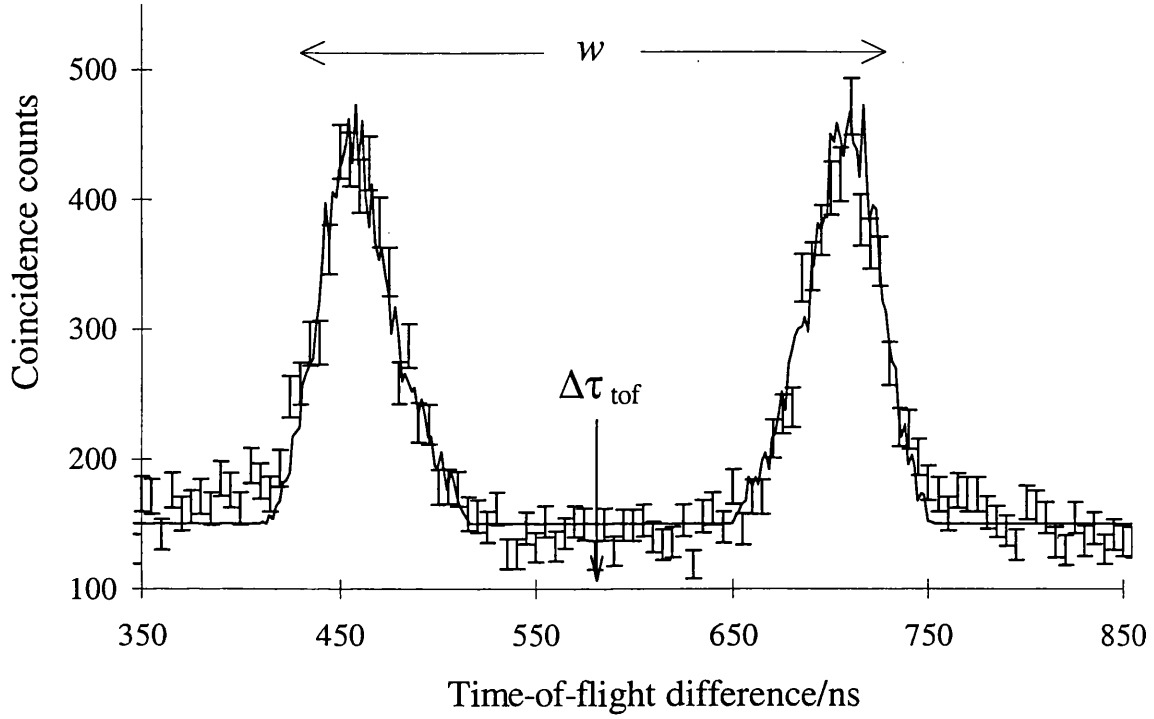

Figure 1.4 A section of a representative electron impact ion-ion coincidence spectrum of width w and peak centre $\Delta\tau_{tof}$ showing the peak resulting from the formation of O^+ and O_2^+ from the dissociation of O_3^{2+}. The ozone dication is generated by electron impact at 150 eV [37]. The solid curve is a simulation of the experimental signal.

To qualitatively consider the effect of the fragment ion's kinetic energy on the width of the coincidence peak, consider a molecular dication XY^{2+} that dissociates to give singly-charged fragment ions X^+ and Y^+ having masses M_X and M_Y and velocities V_Y and V_X respectively. For such a fragmentation, the law of the conservation of linear momentum requires:

$$M_X V_X + M_Y V_Y = 0 \tag{1.16}$$

From Equation 1.15, the difference in the flight times of ions X^+ and Y^+, $\Delta\tau_{tof}$ is given by:

$$\Delta\tau_{tof} = \tau_{0(X)} - \tau_{0(Y)} + \left[\frac{V_Y}{a_Y} - \frac{V_X}{a_X}\right] \tag{1.17}$$

but since the accelerations a_X and a_Y are inversely proportional to the ion mass, the braking times of the fragments are equal in magnitude, but of opposite sign. Hence, Equation (1.17) may be simplified, by using Equation (1.16), giving:

$$\Delta\tau_{tof} = \Delta\tau_0 + 2\frac{V_X}{a_X} \tag{1.18}$$

Since the ions may be produced having initial velocity (V_{MS}) in the range $+V_0$ to $-V_0$, with V_0 being the initial speed of ion and $V_{MS} = V_0\cos\theta$, θ being the angle between the spectrometer's axis and the initial fragment ion trajectory, the resulting coincidence peak will be centred at $\Delta\tau_{tof} = \Delta\tau_0$ and the total peak width w (ns) will be $4V_0/a$. Hence, using Equations 1.16 and 1.17, it can be shown that the total peak width can be expressed in terms of the fragment ion masses and the kinetic energy release U (eV) upon the fragmentation of the dication [18]:

$$w = \frac{5766}{E}\left[\frac{UM_XM_Y}{(M_X + M_Y)}\right]^{0.5} \tag{1.19}$$

where E is the electric field strength (V cm^{-1}) of the source region.

Using a similar procedure to the calculation of an ion's time-of-flight, it can be shown, using a mixture of simple electrostatic equations and Newtonian mechanics, that, for simple molecules, the ion-ion coincidence method can be used to identify the fragment ions:

$$\Delta\tau_{0(XY)} = k\left(\sqrt{M_Y} - \sqrt{M_X}\right) \tag{1.20}$$

where $\Delta\tau_{0(XY)}$ is the time-of-flight difference between ions X^+ and Y^+ of mass M_X and M_Y respectively and k is a constant for a given source electric field. Hence, Equation 1.20 allows the masses of the fragment ions to be readily calculated from the coincidence spectrum. Having identified the masses of the products of the dissociation, the value of the kinetic energy released in the fragmentation may be determined using Equation 1.19.

KER values are an important source of information concerning molecular dications. For example, KER values provide a means of estimating double ionization potentials. In addition, such values offer an insight into the dissociation process. For instance, whether the fragmentation is direct or sequential. KER values also offer a source of information regarding the structure and geometry of molecular dications [18,39]. In addition to the KER data, the ion-ion coincidence technique also provides a means of determining the channels of unimolecular reaction, and the ionization branching ratios.

1.5.3 Photoion-photoion coincidence spectrometry

Photoion-photoion coincidence (PIPICO) is the photoionization analogue of the above technique, differing only in the means of ionization, which, as the name suggests, is achieved by photon impact using either of the methods discussed above.

$$h\nu + XY \rightarrow \left[XY^{2+} + 2e^{-}\right] \rightarrow X^{+} + Y^{+} + 2e^{-} \qquad (1.21)$$

As photon-impact is used to achieve ionization, the advantage of the PIPICO method over its electron-impact rival is that the energy deposition to the molecule is precisely known, although the ease of producing a usable beam of electrons of a suitable flux and energy makes electron-impact an inexpensive and reliable method of ionization.

In common with electron-impact ion-ion coincidence spectrometry, the PIPICO technique has the drawback that it cannot measure the absolute masses of the ions involved in the dissociation, merely the difference in the square roots of their masses. This drawback makes the PIPICO and ion-ion techniques unsuitable for use in identifying the fragment channels of large molecular dications such as the azulene dication ($C_{10}H_8^{2+}$) [23], as there is the possibility of different fragmentation processes giving rise to the same time-of-flight differences.

1.5.4 Photoelectron-photoion-photoion coincidence spectrometry

Photoelectron-photoion-photoion coincidence (PEPIPICO) spectrometry has similarities to the PIPICO method described above. However, PEPIPICO also allows the absolute masses of the fragments to be found. The detection of one of the photoelectrons released during double ionization is used as a time zero. This time zero therefore allows the determination of the photoion's actual times-of-flight and hence their masses. Consequently, the main advantage of the PEPIPICO technique over the PIPICO method is the ability to obtain the absolute masses of the photoions, thus making PEPIPICO particularly well suited for the study of larger dications such as the naphthalene dication ($C_{10}H_8^{2+}$) [23], as the greater number of potential fragmentation channels in larger molecular dications complicates the analysis of PIPICO spectra.

As stated above, the absolute masses of the ionic products of a dissociation event may be obtained using PEPIPICO spectrometry; this ability makes the PEPIPICO technique study especially well suited for investigating the dynamics of three-body dissociations of molecular dications, where there may be many channels of fragmentation. Examples of such work include investigations by Masuoka [26] and Eland [19] into the dissociation dynamics of OCS^{2+} and ICN^{2+}, and provide detailed information concerning the mechanism of dicationic fragmentation.

1.5.5 Doppler-free kinetic energy release spectrometry

The (electron-impact) ion-ion, photoion-photoion and photoelectron-photoion-photoion coincidence methods may all be used to obtain values of the kinetic energy release (KER) upon charge-separating dissociation. Hence, by using Equation 1.19, it is possible to obtain the value of the kinetic energy released in every dissociation event detected in coincidence. Consequently, instead of the flight-time difference of successive ions, it is possible to record the intensity of the coincidence signal as a function of the KER value; this adapted form of coincidence technique is often referred to as kinetic energy release spectrometry.

Prior to 1995, the use of KER spectrometry suffered from poor resolution of the kinetic energy released upon dissociation. The resolution of the kinetic energy released is limited by the Doppler broadening of the coincidence signal due to the thermal velocity of the parent gas molecules. Such broadening is large enough to prevent the observation of vibrational and electronic fine structure. However, the recent introduction of Doppler-free kinetic energy release (DFKER) spectrometry [12,55] has greatly improved the energy resolution.

To eliminate the Doppler broadening, the experimental methodology employed by Lundqvist *et al* [12] utilizes a new apparatus, specifically designed for DFKER spectrometry. The instrument consists of a differentially-pumped gas cell mounted between two adjacent time-of-flight tubes, arranged in a 180° geometry. A pulsed electron beam is used to generate ions in the gas cell by means of electron-impact ionization of neutral precursor molecules.

The use of a two time-of-flight tube arrangement allows the thermal energy of the parent neutral molecule to be removed from the total kinetic energy of the fragment ions. A coincidence signal is produced when both detectors are hit by ions formed from the same dissociation event. The use of the pulsed electron beam provides a time zero and enables the determination of the detected ions flight times. These flight times are converted to individual kinetic energies, and are used to determine the Doppler-free kinetic energy released on dissociation by using Equation 1.22.

$$E_k = E_A + E_B - \frac{\left[\left(E_A m_A\right)^{0.5} - \left(E_B m_B\right)^{0.5}\right]^2}{m_A + m_B} \qquad (1.22)$$

where E_k is the Doppler-free kinetic energy release and E_A and E_B are the individual kinetic energies of the dissociation fragments having masses m_A and m_B respectively.

The significantly increased resolution gained by using the DFKER technique has allowed the kinetic energy release to be examined for fine electronic and vibrational structure, permitting the detailed investigation of the dissociation dynamics of molecular dications. For example, this

technique has been used to examine the kinetic energy released in the dissociation of O_2^{2+} for fine structure, the resolution being of sufficient quality to resolve individual vibrational levels [12]. Thus, the DFKER technique provides an insight into the predissociation and tunnelling processes that are involved in the mechanism of charge-separating fragmentation.

1.5.6 Photoelectron-Photoelectron coincidence

Photoelectron-Photoelectron coincidence (PEPECO) spectrometry is, in effect, the photoelectron spectroscopy of molecular dications [72]. In this technique, both the photoelectrons emitted during double photoionization are detected in coincidence and energy analyzed. This procedure allows the dication state energy $E(XY^{2+})$ to be determined:

$$E(XY^{2+}) = h\nu - \left[E_{e1} + E_{e2}\right] \tag{1.23}$$

where $h\nu$ is the photon energy and E_e is the energy of a photoelectron.

The PEPECO coincidence technique has been used to investigate the spectroscopy of a wide range of dications. For example, an investigation of the mechanism of the double photoionization of mercury [72] has revealed that the mechanism for forming Hg^{2+} in the $^3D_{3,2}$ electronic states is a direct process, whilst the mechanism for forming the $^1S_0$ state is largely indirect, being dominated by the autoionization of Hg^+.

1.6 Non-coincidence methods to study gas-phase molecular dications

1.6.1 Double charge-transfer spectroscopy

Double charge-transfer spectroscopy (DCTS) involves the production of molecular dications by electron-transfer from the neutral molecule to singly-charged ions($\vec{X}^+$) in a fast beam [73], prototypically given by Equation 1.24:

$$\vec{X}^+ + AB \rightarrow \vec{X}^- + AB^{2+} - \Delta E \tag{1.24}$$

The double charge-transfer reaction is generally endothermic, with the energy defect (ΔE) being balanced by a change in the kinetic energy of the fast ion species (X). Therefore measurement of the kinetic energy of the resulting negative ion, together with the projectiles electron affinity, ionization potential and incident ion kinetic energy, allows the calculation of the energy of the dication electronic state $E_{AB^{2+}}$ populated in the double charge-transfer reaction relative to the electronic ground state of the neutral collision partner (AB) .

$$E_{AB^{2+}} = \Delta E + IP_{(X)} + E_{aff(X)} \tag{1.25}$$

where ΔE is the kinetic energy loss of the projectile negative ion, $IP_{(X)}$ is the ionization potential of X and $E_{aff(X)}$ is the electron affinity of X. Hence, the DCTS technique allows a spectroscopy of the dication.

The signals due to the formation of the $\vec{X}^-$, via two sequential single electron-transfers, can be distinguished from the double charge-transfer signals, as the pressure dependence of the sequential process is different. Therefore, the distinction between the two sets of signals may be made by taking the kinetic energy values of the fast ion species (X) at two different pressures of target gas. For example, the DCTS technique has been used to probe the energetics and mechanism of double ionization of HCl [72]. In addition, DCTS has been used to measure the double ionization potentials of a number of species [24,74-76], including CH_4 [77].

1.7 Methods to study the gas-phase reactions of molecular dications

In addition to crossed-beam mass spectrometry, of which the time-of-flight method will be comprehensively described in the next Chapter, the stationary afterglow, flowing afterglow and selected ion flow tube methods may be employed to study ion-neutral reactions at low (thermal) collision energies. The flowing afterglow and selected ion flow tube methods rely on the use of a fast-flow tube reactor in which the rate coefficients for ion-molecule reactions are determined under multiple collision conditions. The use of a multiple collision environment allows the kinetic energy of the reactant ion to be well defined.

The flowing afterglow and selected ion flow tube methods are characterized by the presence of an inert carrier gas (usually helium), this carrier gas is used to convect the reactant ions along the tube to the site of the reaction zone. In the flow tube, the number density of the reactant ion is much less than that of the carrier gas, hence the multiple collisions between the carrier gas and the reactant ions ensures that the ions are efficiently thermalized before undergoing reaction with the neutral reactant. The flowing afterglow is an improved version of the stationary method, with the selected ion flow tube being a further development of the flowing afterglow method. The significant advantages offered by the selected ion flow tube method over the related afterglow techniques are discussed below. However, in order to put the benefits offered by the selected ion flow tube method into context, the specific discussion firstly considers the two prototypical afterglow methods.

1.7.1 Stationary afterglow techniques

In the stationary afterglow (SA) method [78-80], low concentrations of both the neutral reactant gas and the precursor source gas, from which the reactant ion is derived, are mixed with

an inert carrier gas. The mixture of gases is then subjected to a short pulse ionizing DC, RF or microwave discharge, which ionizes the source gas. The ensuing reactions between the ions formed by the discharge and the neutral reactant are studied by means of measuring the currents of the mass analyzed ions; these ions may be either reactant ions that have not undergone reaction or product ions formed in the reaction process.

The principal drawbacks with this experimental method are concerned with the fact that both the precursor source gas and the neutral reactant are subjected to the ionizing discharge; this may lead to the production of ions in excited metastable electronic states, which may complicate the assignment of the reaction products.

1.7.2 Flowing afterglow techniques

Developed in the 1960's, the flowing afterglow (FA) method addresses the shortcomings associated with the SA method described above [81-83]. In the FA method, the carrier gas is subjected to the ionization process at a position in the flow tube that is upstream of the point at which the ion source gas is added, consequently the ion source gas is not subjected to the discharge/electron-impact ionization source. The reactant ions are then formed by means of electron-transfer reactions between the carrier gas ions (He^+) and the ion source gas. This method of producing the reactant ion offers a much greater degree of control of the electronic energy of the reactant ion.

In common with the SA method, the relatively low number density of the reactant ions (10^7-10^9 cm^{-3}) [80] ensures that they are readily thermalized following collisional relaxation with the carrier gas, present in much larger number densities (~10^{16} cm^{-3}), during the period in which the reactant ions are convected by the carrier gas to the reaction region where the neutral reactant is introduced. The reaction is monitored by measuring the reduction in the current of the reactant ion as a function of the amount of neutral reactant that is introduced into the apparatus. The current measurement is achieved by means of a mass spectrometer. The mass spectrometer is also used to identify the charged reaction products. A schematic diagram of a typical flowing afterglow apparatus is shown in Figure 1.5.

Although the FA technique represents a significant improvement over its SA predecessor, it is not without its own problems. Most notably, the presence of the neutral source gas in the reaction zone introduces potential problems due to reactions between the reactant ions and their source gas, complicating the assignment of product ions and the calculation of ion-molecule reaction rate coefficients. The presence of electrons in the reaction site may also complicate the analysis of the reaction products as their presence may lead to a reduction in the reactant ion

current, distorting the product ion intensities through the dissociative recombination of the reactant ion (XY^+), prototypically given by Equation 1.26.

$$XY^+ + e^- \rightarrow [XY] \rightarrow X + Y \qquad (1.26)$$

Other problems associated with the FA method include the possibility of encountering energetic photons originating from the ion source (if applicable) and metastable carrier gas atoms in the reaction site. These are both potential sources of ionization in the afterglow, and may therefore distort the product ion intensities.

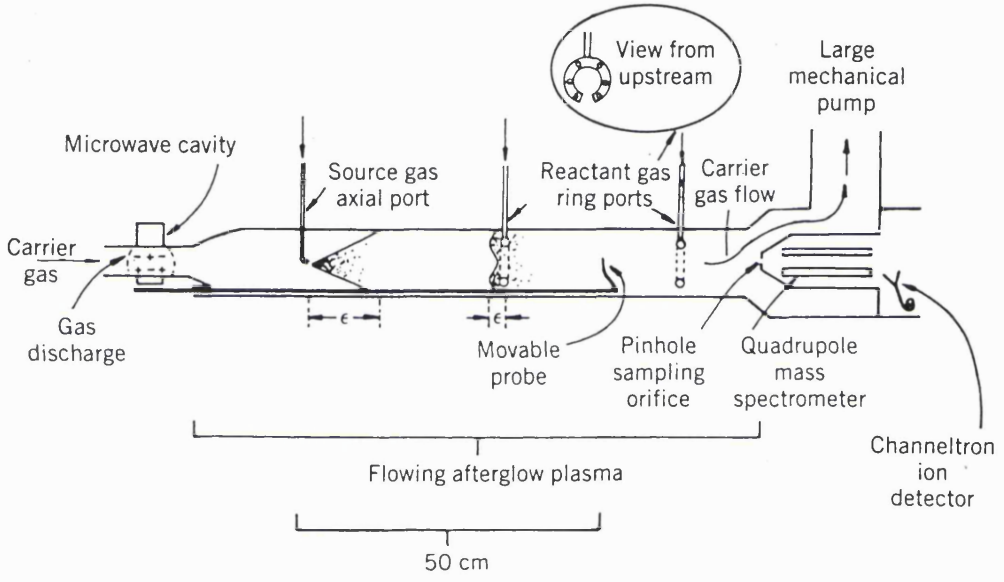

Figure 1.5 Schematic layout of a flowing afterglow apparatus [80]. In this case the ion source is a microwave cavity discharge with a quadropole mass spectrometer employed to mass-analyse the reaction products.

1.7.3 Selected ion flow tube techniques

The selected ion flow tube (SIFT) technique, developed over twenty years ago by Adams and Smith [84,85], was specifically designed to investigate the ion chemistry of the interstellar medium [86], particularly the reactions between positive ions and polyatomic neutrals in interstellar dense clouds. The principal difference between SIFT and the earlier afterglow techniques is that in the case of SIFT, the reactant ions, which may be either positive or negatively charged, are formed in a remote ion source. The employment of a remote source helps to prevent the main problems that are associated with the SA and FA techniques described above, namely the formation of the reactant ion inside the flow tube, which entails the simultaneous presence of the carrier gas, electrons and the neutral reactant species.

As stated above, the SIFT technique is characterized by the formation of the reactant ion in a separate ion source, where ionization is achieved usually by means of electron-impact. After mass analysis, the resulting ions are injected into the flow tube, where the reactant ions are rapidly thermalized by the carrier gas which convects the reactant ions downstream to the reaction site where the neutral reactant is introduced. Following reaction, any unreacted ions and charged products are sampled through a downstream 'pin-hole' orifice situated at the front of a mass spectrometer. The use of the mass spectrometer allows the product ions to be mass-analysed and quantified.

The use of the SIFT technique permits the study of a wide range of ions including atomic dications [87](Equation 1.27), complex ions (Equation 1.28) [88], weakly bound negatively-charged cluster ions (Equation 1.29) [89] and, in a few cases, molecular dications (Equation 1.30) [66,90-92] over a wide range of temperatures.

$$Ar^{2+} + He \rightarrow Ar^{+} + He^{+} \tag{1.27}$$

$$N_2^{+} + N_2 + He \rightarrow N_4^{+} + He \tag{1.28}$$

$$NO_3^{-}(HNO_3) + HCl + He \rightarrow NO_3^{-}(HNO_3) \cdot HCl + He \tag{1.29}$$

$$CO_2^{2+} + N_2 \rightarrow CO_2^{+} + N_2^{+} \tag{1.30}$$

A further development in the field of fast flow tube technology is the *variable-temperature selected ion flow drift tube* (VT-SIFDT) [93]. The VT-SIFDT apparatus consists of a typical SIFT device that incorporates a series of equally-spaced metal rings which are arranged coaxially along the longitudinal axis of the flow tube inside the reaction zone. These rings constitute a drift tube enabling a uniform electric field to be established inside the flow tube. The employment of an electric field accelerates the ions, allowing the reactant ion to be imparted with an amount of kinetic energy which is dependent upon the electric field strength and the collision frequency. Hence, the use of the VT-SIFDT apparatus permits the determination of the thermal and supra-thermal collision energy-dependence of the ion-neutral reaction rate coefficients in addition to the temperature dependence. A schematic of the VT-SIFDT apparatus is illustrated in Figure 1.6

The VT-SIFDT technique provides, as described above, a versatile method of investigating the low collision energy-dependence of ion-molecule reactions. The main drawback with this method is that the presence of the doubly charged reactant ions is likely to result in the ionization of the carrier gas. In addition, the fact that multiple collision conditions are a necessary requirement makes the study of the reactivity of multiply-charged molecular ions difficult to achieve, as a large proportion (~80%) [13] of the charged reactant would be lost through collision-induced charge-separating dissociation with the carrier gas. This would also complicate

the analysis of the reaction products, as the products of dissociative electron-transfer could be indistinct from the fragments of the dissociated reactant ion.

The drawbacks associated with SIFT and VT-SIFDT mentioned above, are not present with crossed beam/time-of-flight (TOF) mass spectrometric methods, where the absence of a carrier gas ensures that single collision conditions are easily achieved. The additional advantages of TOF mass spectrometry are its ability to provide information regarding the energetics of the charged reactants and the increased range of collision energies attainable. For these reasons TOF mass spectrometry is the logical choice of experimental method of investigating the gas-phase reactivity of doubly-charged molecular dications reported in this thesis.

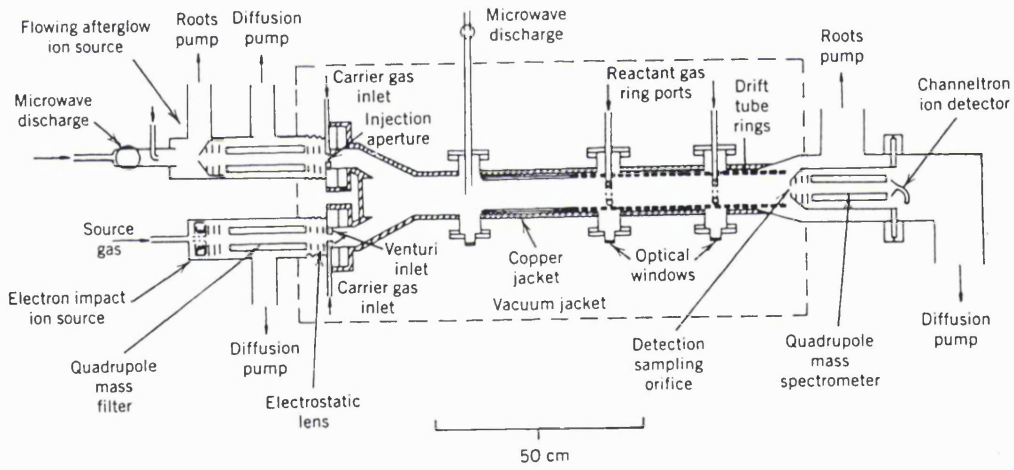

Figure 1.6 Schematic layout of a variable-temperature selected ion flow tube (VT-SIFDT) apparatus [93]. For greater flexibility this particular design incorporates two reactant ion inlets, allowing the reactant ion to be formed by means of both microwave discharge and electron-impact. As illustrated above, mass selectivity of the reactant ion is achieved by means of quadropole mass spectrometry. A quadropole mass spectrometer, situated behind a sampling orifice downstream of the reaction zone, is also employed to mass analyse and quantify the charged reaction products and any unreacted ions.

1.8 Conclusion

As discussed in this Chapter, advances in information technology and the development of new experimental techniques have, over the past two decades, prompted an upsurge of interest in the study of doubly-charged gas-phase molecular ions. However, despite this renewed interest, the majority of work has mainly concentrated on the properties of the isolated species, with the

chemical reactivity of molecular dications with neutral molecular collision partners being particularly under-represented. In attempting to address this shortfall, this thesis presents the first results from a new experiment using a crossed-beam apparatus, incorporating time-of-flight mass spectrometry, specifically designed to investigate the bimolecular reactivity of doubly-charged molecular species.

References

1 D. A. Hagan and J. H. D. Eland, *Rapid Commun. Mass spectrom.*, **3** (1989) 196.

2 K. A. Newson and S. D. Price, *Int. J. Mass Spec. Ion Proc.*, **148** (1995) 203.

3 Z. Dolejsek, M. Farnik and Z. Herman, *Chem. Phys. Letters,* **235** (1995) 99.

4 K. A. Newson and S. D. Price, *Chem. Phys. Letters,* **269** (1997) 93.

5 S. D. Price, S. A. Rogers and S. R. Leone, *J. Chem. Phys.*, **98** (12) (1993) 9455.

6 S. A. Rogers, S. D. Price and S. R. Leone, J. *Chem. Phys.*, **98** (1) (1993) 280.

7 M. Manning, S. D. Price and S. R. Leone, *J. Chem. Phys.*, **98** (11) (1993) 8695.

8 S. D. Price, M. Manning and S. R. Leone, *Chem. Phys. Letters,* **214** (1993) 553.

9 S. D. Price, M. Manning and S. R. Leone, *J. American Chem. Soc.,* **116** (1994) 8673.

10 H. R. Koslowski, H. Lebius, V. Staemmler, R. Fink, K. Wiesemann and B. A. Huber, *J. Phys. B: Atom. Mol. Opt. Phys.*, **24** (1991) 5023.

11 C. J. Reid, J. A. Ballantine and F. M. Harris, *Int. J. Mass Spec. Ion Proc.*, **93** (1989) 23.

12 M. Lundqvist, D. Edvardsson, P. Baltzer, M. Larsson and B. Wannberg, *J. Phys. B: At. Mol. Opt. Phys.*, **29** (1996) 499.

13 J. D. C. Jones, A. S. M. Raof, D. G. Lister, K. Berkinshaw and N. D. Twiddy, *Chem. Phys. Letters*, **78** (1980) 75.

14 X. D. Zhou, A. K. Shukla, R. E. Tosh and J. H. Futrell, *Int. J. Mass Spec. Ion Proc.*, **160** (1997) 49.

15 A. Ehbrecht, N. Mustafa, C. Ottinger and Z. Herman, *J. Chem. Phys.*, **105** (1996) 9833

16 C. P. Safvan and D. Mathur, *J. Phys. B: At. Mol. Opt. Phys.*, **26** (1993) L793.

17 B. P. Tsai and J. H. D. Eland, *Int. J. Mass Spec. Ion Proc.*, **36** (1980) 143.

18 D. M. Curtis and J. H. D. Eland, *Int. J. Mass Spec. Ion Proc.*, **63** (1985) 241.

19 J. H. D. Eland, *Chem. Phys. Letters*, **203** (1993) 353.

20 J. H. D. Eland and D. Mathur, *Rapid Commun. Mass spectrom.*, **5** (1991) 475.

21 G. Dujardin, D. Winkoun and S. Leach, *Phys. Rev. Sect. A.*, **31** (1985) 3027.

22 T. A. Field and J. H. D. Eland, *Chem. Phys. Letters*, **211** (1993) 436.

23 S. Leach, J. H. D. Eland and S. D. Price, *J. Chem. Phys.*, **93** (1989) 7575.

24 P. Millie, I. Nenner, P. Archirel, P. Lablanquie, P. Fournier and J. H. D. Eland, *J. Chem. Phys.*, **84** (1986) 1259.

25 E. Ruhl, S. D. Price and S. Leach, *J. Chem. Phys.*, **93** (1989) 6312.

26 T. Masuoka, *J. Chem. Phys.*, **98** (1993) 6989.

27 T. Masuoka and I. Koyano, *J. Chem. Phys.*, **95** (1991) 909.

28 B. Ernstberger, H. Krause, A. Kiermeier and H. J. Neusser, *J. Chem. Phys.*, **92** (1990) 5285.

29 Z. Fang and V. H. S. Kwong, *Phys. Rev. A.*, **55** (1997) 55.

30 J. J. Thomson, *Philos. Mag.*, **24** (1912) 668.

31 R. Conrad, *Physik. Z.*, **31** (1930) 888.

32 S. D. Price, *J. Chem. Soc., Faraday Trans.*, **93** (1997) 2451.

33 E. Y. Kamber, K. Akgungor, C. P. Savfan and D. Mathur, *Chem. Phys. Letters*, **258** (1996) 336.

34 S. D. Price, Y. Y. Lee, M. Manning and S. R. Leone, *Chem. Phys.*, **190** (1995) 123.

35 P. A. Martin, F. R. Bennett and P. Maier, *J. Chem. Phys.*, **100** (1994) 4766.

36 P. J. Richardson and J. H. D. Eland, *Molecular Phys.*, **55** (1985) 957.

37 K. A. Newson and S. D. Price, *Int. J. Mass Spec. Ion Proc.*, **153** (1996) 151.

38 Y. Y. Lee, S. R. Leone, P. Champkin, N. Kaltsoyannis and S. D. Price, *J. Chem. Phys.*, **106** (1997) 7981.

39 D. Mathur, *Phys. Rep.*, **225** (1993) 193.

40 M. Larsson, *Comm. Atom. Molec. Phys.*, **29** (1993) 39.

41 F. R. Bennett and I. R. McNab, *Chem. Phys. Letters*, **251** (1996) 405.

42 D. Mathur, L. H. Anderson, P. Hvelplund, D. Kella and C. P. Safvan, *J. Phys. B.*, **28** (1995) 3415.

43 T. Weiske, W. Koch and H. Schwarz, *J. American Chem. Soc.*, **115** (1993) 6312.

44 S. S. Prasad and D. R. Furman, *J. Geophys. Rev.*, **80** (1975) 1360.

45 S. Leach, *J.Electron Spec. Rel.Phenom.*, **41** (1986) 427.

46 A. Leger and L. d'Hendecourt, *Astron. Astrophys.*, **146** (1985) 81.

47 L. J. Allamandola, A. G. Tielens and J. R. Barker, *J. Astrophys.* **290** (1985) L25.

48 K. Hogreve, *J. Chem. Phys.*, **102** (1995) 3281.

49 M. Kolbuszwski and J. S. Wright, *J. Phys. Chem.*, **99** (1995) 3455.

50 P. Millie and I Nenner, *J. Chem. Phys.*, **84** (1986) 1259.

51 D. Duflot, J-M. Robbe and J-P. Flament, *J. Chem. Phys.*, **103** (1986) 1259.

52 P. Pyykko, *Chem. Phys. Letters*, **156** (1989) 337.

53 A. Chablo and D. W. J. Cruichshank, *J. Mol. Struct.*, **70** (1981) 95.

54 G. Roberts and A. H. Zewail, *J. Phys. Chem.*, **95** (1986) 1259.

55 S. Hsieh and J. H. D. Eland, *J. Phys. B: At. Mol. Opt. Phys.*, **29** (1996) 5795.

56 P. Kush, A. Hustrulid and J. T. Tate, *Phys. Rev.*, **52** (1937) 843.

57 P. Kush, A. Hustrulid and J. T. Tate, *Phys. Rev.*, 54 (1938) 1037.

58 M. Larsson, P. Baltzer, S. Svensson, B. Wannberg, N. Martenson, A. N. Debrito, N. Correia, M. P. Keane, M. Carlssongothe and L. Karlsson, *J. Phys. B.*, **23** (1990) 1175.

59 G. Parlant, J. Senekowitsch, S. V. O'Neil and D. R. Yarkony, *J. Chem. Phys.*, **94** (1991) 7208.

60 T. A. Field and J. H. D. Eland, *Chem. Phys. Letters*, **211** (1993) 436.

61 L. H. Anderson, J. H. Posthumus, O. Vahtras, H. Agren, N. Elander, A. Nunez, A. Scrinzi, M. Natiello and M. Larsson, *Phys. Rev. Letters*, **71** (1993) 1812.

62 J. Senekowitsch and S. V. O'Neil, *J. Chem. Phys.*, **95** (1991) 1847.

63 F. R. Bennett and I. R. McNab, *Chem. Phys. Letters*, **251** (1996) 405.

64 M. V. V. S. Rao and S. K. Srivastava, *J. Geophys. Rev.*, **96** (1991) 17563.

65 M. Soloman and A. Mandelbaum, *Chem. Commun.*, (1969) 890.

66 P. J. Stephens and K. J. Jalkanen, *J. Chem. Phys.*, **91** (1989) 1376.

67 M. Hamdan and A. G. Brenton, *J. Phys. B: At. Mol. Opt. Phys.*, **22** (1989) L45.

68 K. A. Newson and S.D. Price, *Chem. Phys. Letters,* in press.

69 K. E. McCulloh, T. E. Sharp and H. M. Rosenstock, *J. Chem. Phys.*, **42** (1965) 3501.

70 K. E. McCulloh and and H. M. Rosenstock, *J. Chem. Phys.*, **48** (1968) 2084.

71 W. C. Wiley and I. H. McLaren, *Rev. Sci. Ints.*, **26** (1955) 1150.

72 S. D. Price, *D. Phil. Thesis,* Oxford University 1990.

73 J. Appel, J. Durup, F. C. Fehsenfeld and P. G. Fournier, *J. Phys. B.*, **6** (1973) 197.

74 P. J. Richardson, J. H. D. Eland, P. G. Fournier and D. L. Cooper, *J. Chem. Phys.*, **84** (1986) 3189.

75 P. G. Fournier, M. Mousselmal, S. D. Peyerimhof, A. Banichevich, N. Y. Adam and T. J. Morgan, *Phys. Rev. A.*, 36 (1987) 2594.

76 S. D. Price, J. H. D. Eland, P. G. Fournier, J. Fournier and P. Millie, *J. Chem. Phys.*, **88** (1988) 1511.

77 P. G. Fournier, J. Fournier, F. Salama, P. J. Richardson and J. H. D. Eland, *J. Chem. Phys.*, **83** (1985) 241.

78 D. Smith, A. G. Dean and N. G. Adams, *J. Phys. D.*, **7** (1974) 1944.

79 E. W. McDaniel and E. A. Mason, *The Mobility and Diffusion of Ions in Gases*, J. Wiley, New York, 1973.

80 J. M. Farrar and W. H. Saunders (Jr), *Techniques for the study of Ion-Molecule Reactions*, J. Wiley, New York, 1973.

81 E. E. Ferguson, F. C. Fehsenfeld and A. L. Schmeltekopf, *Adv. Atom. Mol. Phys.*, **5** (1969) 1.

82 D. Smith and N. G. Adams, in M. T. Bowers, *Gas-Phase ion Chemistry*, Academic Press, New York, 1979, vol. 1, pp. 1-44

83 F. C. Fehsenfeld, *Int. J. Mass Spec. Ion Proc.*, **16** (1975) 151.

84 N. G. Adams and D. Smith, *Int. J. Mass Spec. Ion Proc.*, **21** (1976) 349.

85 N. G. Adams and D. Smith, *J. Phys. B.*, **9** (1976) 1439.

86 D. Smith and N. G. Adams, *Int. Rev. Phys. Chem.*, **1** (1981) 271.

87 N. G. Adams and D. Smith, *Int. J. Mass Spec. Ion Proc.*, **35** (1980) 335.

88 H. Bohringer, F. Arnold, D. Smith and N. G. Adams, *Int. J. Mass Spec. Ion Proc.*, **52** (1983) 25.

89 A. A. Viggiano, *J. Chem. Phys.*, **81** (1984) 2639.

90 J. Glosik, A. B. Rakshit, N. D. Twiddy, D. Smith and N. G. Adams, *J. Phys. B.*, **11** (1978) 3365.

91 R. Johnsen and M. A. Biondi, *Phys. Rev. A.*, **18** (1978) 996.

92 N. G. Adams and D. Smith and D. Grief, *J. Phys. B.*, **12** (1979) 2799.

93 D. Smith and N. G. Adams, *Adv. Atom. Mol. Phys.*, **24** (1988) 1.

Chapter 2

Experimental Details

2.1 Introduction

As detailed in the preceding Chapter, this thesis reports the results of experimental work to study the gas-phase reactions of doubly-charged molecular ions following their collisions with neutral molecules. The experiments are performed using a crossed-beam apparatus [1-10]. The charged products formed in the reactive processes, described in the previous Chapter, are quantified and mass analyzed using time-of-flight mass spectrometry [1,5,11-14]. The experimental apparatus is described in two sections. Firstly, a section covering the production of a dication beam and, secondly, a description of the time-of-flight mass spectrometer.

2.2 Experimental Apparatus I: Dication beam generation

2.2.1 Introduction to the crossed-beam spectrometer

The experiments reported in this thesis are performed by intersecting a continuous beam of mass-selected molecular dications with an effusive jet of the neutral target species. The collisions between the dication and the neutral reactants take place in the source region of a TOF mass spectrometer, which is used to quantify and identify the charged products from the various reactive processes.

The spectrometer consists of two stainless steel limbs making up, firstly, the ion/dication gun and secondly, the TOF mass spectrometer. The vacuum chamber is maintained at low operating pressures ($\sim 10^{-6}$ Torr) and is pumped by three Edwards diffstak MK 2 diffusion pumps. These are connected to the detector chamber, the ion source chamber and the main chamber, which houses the source region of the TOF mass spectrometer. A schematic diagram of the complete spectrometer is shown in Figure 2.1.

2.2.2 The ion source

The molecular dications, along with other ionization products, are generated by the electron-impact ionization of suitable precursor gases. This is achieved by directing a focused beam of electrons at ~150 eV onto a perpendicularly orientated jet of the precursor gas inside the ion source block. The electrons are generated by passing a 3.5 A current through a thermionic tungsten filament. This produces an ejected electron current, typically of the order of 20 μA.

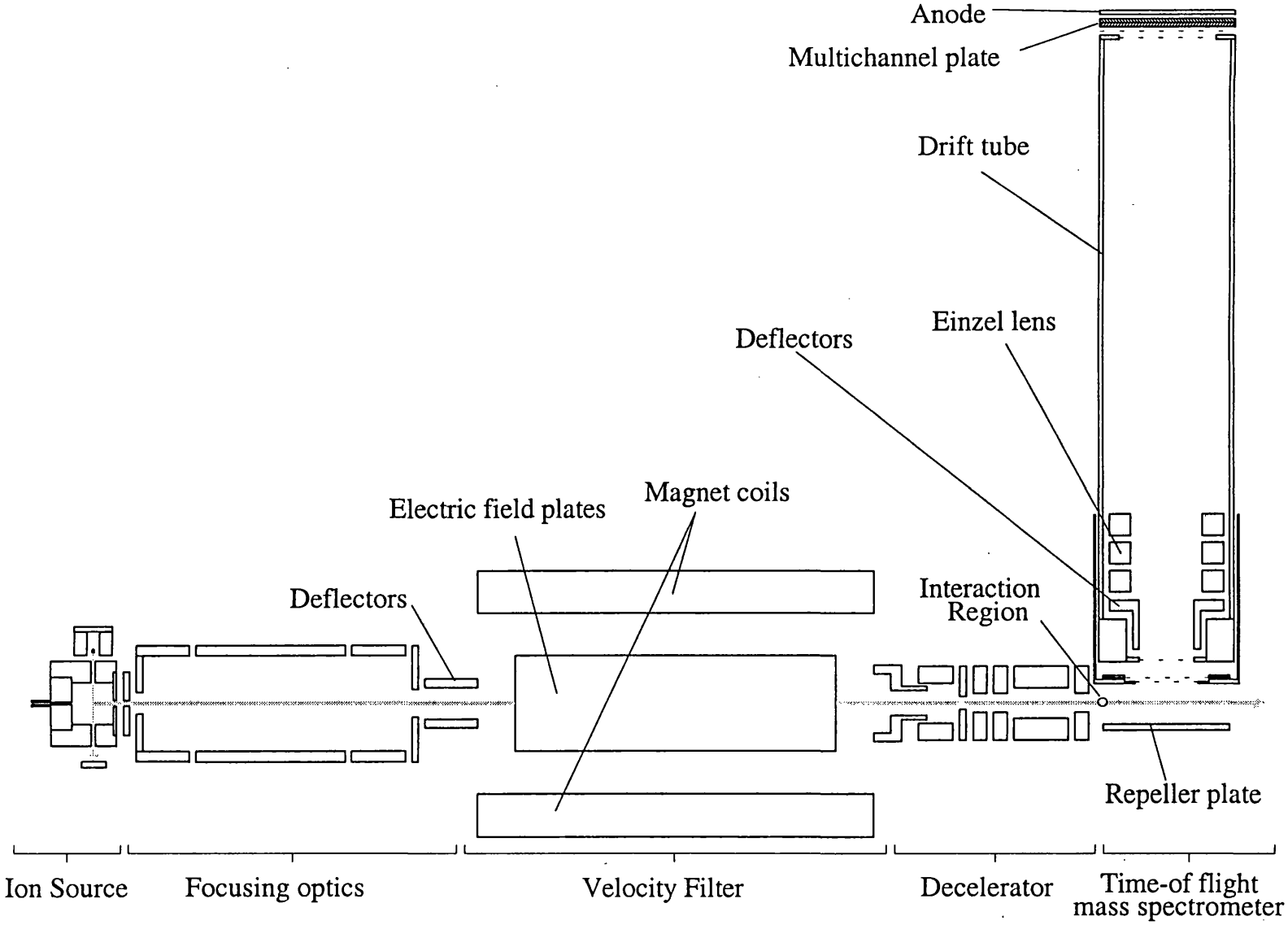

Figure 2.1 Schematic layout of the complete crossed-beam spectrometer.

The background pressure inside the source chamber is kept low enough ($\leq 4 \times 10^{-6}$ Torr) to avoid an excessive number of collisions of the ions with background gas molecules and the neutral precursor gas molecules themselves. Such collisions would result in a decrease in the reactant dication current reaching the interaction region of the TOF mass spectrometer through various collision-induced reaction channels.

In practice, there exists an optimum value of the pressure of the precursor gas inside the source block. Logically, the number of dications generated would be expected to be proportional to the number density of the precursor gas. Indeed, this behaviour is observed as an increase in the dication current with increasing precursor gas pressure. However, if the pressure is increased beyond some optimum value, the dication current falls with increasing pressure. This drop in dication current may be explained as arising because of an increase in the number of collision-induced charge-separating reactions, such as the reaction given in Equation 2.1, occurring inside the source block under elevated pressures.

$$CF_2^{2+} + CF_4 \rightarrow CF^+ + F^+ + CF_4 \qquad (2.1)$$

In addition to causing a reduction of the dication intensity, the presence of the background gas may cause problems in correctly interpreting the TOF mass spectra. Such difficulties arise because many of the products of the reactions between the reactant dication beam and the background gas molecules are indistinguishable from the products of electron-transfer reactions between the reactant dications and the neutral target gas molecules. For example, the CF^+ product ion could be generated when the CF_2^{2+} reactant dication undergoes electron-transfer with either a neutral collision partner, such as NH_3, or species present in the background gas, which, in the ion source, is dominated by CF_4 molecules. Hence, background pressures are kept as low as possible to minimize these adverse effects.

The source block is cubic in shape and is constructed from stainless-steel to withstand the harsh environment of the ionization plasma. A schematic diagram of the ion source is given in Figure 2.1. The ion source consists of the basic block, a thermionic tungsten filament which produces the beam of ionizing electrons, an electron trap, employed to monitor the electron current, and an extraction electrode, which is used to extract newly formed ions from the source block. The precursor gas enters the back of the source block via a flexible PTFE tube, passing through a narrow channel before reaching the central chamber. The ions are generated inside the central chamber, where ionizing electrons are directed perpendicularly to the trajectory of the jet of precursor gas from which the reactant dication is formed. The design of the ion source ensures that the beam of ionizing electrons is very narrow (~2 mm in diameter). Therefore, as the ions are formed in a very small volume of the source block, the ions will have uniform electric potential.

Hence, the kinetic energy of the charged species in the ion beam is also uniform, being defined solely by the potential at which the source block is held. In addition, the design of the source also leads to the efficient extraction of ions, aided by means of an extraction electrode; this prevents an excessive build up of space charge inside the source block.

An array of electrostatic ion optics, consisting of a secondary extraction lens, a pair of vertical deflecting plates and other focusing elements, is employed to extract the ions from the ion source block and collimate them into a beam. The electrostatic potentials at which the ion optics are held were first modelled using appropriate computer software [15] and then optimized to obtain the best quality ion beam. The ion optics are also used to accelerate the ions to a relatively high kinetic energy before they pass into the velocity filter. The source block and extraction electrode arrangement is illustrated in Figure 2.2.

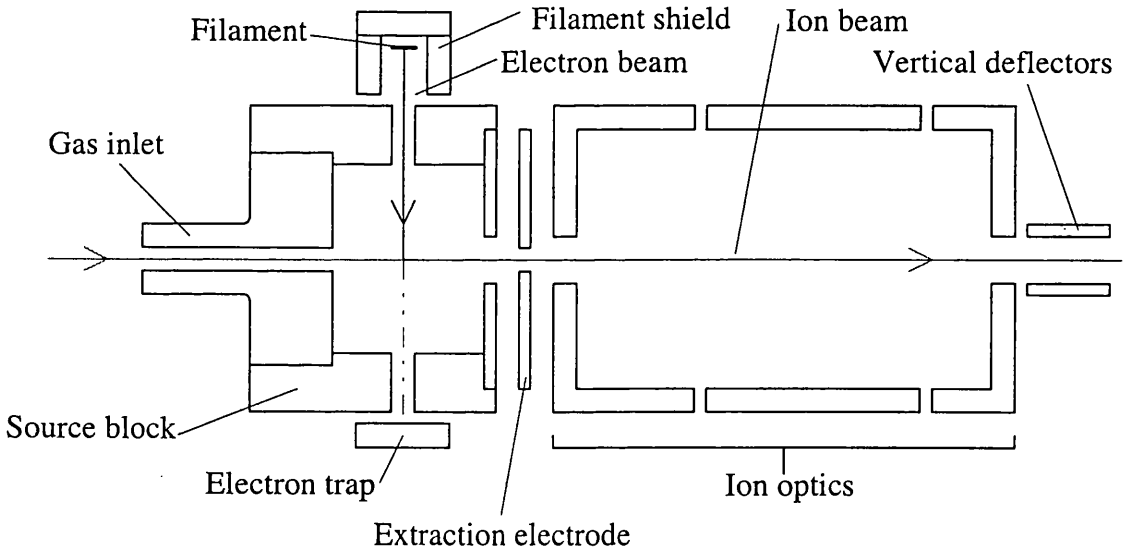

Figure 2.2 Schematic diagram of the ion source block and extraction electrode arrangement.

2.2.3 The velocity filter and mass selection.

The ion beam entering the velocity filter consists of a variety of monocationic and dicationic species formed following the electron-impact ionization of the parent gas molecule. The desired reactant dications comprise only a relatively small fraction of these ions. Many of the products of electron-transfer and collision-induced reactions between the dication and the neutral reactants are identical to these monocations in the raw unfiltered ion beam. Hence, to avoid the product ion intensity being misleadingly enhanced by contributions from the beam of reactant species, it is therefore expedient to obtain a dication beam of the highest possible purity.

Mass selection of the molecular dication is achieved by means of a Colutron velocity filter [16]. The Colutron velocity filter, which is based on the Wien velocity filter [17,18], consists of an electromagnet and a pair of electrostatic deflection plates. The deflection plates are mounted between the poles of the magnet and aligned so as to produce an electric field (E), perpendicular to the magnetic field (B) as shown in Figure 2.3. The force F_E on a particle of charge q in an electric field of strength E is given by:

$$F_E = Eq \tag{2.2}$$

Similarly, the force F_B on a particle of charge q moving with a velocity v in a magnetic field of magnetic flux density B is given by:

$$F_B = Bqv \tag{2.3}$$

a

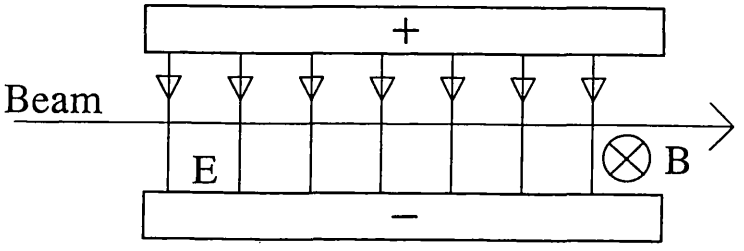

b

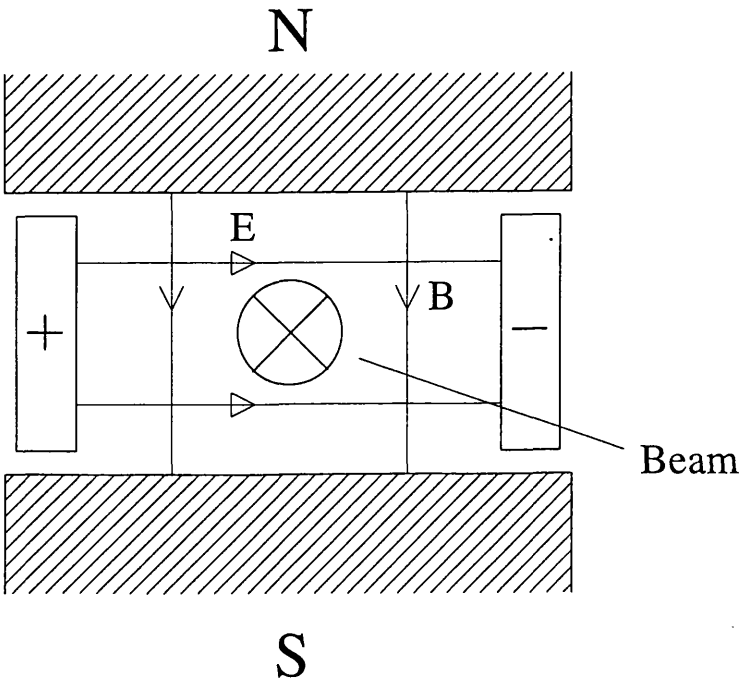

Figure 2.3 (**a**) Arrangement of the electrostatic plates giving rise to the electric field in the velocity filter.
(**b**) The electromagnet arrangement inside the velocity filter.

The combination of the mutually perpendicular magnetic and electric fields results in the two forces F_E and F_B being in opposition. Hence, an ion passing through the velocity filter will be

deflected out of the beam unless the two opposing forces are equal in magnitude. Therefore, as can be seen from Equations 2.2 and 2.3, such a balance in the forces occurs for a unique ion velocity v_0 where:

$$v_0 = E_0 / B_0 \tag{2.4}$$

Thus, if the magnetic flux density and the electric field intensity are set at values B_0 and E_0 respectively, then any ions not having velocity v_0 will be deflected from the beam. All the ions extracted from the ion source are accelerated into the velocity filter by an accelerating potential V. Consequently, all ions of charge q will be accelerated to the same kinetic energy qV, this allows the ion's velocity to be expressed in terms of its mass m:

$$v = \left(\frac{2qV}{m}\right)^{\frac{1}{2}} \tag{2.5}$$

By equating Equations 2.4 and 2.5, it is possible to obtain an expression for an ion of particular mass m_0 remaining undeflected by the opposing magnetic and electric fields for a given set of operating parameters, B, E and V.

$$m_0 = \frac{2qVB_0^2}{E_0^2} \tag{2.6}$$

Any ion not of mass m_0 will be deflected out of the beam. In practice, the magnetic flux density is kept constant to minimize the effects of hysteresis losses and the detrimental effects of the magnet heating or cooling which would result from the current supplied to the electromagnet coils being adjusted. In addition, the Colutron velocity filter achieves its maximum resolution at high values of B. Mass selectivity of the velocity filter is therefore accomplished by varying the electric field strength, this is achieved in practice by scanning the voltage applied to the electrostatic plates.

One problem with the basic velocity filter concerns the natural focusing effect of the crossed electric and magnetic fields [16-21]. Ions in the centre of the ion beam will be undeflected on passing through the filter if the beam and filter are well aligned. However, ions away from the centre of the beam will be drawn to a central focal point, at some distance beyond the filter. This unwanted effect is eliminated by the inclusion of shim plates placed between the electrostatic plates; these shim plates are biased with respect to the electrostatic plate potentials and are connected to potentiometers to allow the sensitive adjustment of their potentials. When correctly biased, the electric field is altered, making the electric field weaker at the positive electrostatic plate and stronger at the negative plate. This produces an electric field shape that compensates for the inherent focusing tendency of the velocity filter.

2.2.4 Ion deceleration

Before ions enter the velocity filter they are accelerated to a relatively high translational energy, typically of the order of 250 eV. The necessity for such an acceleration is that dicationic lifetimes are often of the order of a microsecond or less. Hence, without this acceleration, the transit times of the species in the ion beam to the source region of the spectrometer are of the same order as the dicationic lifetimes. So, to reduce the number of dications lost through natural unimolecular decay, the ions are accelerated to reduce their transit times from the ion source to the collision region. Additionally, higher energy ion beams are easier to handle, as perturbing effects from stray electric fields are less significant. However, despite the above arguments in favour of high energy ion beams, the upper limit to the laboratory frame collision energy used in the research presented in this thesis is of the order of 15 eV. The reason for this limit is that we expect the bond-forming reactivity of molecular dications to be favoured at low collision energies, typically lower than 15 eV in the laboratory frame. In addition to this, at laboratory frame collision energies in excess of 15 eV, the detection efficiency of the experimental arrangement will be markedly reduced as a result of the product ion's transverse velocity component. The detection efficiency is discussed in greater detail in the next Chapter. Hence, before the ions pass into the interaction/source region of the TOFMS, they must be decelerated to the desired collision energy. The deceleration is achieved with the use of appropriate ion deceleration optics.

The ion optics involved in the deceleration process are a commercial assembly. They consist of six independently insulated concentric copper cylinders mounted on a brass base plate which is also independently insulated; a schematic layout of the decelerator assembly is shown in Figure 2.4. The base (**1**), first, second and fourth cylinders (**2**, **3**, **5**) are held at approximately the same potential as the accelerated ion beam, the third and fifth cylinder are held at lower potentials which are controlled by potentiometers. The final cylinder (**7**) is held at ground potential. The aim of this is to gradually reduce the beam energy. The fifth cylinder (**6**) is an Einzel lens which has a cylindrical focusing capability which enables the ion beam to be refocused before the beam reaches the interaction region, as the process of deceleration causes the strong divergence of the ion beam. Such divergence can be explained as arising because the decelerator is only able to reduce the ion's longitudinal velocity component. Hence, the ion's transverse velocity is left unaffected by the 'deceleration' process. Beam focusing is controlled by varying the potential on the third and sixth cylinders by means of adjusting the potentiometers. On leaving the deceleration optics, the collimated beam of molecular dications, now at the desired collision energy, enters the interaction region which is inside the source region of the TOFMS.

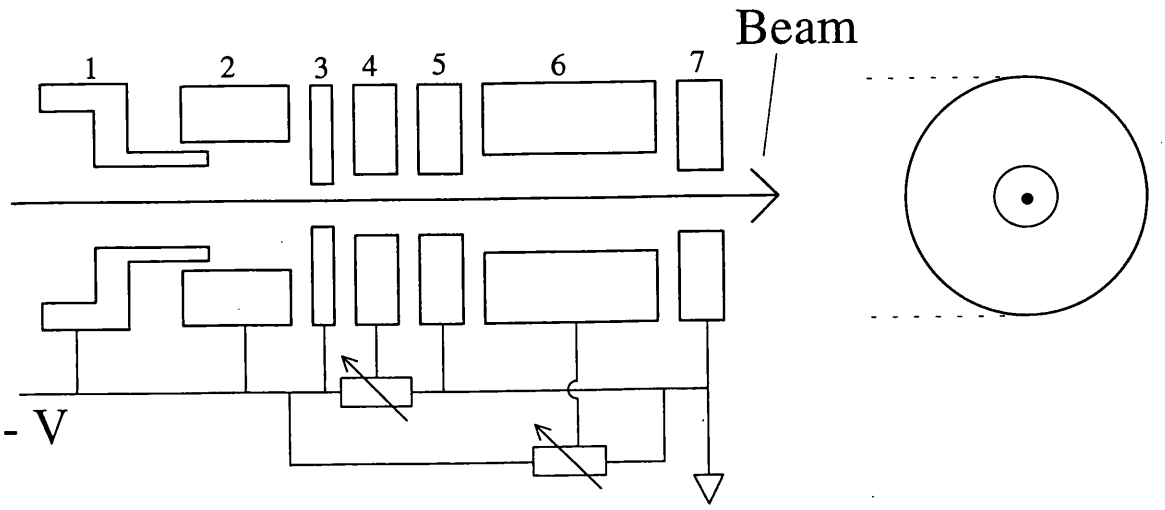

Figure 2.4 Schematic layout of the decelerator assembly.

2.3 Experimental Apparatus II: Time-of-flight mass spectrometry

2.3.1 Introduction to time-of-flight mass spectrometry

Time-of-flight mass spectrometry (TOFMS) has, in recent years, become a versatile experimental technique for the analytical scientist. TOFMS employs as its method of mass separation the fact that ions of differing mass, when accelerated to the same kinetic energy, will, as a virtue of their differing masses, possess different velocities. Hence, their times of flight over a given path length will also be different. Thus, the theoretical concept behind TOFMS is comparatively simple. The fundamental dynamics of a non-relativistic ion of mass *m*, moving in an electric field are described by a combination of simple electrostatics and Newtonian mechanics. It can be shown (Appendix 1) that the time-of-flight of an ion in a series of electric fields (τ_{tof}) is given by:

$$\tau_{tof} = k\sqrt{m} \tag{2.7}$$

Where *k* is a constant that is determined from the internal dimensions of the spectrometer and the magnitude of the electric potentials used to accelerate the ions.

The advantages of TOFMS over rival mass spectrometric techniques, which include magnetic sector mass spectrometry, are many and include such features as the fact that TOFMS offers an unlimited mass range, fast scanning rates (~100 kHz), the fact that each ionization event produces a complete mass spectrum (multiplex operation), relatively low cost of construction and the inherent suitability for using the technique in conjunction with pulsed ionization [14]. The simplicity of the design of a time-of-flight (TOF) mass spectrometer is also a significant

advantage, as other mass spectrometric methods rely heavily upon the accuracy of mechanical alignment and require involved and costly apparatus design and construction [11].

Although TOFMS techniques have been in use for more than sixty years, the use of this particular method of mass spectrometry was not widespread until the late 1950's, when the ground-breaking work of Wiley and McLaren produced a twin electric field design which prompted a renaissance in the use of TOFMS. The availability of modern electronic timing equipment has further increased the applicability of this spectrometric method.

2.3.2 The operational methodology of TOFMS

As mentioned previously, one of the main advantages of TOFMS is the conceptual simplicity of obtaining a value of the mass to charge ratio of an ion, by measuring the ion's flight time along a fixed path length. Ideally, the ion flight times would be uniform for a given ion mass. However, the ions to be analyzed usually have a distribution of initial velocities and initial positions. This has the effect of causing ions of the same mass and charge to have a range of flight times. In an attempt overcome, or at least reduce, this detrimental effect, the spectrometer is designed so that the ions are 'focused'. Focusing attempts to ensure that, irrespective of the above effects, ions of a given mass arrive at the ion detector at the same time. A situation in which the ions are focused may be described mathematically:

$$\frac{dt}{ds} = 0 \tag{2.8}$$

that is, there is no variation in the ion's flight time t, with the ion's initial position s in the source region. The mathematical details of focusing are given in Appendix 2.

In practice, the ion peaks in the mass spectrum have finite half widths corresponding to a range of ion flight times; this is a physical consequence of the ions having a distribution of kinetic energies together with the fact that the ions are formed over a range of positions in the source region and that the focusing is not perfect. Although focusing can help to reduce the spread the ion flight times of ion of a given mass arising because of the ion's initial positions, it is very much more difficult to reduce the detrimental effects of the ions having differing initial velocities. Hence, in addition to having differing initial speeds, the ion's initial trajectories may be in different directions; this further complicates the problem of focusing since ions with initial trajectories directed away from the detector will require a finite time for the electric field to change the direction of their motion. This additional time is known as the *'turn around time'* and adds to the width of a given mass spectral peak. A schematic diagram of a linear, twin electric field design of time-of-flight mass spectrometer is shown in Figure 2.5.

Perhaps the most important feature of the Wiley-McLaren design of twin electric field TOF mass spectrometer is the relative ease of achieving focusing [11]. As discussed in Appendix 2, the focusing is attained by simply adjusting the ratio of the electric fields (Figure 2.5). In general, ions are generated in the source region of the spectrometer either by electron-impact or photon-impact ionization of the precursor sample gas. Alternatively, ions may be produced in a separate ion gun, as in the case of the crossed-beam spectrometer, prior to being transported to the mass spectrometer's source region. The mass spectrum is usually recorded by periodically pulsing on a positive potential to the repeller plate in the spectrometer's source region, whilst simultaneously a START signal is sent to an electrical timing device such as a multichannel scalar (MCS). The positive voltage pulse applied to the repeller plate creates an electric field in the source region. This electric field extracts the positively charged ions out of the source region. A second electric field accelerates the ions further before they pass into a field-free drift region. After the drift region the ions reach the detector, where the arrival of an ion results in a STOP signal being sent to the MCS. The ion's time-of-flight is simply the difference between the stop and start times.

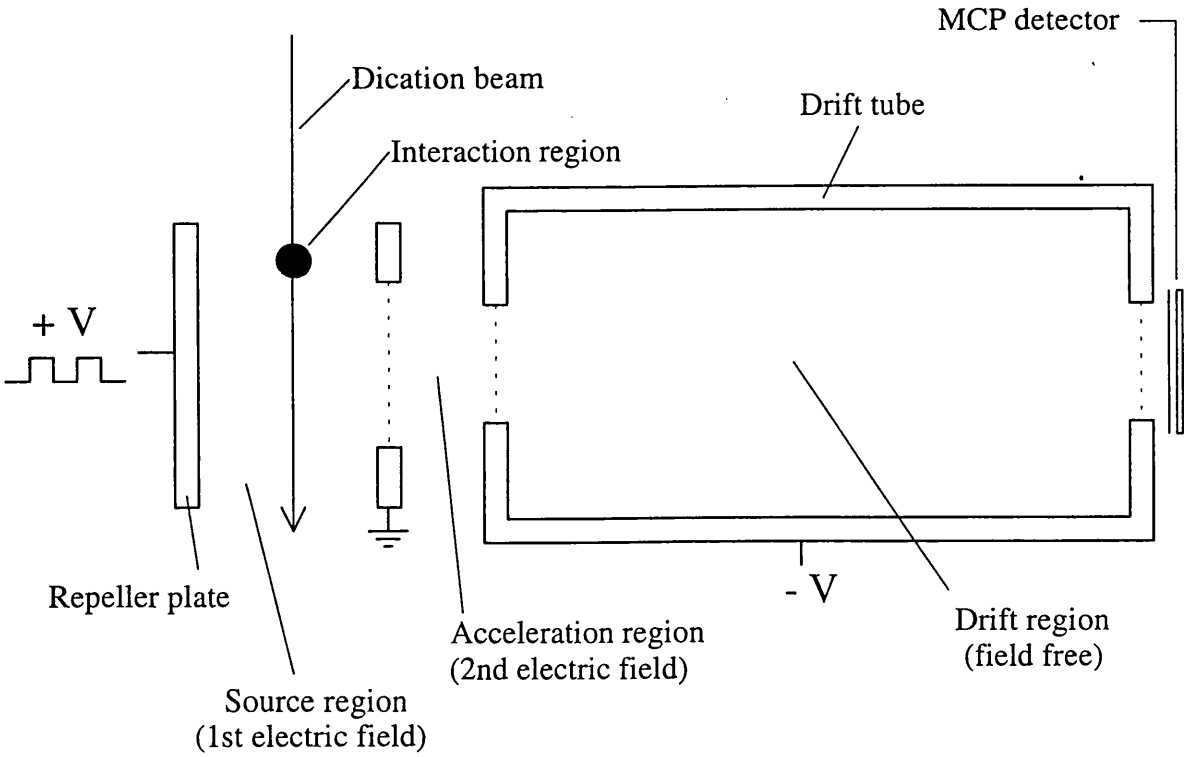

Figure 2.5 Schematic diagram of a twin electric field time-of-flight mass spectrometer, including the interaction/source region.

2.3.3 Collision processes and ion detection

Upon leaving the decelerator, the beam of molecular dications enters the source region of the TOF mass spectrometer. The interaction region, where the dication encounters the neutral reactant, lies approximately mid-way between the end of the decelerator and the central longitudinal axis of TOF mass spectrometer, inside the source region as illustrated in Figure 2.8. The neutral target species enter the interaction region in the form of an effusive jet, delivered via a brass needle which is oriented perpendicularly to the dication beam. This orientation ensures that the neutral species have no significant velocity component in the direction of the dication beam or along the longitudinal axis of the spectrometer. This ensures optimum product ion spatial focusing and greatly simplifies the calculations of the product ion dynamics.

The product ions formed in the reactions between the dications and neutrals in the interaction region, in addition to the unreacted dications, are extracted from the source region of the TOFMS by a periodically pulsed positive voltage pulse on the repeller plate of the TOFMS which, as can be seen in the schematic diagram in Figure 2.5, is situated at the rear of the source region. On leaving the source region, the ions are further accelerated by a second electric field, in the acceleration region, before entering an electric field free drift region. After leaving the drift region the ions hit the front plate of the multichannel plate detector (MCP), which produces an electrical signal signifying the detection of the ions.

2.3.4 Time-of-flight measurement

As briefly mentioned above, the time-of-flight (TOF) of the ions is measured electronically. The components involved in the timing operation are shown schematically in Figure 2.6. Timing the ion's flight is achieved by measuring the difference in times of a START signal to initiate the ion's transit from the source region and a STOP signal generated by the ion when it reaches the detector. The START signal is generated by a Stanford 535 digital delay/pulse generator. The START signal is sent to a pulser unit which then delivers a +400 V pulse to the repeller plate of the TOFMS which initiates the extraction of the ions from the spectrometer's source region. Simultaneously, the pulse generator sends the same START signal to a LeCroy 4208 time-to-digital converter, thus commencing the timing cycle. The arrival of the ion at the front plate of the MCP detector triggers a STOP signal, this signal is amplified and discriminated to remove electronic noise before reaching the same LeCroy 4208 time-to-digital converter (TDC), thus ending the timing cycle. The TDC then passes the digitalized ion flight times to a PC via a GPIB interface. Note that the choice of a time-to-digital converter was made to allow provision for ion coincidence experiments to be performed in future work.

Although the TOFMS part of the apparatus is based upon the Wiley-McLaren twin field design, the TOFMS used in the experiments described in this thesis does incorporate a number of refinements for studying dication reactions [1,5-9,22,23], as illustrated in the schematic diagram in Figure 2.1. These refinements include an Einzel lens and ion deflectors, both of which are situated at the start of the spectrometer's drift tube. These electrostatic elements are only useful at large laboratory-frame collision energies, and for the work reported in this thesis they were not utilized but were merely held at the same potential as the drift tube. A further addition to the Wiley-McLaren design is a grid situated between the grounded acceleration grid and the drift tube grid (Figure 2.5). This grid is held at a low positive potential (~5V) which prevents stray ions from entering the acceleration region during that part of the duty cycle of the TOFMS when the repeller plate is held at ground potential. A Faraday cup is situated beyond the source region, allowing the dication beam intensity (current) to be measured independently of the TOFMS.

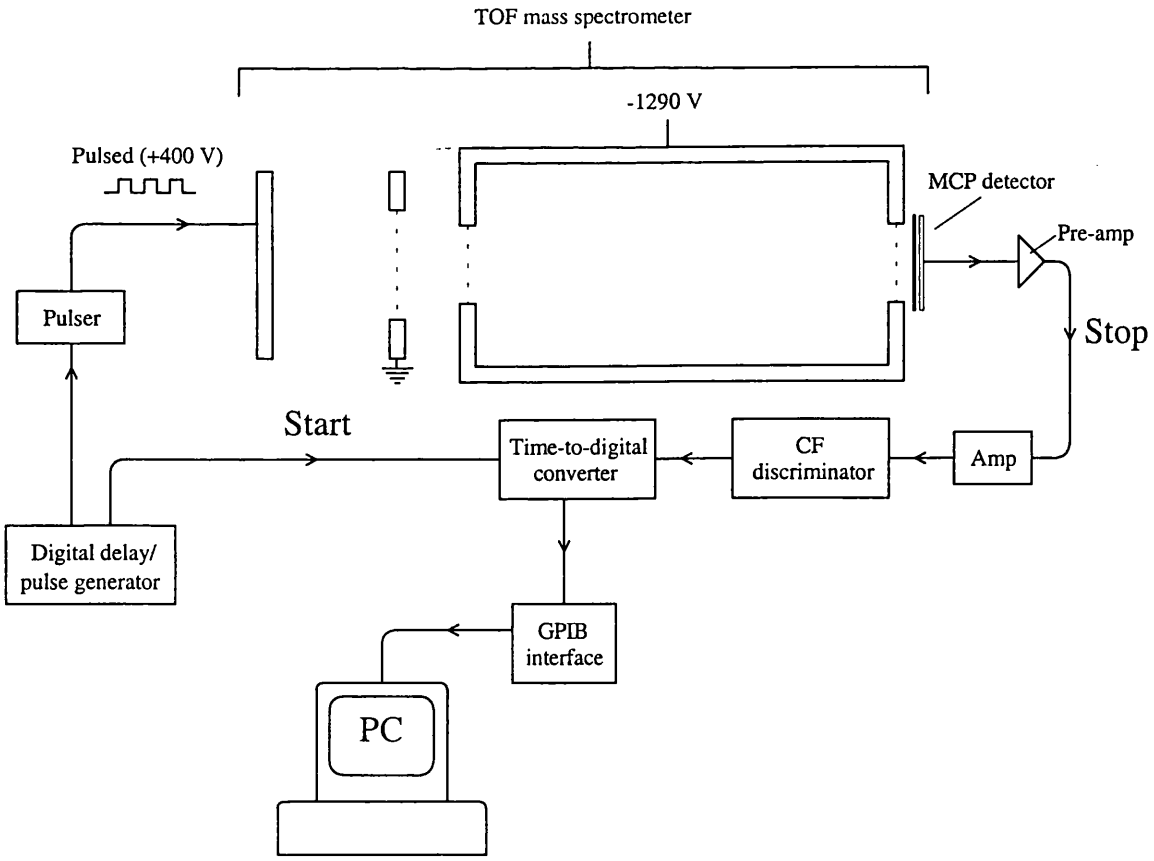

Figure 2.6 Schematic diagram of the timing components of the TOFMS.

2.3.5 Recording the mass spectrum

The target gas pressure is rigidly maintained at a constant value, typically 4×10^{-6} Torr during the recording of a mass spectrum. This pressure is low enough to eliminate the possibility of forming an excessive number of product ions which could cause potential problems by saturating the sensitive ion detector. In addition, this pressure is sufficiently low to guard against the possibility of multiple collisions [24] inside the source region of the spectrometer. A multiple collision may be defined as the situation when an ion experiences two or more collision events in the time between it entering the TOF source region and reaching the ion detector. Multiple collision processes would unnecessarily complicate the identification of the reaction channel leading to the formation of a given product ion, as the same product ion could be formed in two or more different reaction processes. The conditions required to eliminate the possibility of multiple collisions are described fully in Appendix 3 [24]. These conditions are carefully tested to ensure that multiple collisions are not occurring by measuring the product ion intensity as a function of the target gas pressure. A linear relationship, such as that shown in Figure 2.7, confirms the presence of single collision conditions.

Time-of-flight mass spectra are recorded for typically 10^6 data acquisition cycles to identify and adequately quantify the product ions formed in the reactions between the reactant dications and neutral molecules. The precise number of data acquisition cycles required to generate a statistically viable mass spectrum is dependent upon the collision energy, the intensity of the beam of reactant dications and the cross-section of the reaction process for a given collision system of interest. Additionally, as described in the next Chapter, background mass spectra are also taken in the absence of the neutral collision partner. These background spectra are used to correct the product ion mass spectra for background ion contributions. A representative background time-of-flight mass spectrum is shown in Figure 2.8. As can be seen from the mass spectrum of the CF_2^{2+} reactant dication in Figure 2.8, the experimental apparatus produces a highly pure beam (~ 99 %) of the reactant ion, with the intensity of ions other than the reactant species being at low background levels.

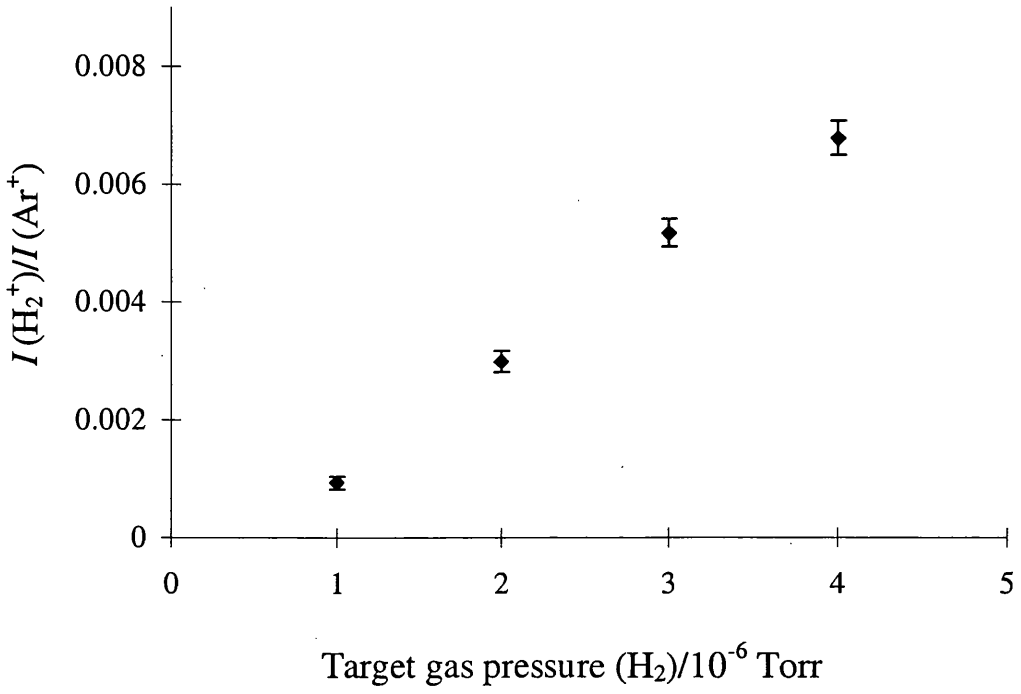

Figure 2.7 Graph of the relative product ion (H^+) intensity produced following collisions between Ar^+ and H_2 as a function of the target gas pressure. The linear relationship observed is indicative of single collision conditions.

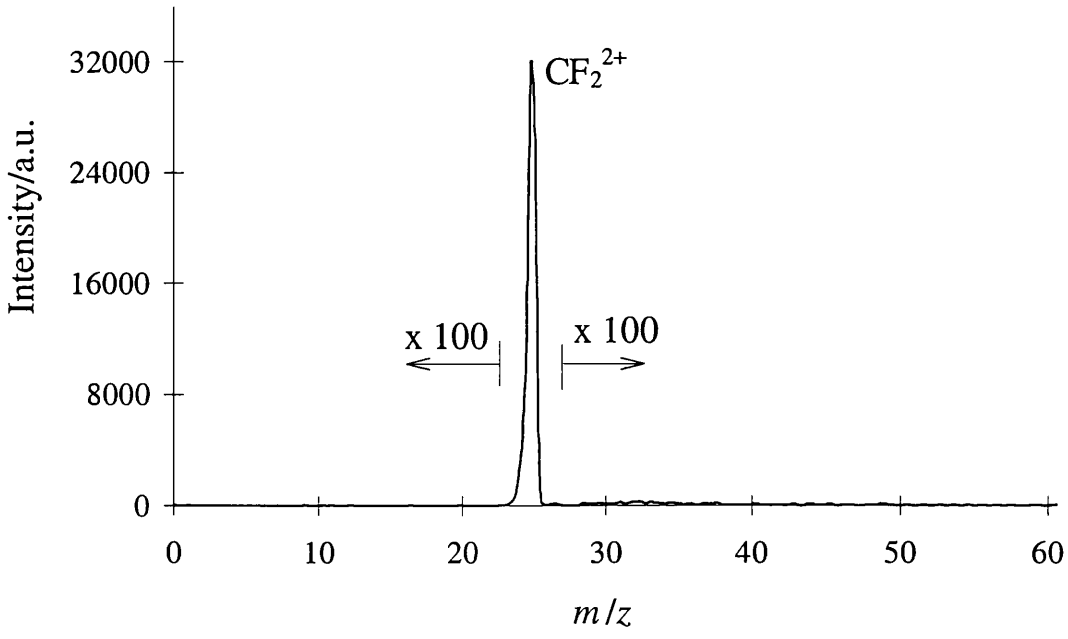

Figure 2.8 Representative background time-of-flight mass spectrum of a CF_2^{2+} molecular dication beam.

2.4 Operational parameters

Typical settings of the operating parameters used in the running of the experimental apparatus are listed in the tables below.

Table 2.1a Miscellaneous operating parameters.

Parameter	Typical setting
Laboratory frame collision energy	3-13 eV
Repeller plate pulsing frequency	330 Hz
Typical number of ions per pulse	0.71
Typical dication current	50 pA
CF_4 precursor gas pressure	4×10^{-6} Torr
Neutral target gas pressure (NH_3)	4×10^{-6} Torr

Table 2.1b Typical spectrometer operating electrical parameters.

Parameter	Typical setting
Repeller plate voltage	0 to + 400 V
Drift tube potential (TOF deflectors/Einzel lens)	-1230 V
MCP detector front plate voltage	-2050 V
MCP detector back plate voltage	40 V
Sandwich Grid potential	5 V
Extraction Electrode potential	-7 V
Accelerating potential	250 V
Filament voltage	150 V
Velocity filter electric field potential	~50 V
Filament shield potential	-25.3V
Ion lens potential	-25.2V
Vertical deflector plate potential	~0.1 V
Electromagnet voltage	~13 V
Electromagnet current	2.1 A
Decelerator element potential	0 to -150 V

2.5 Conclusion

A new spectrometer has been developed to investigate the reactivity of molecular dications with neutral species. The spectrometer consists of an ion gun coupled to a TOF mass spectrometer, incorporating a number of special features enabling the apparatus to be used with short-lived species.

References

1 K. A. Newson and S. D. Price, *Chem. Phys. Letters*, **269** (1997) 93.

2 C. Y. Ng, T. Baer and I. Powis, *Unimolecular and Bimolecular Ion-Molecule Reaction Dynamics*, John Wiley and sons Ltd, Inc. New York 1994

3 T. Baer and C. Y. Ng, *State Selected and State-to-State Ion-Molecule Reaction Dynamics Part 2 (Theory)* John Wiley and sons Ltd, Inc. New York 1992

4 R. D. Levine and R. B. Bernstein, *Molecular Reaction Dynamics and Chemical Reactivity* Oxford University Press, Inc. New York 1987.

5 S. D. Price, *J. Chem. Soc., Faraday Trans.*, **93** (1997) 2451.

6 M. Manning, S. D. Price and S. R. Leone, *J. Chem. Phys.*, **99** (11) (1993) 8695.

7 S. D. Price, S. A. Rogers and S. R. Leone, *J. Chem. Phys.*, **98** (12) (1993) 9455.

8 S. D. Price, M. Manning and S. R. Leone, *J. Am. Chem. Soc.*, **116** (1994) 8673.

9 S. A. Rogers, S. D. Price and S. R. Leone, *J.Chem. Phys.*, **98** (1) (1993) 280.

10 S. D. Price, M. Manning and S. R. Leone, *Chem. Phys. Letters*, **214** (1993) 553.

11 W. C. Wiley and I. H. McLaren, *Rev Scientific instruments*, **26** (1955) 1150.

12 K. A. Newson, S. Luc, N. J. Mason and S. D. Price, *Int. J. Mass Spectrom. And Ion Processes*,. **148** (1995) 203.

13 R. B. Opsal, K. G. Owens and J. P. Reilly, *Analytical Chem.*, **57** (1985) 1884.

14 R. D. Macfarlane, *Analytical Chem.*, **55** (1983) 1247A.

15 D. A. Dahl, J. E. Delmore and A. D. Appelhans, *Rev Sci inst.*, **61** (1990) 607.

16 L. Wahlin, *Nuc Instrom. and Methods.*, **27** (1964) 55.

17 W. Wien, *Ann. Physik.*, **65** (1898) 440.

18 M. L. Oliphant, E. S. Shire and B. M. Crowther, *Proc. Royal Soc. (London)*, **A146** (1934) 922.

19 O. Klemperer and M. E. Barnet, *Electron Optics*. Cambridge. Cambridge University Press (1971).

20 M. Szilagyi, *Electron Optics*. Plenum, New York (1988).

21 A. R. Kip, *Fundamentals of Electricity and Magnetism*. Singapore. McGraw-Hill (1969).

22 K. A. Newson and S. D. Price, *J. Chem. Soc., Faraday Trans.*, in press.

23 K. A. Newson and S. D. Price, *Chem. Phys. Letters*, in press.

24 K. Yamasaki and S. R. Leone, *J. Chem. Phys.*, **90** (1989) 964.

Chapter 3

Data analysis

The experimental methodology employed in the investigation of the gas-phase reactivity of doubly-charged molecular ions involves recording time-of-flight mass spectra of the products formed following collisions between molecular dications and neutral collision partners. The previous Chapter contained a description of the experimental apparatus. This Chapter deals with the collection and analysis of the experimental data.

3.1 The time-of-flight mass spectrum

As stated in the previous Chapter, the computer receives the experimental data, which consists of flight times of the detected ions, via the GPIB interface and processes this data to generate mass spectra. The heart of the data analysis software involves an array of 500 time channels for a given range of ion flight times [1-3]. Typically, the times-of-flight of the ions measured in these experiments would be between 2 and 6 μs. Hence, for such a range of flight times, the width of each of the 500 channels in the data array is 8 ns. The first time channel contains counts for those ions having flight times between 2000 and 2008 ns, the second channel contains those ions with flight times between 2009 and 2016 ns and so on up till the 500th channel, which contains counts for those ions having flight times between 5993 and 6000 ns.

The computer assigns each of the counts to a time channel, building up a histogram of ion flight times. The number of counts in each channel is representative of the intensity of the detected signal of the ion having a flight time within the range of that particular channel. The total array of all 500 of the channels is, hence, the complete TOF mass spectrum. The minimum and maximum times of the array of time channels are variable parameters, set according to the particular collision system under investigation; this allows the various product ions to be represented in a mass spectrum of any desired mass range.

3.2 Data extraction and analysis

3.2.1 Analysis of the mass spectra

The arrangement described above, involving a histogram of time channels to represent the mass spectrum, is a distinct advantage for analysis, as the values of the ion intensities are obtained by simply summing the counts for each of the channels making up a peak. This avoids using considerably more complicated analytical methods such as the numerical integration of a trace of the ion peaks on an oscilloscope [4]. The TOF mass spectra are calibrated using the flight times for simple ions, for example Ar^+ and Ar^{2+}, using the equation:

$$\tau_{tof} = k\sqrt{m} + c \qquad (3.1)$$

If the times-of-flight of two ions of known mass are obtained, then k and c may be calculated by solving Equation 3.1 simultaneously. Hence, having obtained k and c, the time-of-flight of any ion of mass m can be calculated by using the above equation. Note that the parameter k depends solely on the various voltages applied to set up the electric fields inside the spectrometer. Therefore, if these spectrometer voltage settings are held constant then the masses of ions formed in any collision system may be calculated without the need for repeated calibration. The c constant is a mass-independent timing constant that is required due to the 'dead time' in the duty cycle of the time-of-flight electronics.

The time channels can, by using the above method, be converted to channels of mass. Hence, the intensity of a particular ion can be found by summing the number of counts of each of the channels making up the ion peak. The computer software allows the intensities of the ion peaks to be rapidly obtained as the analysis program contains a function that sums up the counts in all the channels within a selected minimum and maximum mass or channel value.

3.2.2 Background correction methodology

In addition to mass spectra of the product ions formed as a result of collisions between the reactant dications and neutral target molecules, background spectra are also recorded. These background spectra are recorded in exactly the same manner as the product-ion mass spectra, the only difference being that no neutral target molecules are introduced into the apparatus [5]. A 'background' ion is an ion recorded in the absence of a target gas. When a spectrum is recorded in the presence of a target gas, such background ion signals may artificially enhance the experimental product ion intensities. The dominant source of the background ions is the dication beam itself, which although of high purity (> 99 % in most cases), will still contain a number of contaminant ions that have managed to traverse the velocity filter. Another possible source of background ions is singly-charged ions formed as a direct result of the unimolecular decay [6-8] of the dicationic species making up the reactant ion beam. For example:

$$CF_2^{2+} \rightarrow CF^+ + F^+ \qquad (3.2)$$

Additionally, background ions may also be formed following collisions between the reactant dications and residual gas molecules in the spectrometer. For example:

$$CF_2^{2+} + N_2 \rightarrow CF_2^+ + N_2^+ \qquad (3.3)$$

In certain cases where the reaction cross-section is low, for example in the case of some bond-forming reactions [3,9-12], the background contribution to the product ion peaks may be significant. Hence, the precise determination of the true yields of the product ions demands an

accurate evaluation of the background ion contribution. To correct the product ion mass spectra for these background ion signals, several mass spectra are recorded, both with and without the neutral target gas. The true product ion intensities I_{real} are then obtained by subtracting the background ion signal I_{bg} from the raw product ion intensity I_{raw} which, unlike the background ion intensity, is obtained from the mass spectra recorded in the presence of the neutral target gas. The background ion signal is normalized by the ratio of the intensities of the unreacted dications I_{dic}:

$$I_{real} = I_{raw} - I_{bg}\left(\frac{I_{dic}(rxn)}{I_{dic}(bg)}\right) \tag{3.4}$$

3.2.3 Product ion detection efficiency

If a reaction occurs during the collision between the reactant dication and the neutral collision partner, the dynamics of the reaction process may result in a substantial release of kinetic energy. Such large releases of kinetic energy are common to many reaction processes involving molecular dications, due to the presence of the double charge. An example of such a reaction is given in Equation 3.5. The kinetic energy is released because of the Coulombic repulsion between the pair of singly-charged ions formed in the reaction. This kinetic energy is released in the centre-of-mass frame and affects the product ions translational energy component in the laboratory frame [3].

$$CF_2^{2+} + Ar \rightarrow CF_2^{+} + Ar^{+} \tag{3.5}$$

Each reaction channel may have a different average kinetic energy release (KER) together with a different distribution of the kinetic energy releases [12]. Hence, the product ions may, by virtue of their different masses and total kinetic energies, have different transverse velocities across the source region of the mass spectrometer. Thus, as can be seen from figures 3.1 and 3.2, owing to these different velocities, the product ions may travel different transverse distances as they pass down the length of the mass spectrometer to reach the multichannel plate (MCP) detector. Those ions with larger transverse kinetic energies in the laboratory frame will be faster, and therefore travel a greater distance away from the central axis of the spectrometer (following trajectory A) than the less energetic ions which would follow trajectory B. Due to this effect, the length L of the source region of the TOF mass spectrometer which is imaged onto the MCP detector, varies with the total kinetic energy of the product ions as shown in Table 3.1. In addition, a schematic of the TOFMS source region in Figure 3.2 shows the product ion trajectory range which gives rise to the differential imaging of the flux on to the ion detector.

The product ion flux is proportional to the cross-section of the reaction process leading to the formation of that particular product ion. Hence, the ratio of the cross-sections σ of two reaction processes A and B would be given by the ratio of the fluxes F of the ions across the same region.

$$\frac{\sigma_A}{\sigma_B} = \frac{F_A}{F_B} \tag{3.6}$$

However, as mentioned above, all the ions, both the unreacted dications and product ions formed in the TOF mass spectrometer, will posses a component of velocity perpendicular to the longitudinal axis of the TOF spectrometer. The origin of this 'transverse velocity' component lies in the fact that the reactant dications are delivered to the TOF mass spectrometers source region, via the ion gun, in a direction perpendicular to the longitudinal axis of the TOF mass spectrometer. In addition to this intrinsic component of transverse velocity, the reaction processes are highly energetic, therefore the product ions may, as a result of reactive scattering, have enhanced transverse velocity components.

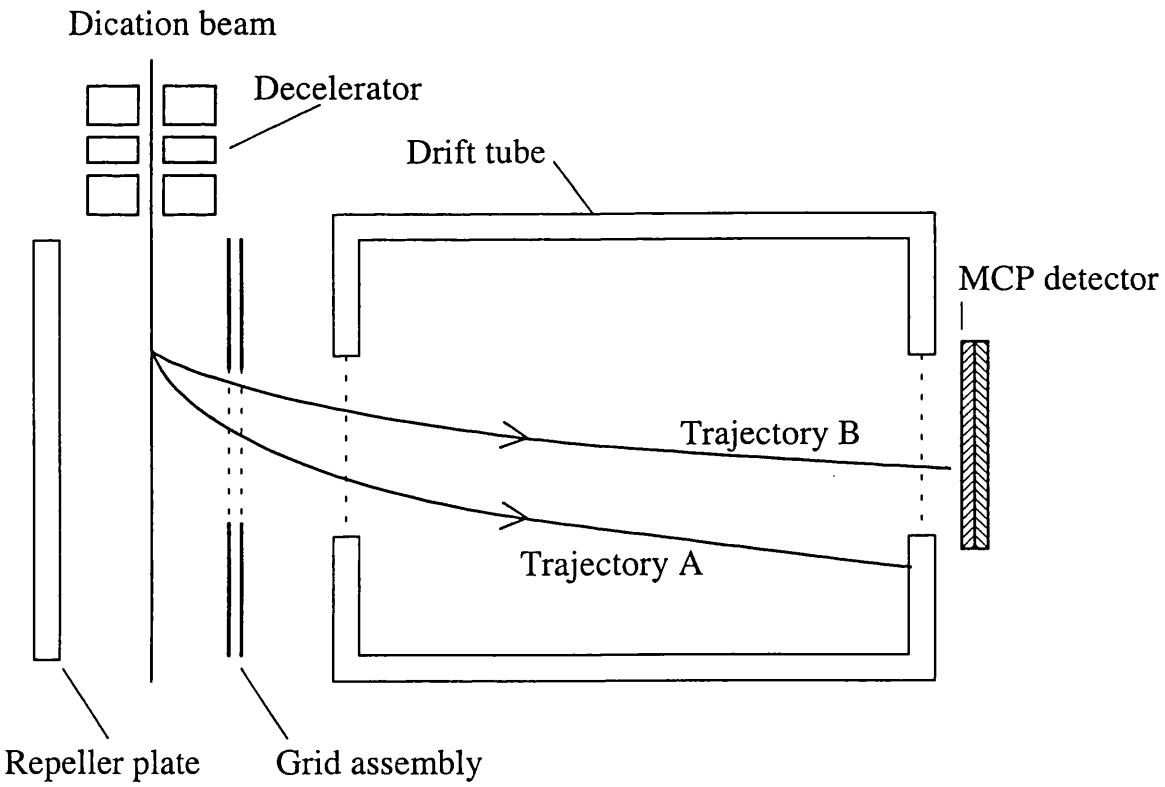

Figure 3.1 Schematic diagram of the TOFMS showing the trajectories of product ions formed at the same point in the ion source. In the diagram trajectory **A** represents the path taken by an ion formed in a reactive encounter in which there is a large kinetic energy release, whilst trajectory **B** represents the analogous case where the kinetic energy release is significantly smaller .

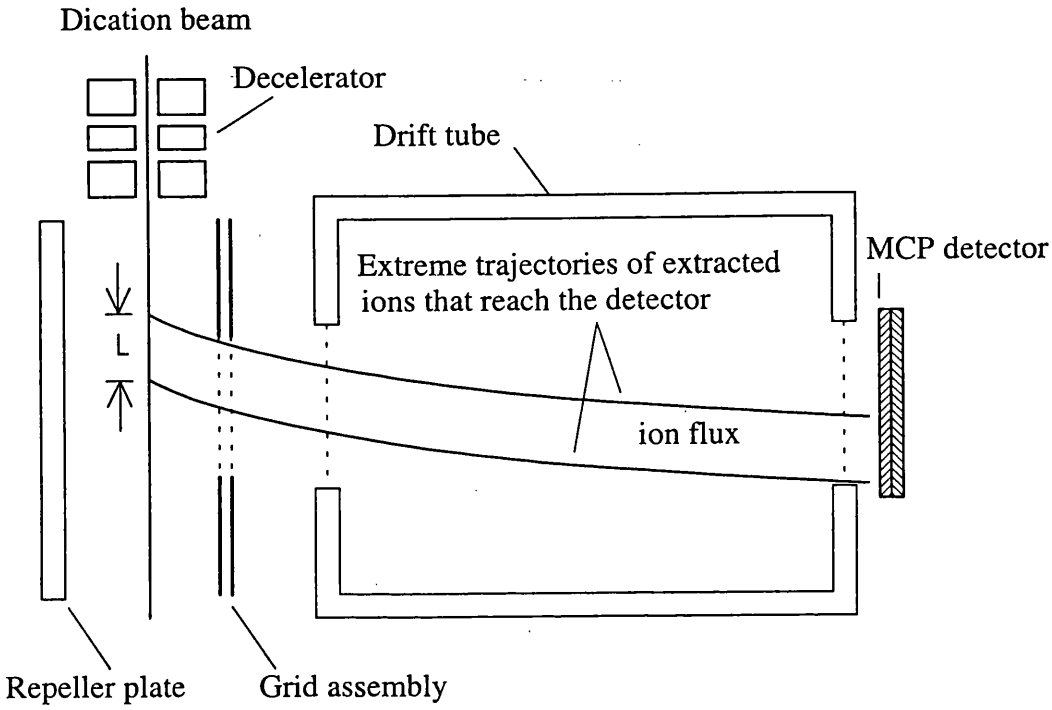

Figure 3.2 Schematic diagram of the TOFMS showing the distance '*L*' between the extreme trajectories reaching the front plate of the ion detector.

As a result of the ions having a component of transverse velocity, some of the ion flux may not reach the ion detector. This can be viewed as a reduction in the efficiency with which an ion is detected. That is, those ions with relatively high transverse velocity components will have a greater chance of failing to reach the detector than those ions that have relatively low transverse velocity components. In practice, to correct the detected ion signals (intensities) for the effects of the transverse velocity upon the ion's detection efficiency it is necessary to consider the ion's mass, its time-of-flight and, in the case of a product ion, the distribution of the kinetic energy released on reaction.

To make allowance for the KER affecting the detection efficiency, the reaction dynamics of the collision system is assumed to be dominated by forward-scattering of the product ions. This assumption is based on the results of the only angularly resolved investigation of dication reactivity [12]. The results of which indicate that forward-scattering is the dominant mechanism of bond forming and electron-transfer reactions for dication-neutral collision systems.

The intensity I of an ion signal reaching the detector is proportional to the ion density n in a volume V of the interaction region that is imaged onto the ion detector in the TOFMS:

$$I = nVj \tag{3.7}$$

where j is a mass-independent ion detection efficiency and is an intrinsic property of the ion detector and timing electronics. The flux F of a product ion is related to its velocity v across the ion source region and the ion density n :

$$F = nv \tag{3.8}$$

By considering Equations 3.8 and 3.9 it is possible to obtain an expression for the relationship between the ion flux and the detected ion intensity:

$$F = \frac{Iv}{Vj} \tag{3.9}$$

The volume V of the interaction/source region imaged onto the ion detector may be expressed in terms of its cross-sectional area A and length L giving:

$$F = \frac{Iv}{ALj} \tag{3.10}$$

The cross-sectional area of the volume imaged onto the detector depends upon the internal bore of the decelerator assembly and its focusing characteristics. Hence, the cross-sectional area A is constant for any reaction process, and for two such processes, denoted A and B, the relative ion fluxes are given by:

$$\frac{F_A}{F_B} = \frac{I_A}{I_B}\frac{v_A}{v_B}\frac{L_B}{L_A} \tag{3.11}$$

The relative cross-sections for the reaction processes are proportional to the relative product ion fluxes. Therefore, the relative cross-sections for reaction processes A and B can be determined from the mass spectrometric product ion intensities by:

$$\frac{\sigma_A}{\sigma_B} = \frac{I_A}{I_B}\frac{v_A}{v_B}\frac{L_B}{L_A} \tag{3.12}$$

In the above correction L is the effective length of the source region of the TOFMS that is imaged on to the ion detector, shown schematically in Figure 3.2. The length L is dependent upon the internal geometry of the spectrometer, the transverse velocity v of the product ion and the ion's time-of-flight. The value of v is given by the centre-of-mass velocity (collision energy) and the energy imparted to the ion in the reaction process [3]. Representative values of v and L at various laboratory frame collision energies E_{lab}, for the CF_2^+ product ion formed in the reaction between CF_2^{2+} and NH_3 [13], are given in Table 3.1. The value of the kinetic energy released (KER) in the centre-of-mass frame to the products of the bond-forming reaction between CF_2^{2+} and NH_3, used in calculating the values listed in Table 3.1, is 6.5 eV [12].

The analysis procedure detailed above, provides a reliable and versatile means of accurately determining the relative intensities of the charged products of reactions between molecular dications and neutral species. It is certainly pleasing to note that the relative intensities for ions generated in bond-forming and electron-transfer reactions between CF_2^{2+} and D_2, that were

obtained using the apparatus and methodology described above, are, within experimental error, the same as those obtained by another research group which employed a different experimental technique [12].

Table 3.1 Representative values of v and L at given laboratory frame collision energies E_{lab} for the $HNCF^+$ product ion formed in the reaction between CF_2^{2+} and NH_3. The value of the kinetic energy release (KER) used in the calculation of v is 6.5 eV.

E_{lab}/eV	v/m s^{-1}	L/mm
10.0	5268.66	12.61
9.0	5030.81	13.53
8.0	4779.33	14.50
7.0	4511.57	15.54
6.0	4223.91	16.65
5.0	3911.09	17.86
4.0	3565.07	19.20

3.3 Conclusions

A data analysis methodology for the calculation of relative cross-sections of reaction processes based upon measurements of product ion intensities has been developed. The analysis procedure corrects the observed ion intensities for background ion contributions and differences in the ionic detection efficiency, and provides an accurate, reliable and uncomplicated means of obtaining product ion intensities.

References

1 K. A. Newson, S. Luc, N. J. Mason and S. D. Price, *Int. J. Mass Spectrom. And Ion Proc.*, **148** (1995) 203.

2 K. A. Newson and S. D. Price, *Int. J. Mass Spectrom. and Ion Proc.*, **153** (1996) 151.

3 K. A. Newson and S. D. Price, *Chem. Phys. letters,* **269** (1997) 93.

4 W. C. Wiley and I. H. McLaren, *Rev Scientific instruments.*, **26** (1955) 1150.

5 S. A. Rogers, S. D. Price and S. R. Leone, *J.Chem. Phys.*, **98** (1) (1993) 280.

6 C. Y. Ng, T. Baer and I. Powis, *Unimolecular and Bimolecular Ion-Molecule Reaction Dynamics*, 1994 John Wiley and sons Ltd, Inc.

7 T. Baer and C. Y. Ng, *State Selected and State-to-State Ion-Molecule Reaction Dynamics Part 2 (Theory),* 1992 John Wiley and sons Ltd, Inc.

8 R. D. Levine and R. B. Bernstein, *Molecular Reaction Dynamics and Chemical Reactivity* 1987 Oxford University Press, Inc.

9 S. D. Price, M. Manning and S. R. Leone, *J. Am. Chem. Soc.*, **116** (1994) 8673.

10 S. D. Price, *J. Chem. Soc., Faraday Trans.*, **93** (1997) 2451.

11 K. A. Newson and S. D. Price, *Chem. Phys. Letters*, in press.

12 Z. Dolejsek, M. Farnik and Z. Herman, *Chem. Phys. Letters*, **235** (1995) 99.

13 K. A. Newson and S. D. Price, *J. Chem. Soc., Faraday Trans.*, in press.

Chapter 4

Ion-neutral reactivity and reaction dynamics: a theoretical perspective

4.1 Introduction

Theoretical investigations of the chemical and physical properties of gas-phase molecular dications play a vital role in the attempt to rationalize the behaviour of these reactive species. Clearly, a comprehensive understanding of the relevant areas of the theory of reaction dynamics is also a necessary prerequisite to establishing a thorough explanation of the collisional behaviour exhibited by dicationic species. The theoretical studies of molecular dicationic behaviour performed to date have concentrated mainly upon the properties of the isolated species. These studies cover such topics as the ionization cross-sections for forming dications [1,2], the potential energy surfaces of dications [3-8] and the influence the potential energy surfaces have in determining the stability and lifetimes of the dicationic species [9-11].

In contrast, the theory underpinning the reactive processes that may occur following the collision of a molecular dication with neutral target species have received limited attention. A theoretical model of the bimolecular electron-transfer reactivity of molecular dications with neutral targets [12-16] has been attempted with some success, using an adaptation of the Landau-Zener theory of electron transfer between singly-charged atomic ions and neutrals [17,18]. However, the bond-forming (chemical) reactivity occurring in certain molecular dication/neutral collision systems at low laboratory frame collision energies (<13 eV) has not, to date, received significant attention from theoreticians. An attempt to model the mechanism of bond forming reactions, based on the principles of the Landau-Zener theory, has been attempted. However, the applicability of this non-chemical model of the bond-forming reactivity of molecular dications will be shown in this thesis to be inappropriate [19].

This Chapter examines aspects of the theory relating to gas-phase ionic reactivity that are of primary importance to understanding the experimental work presented in this thesis and explaining the subsequent results. Specifically, a discussion of the Landau-Zener theory of electron-transfer and its offshoot, the reaction window theory, is presented. As will become clear, the Landau-Zener theory is not only a valuable tool with which to gauge the likelihood of electron-transfer, it can also be used to accurately determine the precise channels of dissociative electron-transfer.

The bulk of the experimental work contained in this thesis concerns the measurement of product ion intensities, from which relative cross-sections are calculated. However, the ability to interpret the results and draw the necessary conclusions requires a thorough understanding of the theory appertaining to ion chemistry, including such subjects as collision kinematics and reaction

dynamics. Therefore, these subjects will also be considered from a theoretical perspective. Finally, the interpretation of isotope effects in ion-molecule reactions involving molecular dications will be examined. Such isotope effects are used in this work as a probe of the reaction dynamics.

4.2 Reaction window theory and the Landau-Zener model

The Landau-Zener model (LZ) [17,18] is a semi-classical picture of electron transfer reactivity for purely atomic collision systems. The model determines the probability of charge transfer between given reactant and product electronic states. The LZ model considers the reaction as occurring at the crossing (R_c) of two diabatic potential curves corresponding to the reactants and products. Such a crossing is illustrated in Figure 4.1 below.

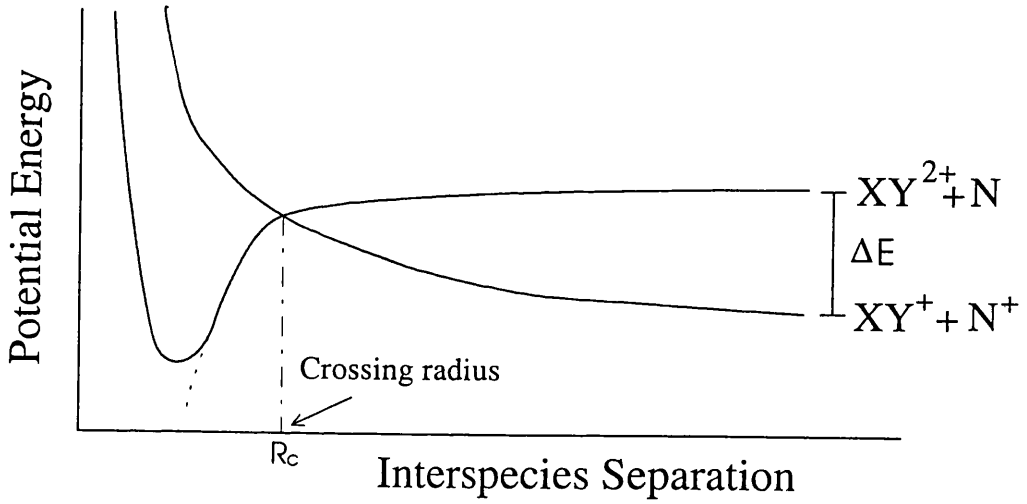

Figure 4.1 The crossing of product and reactant potential energy curves for a dication-neutral electron-transfer reaction.

For an electron-transfer reaction the curve crossing may occur either on the incoming or outgoing trajectories. Hence the total probability P for electron transfer is given by:

$$P = 2\delta(1-\delta) \tag{4.1}$$

where δ is the probability of remaining on the diabatic curve on one pass through the avoided crossing. Hence, the quantity δ is a measure of the coupling between the product and reactant potential curves and is a function of $|V_1' - V_2'|$ which is the magnitude of the difference in the gradients of the two potential energy curves at the crossing radius (R_c), the relative radial velocity υ_b and the electronic coupling matrix H_{12} between the product and reactant electronic states. Explicitly, δ is given by:

$$\delta = \exp\left(\frac{-\pi|H_{12}|^2}{2\hbar|V_1' - V_2'|\upsilon_b}\right) \tag{4.2}$$

In the case of the pseudo Landau-Zener theory, which models the charge transfer between a molecular dication and a neutral target, the approximate potential energy curves are modelled using simple standard electrostatic equations:

$$V_1 = -\frac{z^2 e^2 \alpha}{2R^4} + \Delta E \tag{4.3}$$

$$V_2 = \frac{e^2}{R} \tag{4.4}$$

In the above, the potential of the reactant channel V_1 is given as the sum of the reaction exothermicity (ΔE) and a standard polarization attraction function that is determined from the polarizability (α) of the neutral target species. This simple model of reactant potential makes no allowance for the repulsive wall encountered at very small values of R. This is not a major approximation as the repulsion is only significant at very small interspecies separations, and may therefore be ignored over the range of interspecies separations where the reactant and product curves intersect. The potential V_2 of the electron-transfer product channel is modelled as being purely repulsive, due to Coulombic repulsion between the singly-charged product ions.

The curve crossing radius R_c is obtained by equating the reactant and product potentials V_1 and V_2 (Equations 4.3 and 4.4) and solving the equation for R. Differentiation of V_1 and V_2 at $R = R_c$ allows the value of $\left|V_1' - V_2'\right|$ to be calculated. The relative radial velocity υ_b may be calculated from the impact parameter b, the initial velocity of the reactants and the energy gained by the collision partners as a result of the polarization attraction as the separation between the two reactants approaches R_c. The calculation of the electronic coupling matrix elements H_{12} requires precise details of the electronic wave functions of the collision system at $R = R_c$. However, several empirical functions [20-22] have been proposed for the calculation of H_{12} for the general charge-transfer reaction between a dicationic species and a neutral:

$$A^{2+} + B \rightarrow A^{+} + B^{+} \tag{4.5}$$

In all cases, the empirical functions are dependent on the crossing radius R_c, predicting that $\left|H_{12}\right|^2$ decreases exponentially with R_c. The functions are also dependent upon the ionization potential of B, I_B, and the ionization potential of A^+ from its product electronic state to the reactant state A^{2+}, I_A. One particular function given by Olsen *et al* [22] has been extensively used to estimate H_{12}. This function gives the electronic coupling matrix element as:

$$\left|H_{12}\right|^2 = \left(I_A I_B\right)\left(R_c^*\right)^2 \exp\left(-1.72 R_c^*\right) \tag{4.6}$$

where:

$$R_c^* = \left(\frac{\sqrt{I_A} + \sqrt{I_B}}{\sqrt{2}}\right) R_c \tag{4.7}$$

According to the LZ model, crossings between the reactant and product channels at interspecies separations greater than ~ 0.6 nm are strongly diabatic ($\delta \rightarrow 1$) due to the great distance over which the electron must quantum mechanically tunnel from the neutral to the dication. Hence the probability of electron transfer is small. For crossings at radii less than ~0.2 nm the character of the crossing becomes significantly adiabatic ($\delta \rightarrow 0$). As a result of this adiabaticity, the interaction between the product and reactant channels is large and so the probability of the electron being transferred on a single pass through the crossing radius is high. However, the reactants make two passes through the crossing radius. That is, once as the reactants approach and then again as the reactants depart from each other. Hence, those species having crossed over to the product potential curve will cross back to the reactant potential curve, with the overall result being no net electron-transfer. For crossings in the so-called reaction window at between $R \approx 0.2$ and 0.6 nm, the value of δ lies between 0 and 1 and at the point corresponding to $\delta = 0.5$, it may be shown, using Equation 4.1, that the reaction probability P, reaches its maximum value of 0.5.

The above algorithm has been used to qualitatively model electron-transfer reactions. If the reactant and product curves cross within a range of interspecies separations between 0.2 and 0.6 nm, that is inside the reaction window, then the probability of entering on the reactant potential and leaving on the product potential is relatively high. Hence, the reaction probability will also be high. For a given collision system there may be many possible reaction channels each having its own value of exothermicity, which may be defined as the difference in the asymptotic energies of the product and reactant potentials. Representative values of reaction exothermicity are listed in Table 4.1 for the CF_2^{2+}/rare gas collision system. As can be seen from Equations 4.3 and 4.4, the form of the reactant and product potentials, for any dication-neutral collision system, are almost identical, differing only in the value of the reaction exothermicity and the polarizability of the neutral collision partner α. However, the polarizabilty has relatively little influence on the position of the crossing radius R_c in comparison with the exothermicity. Hence, for a given collision system, it is largely the exothermicity that determines R_c. Consequently there exists a window of reaction exothermicities of approximate range (2-7 eV) over which electron-transfer is favourable. As can be seen from Figure 4.2, if the exothermicity is small, then the curves will cross at large values of the interspecies separation, outside the reaction window. Conversely, if the exothermicity is large then the curves will cross at too small a value of the interspecies separation, also outside the reaction window. Therefore, the Landau-Zener model can be used as a qualitative tool to predict the feasibility of electron-transfer given just the reaction exothermicity.

The applicability of this model has been confirmed by analysis of the electron-transfer reactions between molecular dications and rare gas collision partners [12-16]. Here the electron-transfer

reactions with the lighter rare gases (He and Ne) are not favoured because the reactions are either endothermic or barely exothermic. However, electron-transfer reactions are observed with the heavier rare gas targets (Ar, Kr and Xe) which have larger reaction exothermicities, that lie within the reaction window.

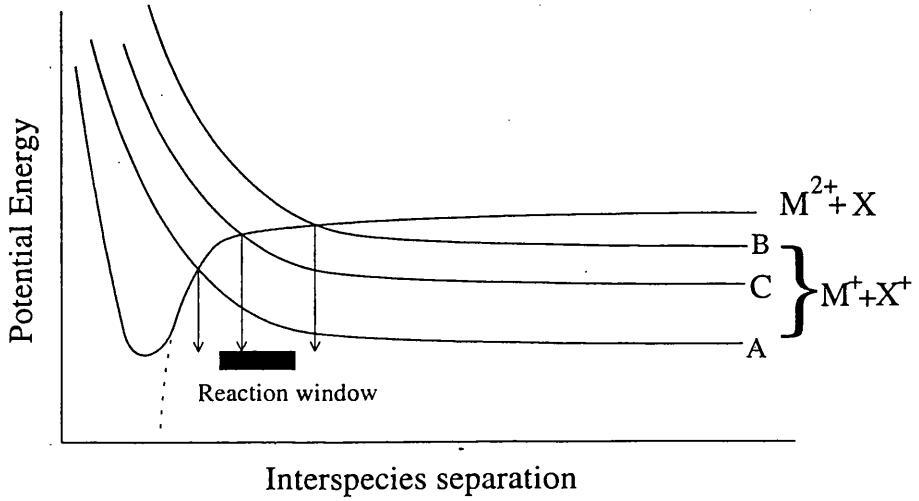

Figure 4.2 Representative potential curve crossings of product and reactant curves for the electron-transfer reaction between a dication and a neutral species. The three product curves correspond to: **A** large reaction exothermicity, **B** small reaction exothermicity, and **C** optimum reaction exothermicity.

An additional feature of this application of the reaction window theory is its ability to predict whether an electron-transfer reaction will be dissociative or non-dissociative. As mentioned above, the exothermicity of an electron-transfer reaction determines the feasibility of the reaction. However, a collision system may have many channels of electron-transfer reactivity, such as those in Table 4.1, with each channel having a particular value of exothermicity. Therefore, given the window of exothermicities, the electron-transfer reactivity of any dication-neutral collision system can be rationalized using the above approach.

Consider the electron-transfer reactivity between a prototypical molecular dication XY^{2+} and neutral target Rg. As illustrated in Figure 4.3, two general channels of electron-transfer are possible. Firstly, a non-dissociative channel leading to the formation of XY^{+}, and secondly a dissociative channel that results in the formation of the molecular monocation in an excited state XY^{+*} that dissociates to give $X^{+}+Y$. Note in both cases, the other product is the ionised collision partner Rg^{+}. In this general example, the exothermicity of the non-dissociative electron-transfer reaction is relatively large compared to that of the dissociative process. Hence, as shown in Figure 4.3, the reactant and (non-dissociative) product potential curves cross at values of R_c smaller than the reaction window minimum, whilst the crossing radius of the reactant and the less exothermic dissociative product potential curves lies within the reaction window. Thus, in this particular case population of the XY^{+*} state through the dissociative channel is predicted, whilst the non-dissociative channel is disfavoured.

The Landau-Zener model has been successfully used to predict electron-transfer reactivity in molecular dication-neutral collision systems [12-16]. For example, consider the electron-transfer reactivity of CF^{2+} with rare gas collision partners [12]. As can be seen from Table 4.1, the exothermicities of the relevant electron-transfer reactions increase with the mass of the rare gas target, this arises because the ionization potential of the rare-gas neutral decreases with increasing mass. Table 4.1 also reveals that the exothermicities of the dissociative electron-transfer reaction are lower than the corresponding non-dissociative process. Hence, as the exothermicities of the channels of electron-transfer for a given collision system are distinct, the imposition of a window of reaction exothermicities provides a means of predicting the likely channel of electron-transfer reaction. For example, in the case of the CF^{2+}-He collision system, the electron-transfer processes are either endothermic or barely exothermic. Consequently, electron-transfer is not expected to be a major reactive pathway for this system. In contrast, non-dissociative electron-transfer reactivity is expected in the CF^{2+}-Ne collision system, as the exothermicity of 5 eV lies inside the window of exothermicities, whilst the dissociative electron-transfer channels are endothermic, and therefore disfavoured.

For the remaining CF^{2+}-Ar, Kr, and Xe collision systems the exothermicity of non-dissociative electron-transfer increases to the point where it is outside the window of exothermicities, whilst the exothermicity of dissociative electron-transfer is now inside the window. Consequently, as the mass of the rare gas target increases from Ar through to Xe, the nature of the electron-transfer reactivity is predicted to favour the dissociative process at the expense of the non-dissociative channel. It is reassuring to note that the above predictions are in excellent agreement with experimental observations [12]. Thus, the Landau-Zener model is a powerful predictive tool of electron-transfer in molecular dication-neutral atomic collision systems.

Table 4.1 Electron-transfer exothermicities (shown as positive eV) for the reaction of groundstate CF^{2+} with rare gas targets.

	Electron-transfer products[a]		
Rare gas	CF^+	$C^+ + F$	$F^+ + C$
He	2.0	-5.3	-11.4
Ne	5.0	-2.3	-8.4
Ar	10.8	3.5	-2.6
Kr	12.6	5.3	-0.8
Xe	14.5	7.2	1.1

[a]The other product is the corresponding rare gas ion

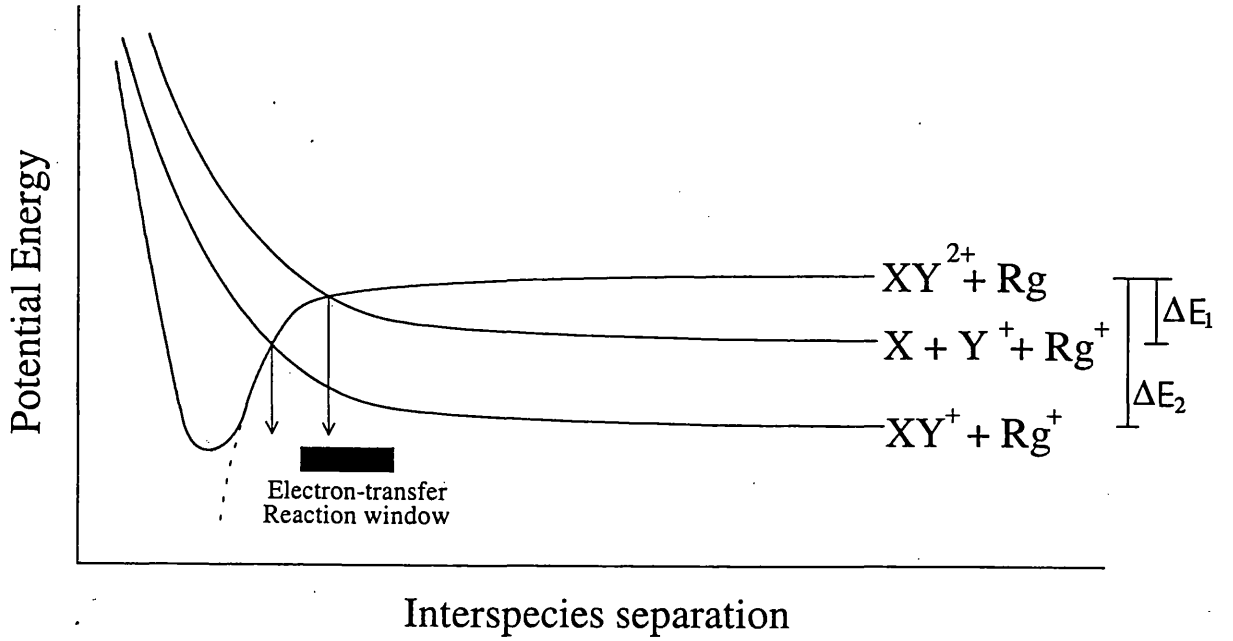

Figure 4.3 Schematic representative of potential curves to illustrate how the reaction exothermicity (ΔE) determines the crossing radius and therefore the favoured electron-transfer channel.

4.3 Reaction Dynamics

The subject of 'reaction dynamics' attempts to explain the dynamic behaviour of a reactive system, both qualitatively and quantitatively. An appreciation of reaction dynamics is essential to understand the phenomena of reactive collisions at the microscopic molecular level, which in itself plays a vital role in the interpretation of chemical reactivity at the bulk macroscopic level.

The succeeding sections of this Chapter examine the areas of reaction dynamics that are fundamentally important in the study of ion-molecule reactions. These subjects include the reaction cross-section which, being a measure of reaction probability, provides a means of quantifying the strength of a reaction channel. Other areas considered include the factors that influence the collision process and therefore the reaction cross-section; these areas include the collision energy-dependence, the form of the intermolecular potential and the nature of the reaction mechanism.

4.3.1 The reaction rate constant

Classically, chemical reaction rates may be expressed in terms of a temperature-dependent rate constant $k(T)$. For a simple bimolecular reaction:

$$A + B \rightarrow C \tag{4.8}$$

a typical reaction rate equation is of the form:

$$\text{Rate} = -\frac{dA}{dt} = -\frac{dB}{dt} = \frac{dC}{dt} = k(T)\,[A]^n[B]^m \tag{4.9}$$

where n and m are the orders of the reaction and [Y] is the concentration of reactant Y.

To best consider the detailed reaction dynamics of gas-phase reactions it is necessary to consider individual collision events. To allow this, a detailed knowledge of the energetics of the individual collision partners is required. Hence, the macroscopic bulk temperature dependent rate constant is replaced with a velocity dependent rate constant $k(v)$.

4.3.2 The centre-of-mass reference frame

Consider a collision system comprising of two colliding species A and B of mass m_a and m_b respectively. In the laboratory frame the origin is taken as the point of collision. The velocities of the collision partners and their position vectors are given by v_a, v_b and R_A, R_B respectively, as shown in Figure 4.4 below. The use of this reference frame is not, however, the most convenient for use in the calculations involved in reactive collisions. The principle reason for this is that a relatively large number of parameters need to be evaluated in the calculation. To overcome this problem most calculations are performed in the centre-of-mass reference frame.

The centre-of-mass (CM) system, although being conceptually greater in complexity than the laboratory frame system, does however greatly simplify the calculation process. In addition to the reduced number of parameters in the CM system, further simplification is achieved, as by definition the total linear momentum in the CM is zero. A proof of this is given below.

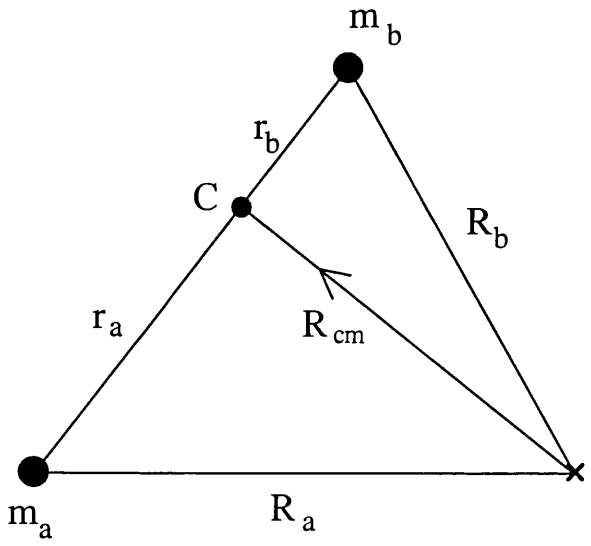

Figure 4.4 The collision of reactants A and B of masses m_a and m_b respectively in the centre-of-mass and laboratory frames. By definition, the origin in the laboratory frame X corresponds to the collision point. The centre-of-mass origin **C** lies at a distance R_{cm} from the laboratory origin.

In the CM system, the centre-of-mass of the two collision partners moves at a constant velocity relative to the laboratory along the line between the two reactants. Note, if the velocity of one of the reactants is very much larger than that of the other collision partner, as is the case in the experiments reported in this thesis, then the CM can be considered as moving along the line that is given by the path of the fast reactant. Figure 4.4 indicates the connection between the centre-of-mass and laboratory frames of reference.

The centre-of-mass origin has a position vector R_{cm} with respect to the point of collision, that is the origin in the laboratory frame. The separation of the collision partners r_a and r_b, with respect to the centre-of-mass is given by:

$$r_a = \frac{m_b}{m_a + m_b}(R_a - R_b) \tag{4.10}$$

similarly:

$$r_b = \frac{-m_a}{m_a + m_b}(R_a - R_b) \tag{4.11}$$

The velocity vectors of A and B in the CM frame u_a and u_b are easily obtained by differentiating Equations 4.10 and 4.11 with respect to time:

$$u_a = \frac{dr_a}{dt} = \frac{m_b}{m_a + m_b}(v_a - v_b) \tag{4.12}$$

and

$$u_b = \frac{dr_b}{dt} = \frac{-m_a}{m_a + m_b}(v_a - v_b) \tag{4.13}$$

Equations 4.12 and 4.13 may therefore now be used to find the sum of the linear momenta (ΣP_{cm}).

$$\Sigma P_{cm} = m_a u_a + m_b u_b = \frac{m_a m_b}{m_a + m_b}(v_a - v_b) - \frac{m_a m_b}{m_a + m_b}(v_a - v_b) = 0 \tag{4.14}$$

Hence, the total linear momenta in the CM system is indeed zero.

A similar analysis may be used to obtain the relative kinetic energy of the reactants in the CM system. The centre-of-mass kinetic energies T_a and T_b are given by:

$$T_a = \frac{1}{2}m_a u_a^2 = \frac{1}{2}m_a\left[\frac{m_a}{m_a + m_b}(v_a - v_b)\right]^2 \tag{4.15}$$

$$T_b = \frac{1}{2}m_b u_b^2 = \frac{1}{2}m_b\left[\frac{-m_b}{m_a + m_b}(v_a - v_b)\right]^2$$

Hence, the combined CM kinetic energy T is given by:

$$T = T_a + T_b = \frac{1}{2}\frac{m_a m_b}{m_a + m_b}(v_a - v_b)^2\left(\frac{m_b}{m_a + m_b} + \frac{m_a}{m_a + m_b}\right) \tag{4.16}$$

this can be simplified to give:

$$T = \frac{1}{2}\mu v \tag{4.17}$$

where μ is the reduced mass and v is the relative velocity (v_a-v_b), of the collision partners.

At large separations R, the relative velocities and, hence, the relative kinetic energy T are constant. Therefore, the total collision energy E_T is equal to the relative kinetic energy T at large interspecies separations where any forces between the collision partners are negligible. However, as the two particles converge, the relative kinetic energy is changed as a result of the interaction between the collision partners and only the total collision energy is conserved.

$$E_T = \frac{1}{2}\mu v^2 = T + V(R) \tag{4.18}$$

where v is the initial value of the relative velocity of the collision partners (i.e. at large values of separation R where $V(R)$ is effectively zero). Hence, the relative kinetic energy available at the point of interaction T, is dependent upon the separation R:

$$T = E_T - V(R) \tag{4.19}$$

4.3.3 The collision cross-section and impact parameter.

For a chemical reaction to take place, the reactant species must come into close enough contact to allow the chemical rearrangement of the collision partners. As a first approximation, the assumption is made that the reactants are hard spheres of diameter d and, as illustrated in Figure 4.5, must collide before a reaction can take place. Hence, the interspecies centre-centre separation R upon collision is given by $R = d$. In other words, a collision occurs whenever the centre of one molecule enters a sphere of radius d around the second molecule. For an incident reactant molecule this sphere presents an effective area centred around its collision partner, into which its centre must enter for a collision to occur. The physical size of the collision partners therefore determines the collision cross-section. The *collision cross-section* σ_c can be defined as the constant of proportionality such that:

$$\frac{1}{\lambda} = \sigma_c n_b \tag{4.20}$$

Where λ is the mean free path and n_b is the number density of the collision partner. As can be seen from Equation 4.20 above, increasing the collision cross-section has the effect of increasing the chances of a collision occurring. This is quantitatively observed as a reduction in the distance the reactant travels before colliding (the mean free path).

For real molecules the collision cross-section can be considered in terms of the *impact parameter b*. The impact parameter may be defined as being the distance of closest approach of the particles in the absence of an interaction between the two collision partners. As can be seen from Figure 4.6, if one considers the incident ion trajectories having impact parameters in the range b to $b+db$ and assuming cylindrical symmetry of the ion flux, then the ion trajectories have to pass through an annular volume of radius b and thickness db in a plane perpendicular to the original direction of

motion. Any trajectory with a relative separation vector R inside the area of the annulus will result in a collision. Hence, this gives an element of the collision cross-section $d\sigma_c$ where:

$$d\sigma_c = 2\pi b db \tag{4.21}$$

Integrating Equation 4.21 for all values of the impact parameter up to a maximum (b_{max}) that will result in a collision at a given collision energy gives:

$$\sigma_c = \pi b_{max}^2 \tag{4.22}$$

For example, in the hard sphere model b_{max} is equal to the hard sphere diameter d, giving a hard sphere collision cross-section $\sigma_c = \pi d^2$.

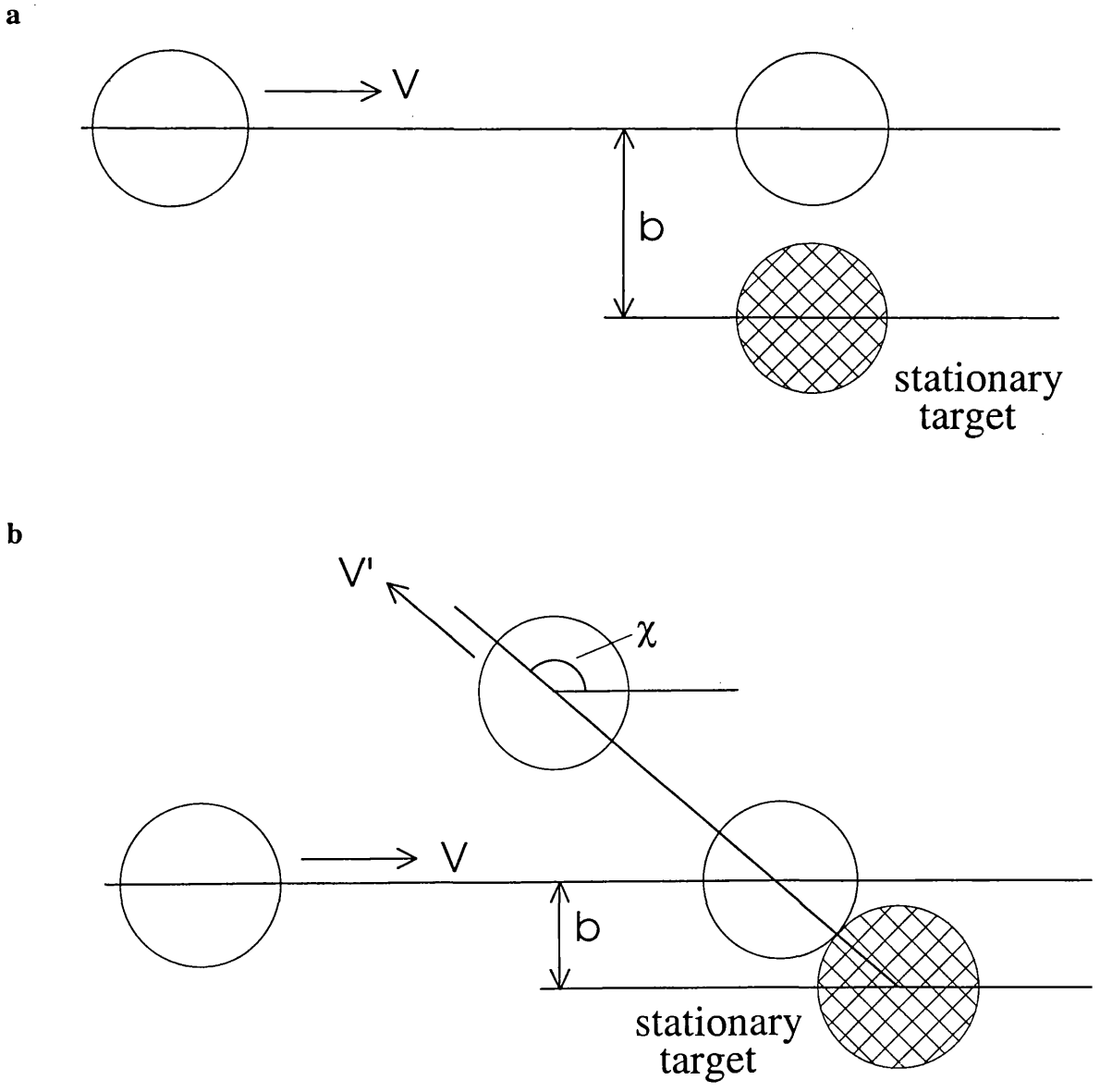

Figure 4.5 Collisions between identical non-interacting hard spheres of diameter d. (**a**) A collision does not occur if the impact parameter b is greater than d the hard sphere diameter. (**b**) If $d \geq b$ then collision occurs with a deflection angle χ.

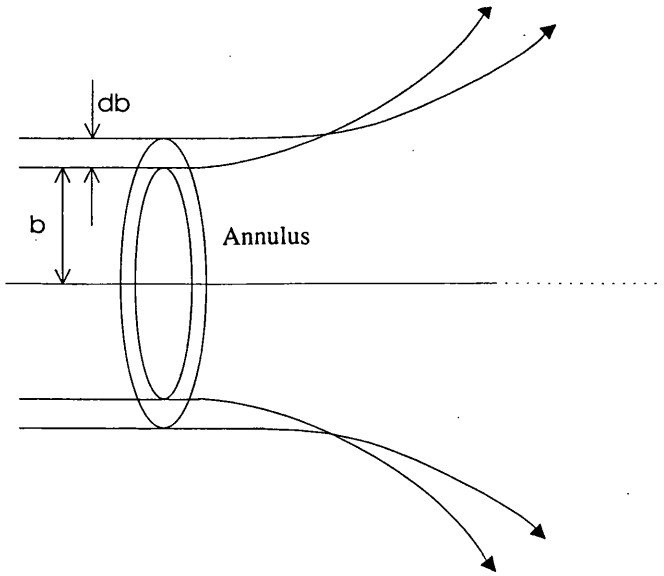

Figure 4.6 Schematic representation of the trajectories of collision partners having impact parameter in the range b to b+db, forming an annular area of radius b and thickness db.

4.3.4 The centrifugal barrier and intermolecular potential

In reality molecules are not hard spheres. The collision partners are subject to attractive and repulsive forces, these forces have a considerable effect upon the trajectory of a pair of colliding particles and the energetics of the collision process. This is best illustrated by the fact that a collision event may still occur between two particles where the internuclear separation at the point of closest approach is greater than the sum of the atomic radii of the collision partners. The contrast of this situation to the situation of the non-interacting hard sphere model of atomic collisions is shown in Figure 4.7.

The relative motion of two reactant species can be specified in terms of a relative position vector $\boldsymbol{R}$ of magnitude R, aligned at an angle ψ with respect to a fixed direction as shown in Figure 4.7. The presence of the intermolecular forces directly affects both the separation R of the two reactants and the orientation angle ψ. The magnitude of the interspecies separation with time $R(t)$, describes the approach of the reactants and the subsequent separation of the reaction products. However, to fully describe the reaction dynamics and relative position of the species, it is also necessary to consider the angle of the relative orientation ψ of the reactants with respect to a fixed direction. The necessity for this is that the relative rotation of the reactants, that is the change in the orientation angle ψ with time, results in a net reduction in the energy available for reaction. The moment of inertia of the reactants is given by $I = \mu R^2$ hence, the smaller the interspecies separation, the lower is I and by virtue of the conservation of angular momentum ($I\omega$) the higher will be the angular velocity ω. Hence, by

reducing R and thereby increasing ω the net effect, as demonstrated in Equation 4.23, is to increase the rotational kinetic energy E_R

$$E_R = \frac{I\omega^2}{2} = \frac{\mu R^2}{2}\left(\frac{d\psi}{dt}\right)^2 \tag{4.23}$$

As the two reactants converge, there is therefore an effective reduction in the amount of kinetic energy available to overcome the potential barrier $V(R)$. We see the relative rotation itself acting as a barrier to reaction which prevents the two reactant species from getting as close as would be possible if ω had zero value. Hence, the total collision energy E_T is the sum of the relative kinetic energy and the potential energy as given in Equation 4.24:

$$E_T = T + V(R) = \frac{\mu}{2}\left(\frac{dR}{dt}\right)^2 + \frac{\mu}{2}R^2\omega^2 + V(R) \tag{4.24}$$

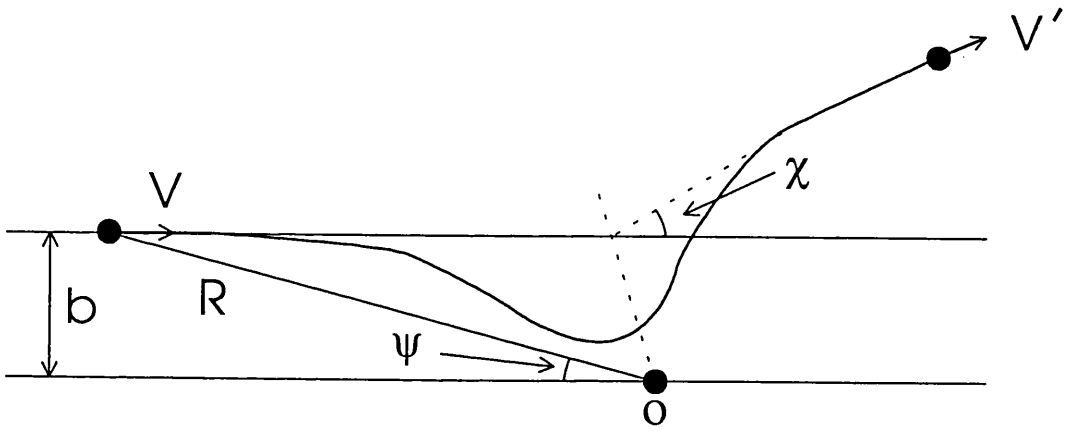

Figure 4.7 The trajectory in the centre-of-mass frame of a collision between two 'real' particles at impact parameter b, relative velocity v and reduced mass μ. The relative separation $\boldsymbol{R(t)}$ can be viewed as the path taken by particle of mass μ and initial velocity v, when deflected by a potential $V(R)$ centred on the stationary target at **O.**

Note, the kinetic energy is expressed as two terms in Equations 4.23 and 4.24. This is explained as arising because the kinetic energy is defined in terms of the relative position vector $\boldsymbol{R(t)}$. Consequently, as the colliding particles approach one another, $\boldsymbol{R(t)}$ changes with time and the kinetic energy term therefore requires two terms. Firstly, a term that corresponds to the magnitude of the relative separation of the colliding species, and secondly, a term corresponding to the changing direction ψ of the relative position vector.

From Appendix 4, consideration of the angular momentum L of the relative motion gives a relationship between the angular velocity ω and the impact parameter b:

$$L = \mu v b = I\omega = \mu R^2 \omega \tag{4.25}$$

Hence, from Equation 4.25 we get:

$$\omega = \frac{vb}{R^2} \tag{4.26}$$

If the collision partners are at initial separations large enough so that the potential energy $V(R)$ has zero value, the total energy of the collision E_T may be described purely in terms of the initial relative velocity v and the reduced mass μ:

$$E_T = \frac{1}{2}\mu v^2 \tag{4.27}$$

Therefore, by substituting the expressions for ω given in Equation 4.26 into Equation 4.24 we get:

$$E_T = T + V(R) = \frac{\mu}{2}\left(\frac{dR}{dt}\right)^2 + \frac{\mu}{2}\frac{v^2 b^2}{R^2} + V(R) \tag{4.28}$$

Equating the two expressions for E_T in Equations 4.27 and 4.28 gives:

$$E_T = E_T\left(\frac{b}{R}\right)^2 + \frac{\mu}{2}\left(\frac{dR}{dt}\right)^2 + V(R) \tag{4.29}$$

Thus, the energy of rotation acts to reduce the kinetic energy available to overcome the intermolecular potential. A convenient representation of the effective kinetic energy, which is sometimes known as the *line of centres energy*, is therefore obtained by rearranging Equation 4.24 to give:

$$E_T\left(1 - \frac{b^2}{R^2}\right) = \frac{\mu}{2}\left(\frac{dR}{dt}\right)^2 + V(R) \tag{4.30}$$

Hence, the motion of the approaching particles may be viewed as the motion of a particle of mass μ, in a potential $V(R)$ with an effective kinetic energy $E_T\left(1 - b^2/R^2\right)$.

An alternative perspective combines the energy of rotation (centrifugal energy) and the potential energy, such that the centrifugal energy acts as a repulsive contribution to an effective potential V_{eff} giving:

$$V_{eff}(R) = V(R) + E_T\frac{b^2}{R^2} \tag{4.31}$$

The energy of rotation therefore contributes to V_{eff}, which acts as a repulsive potential to prevent the close convergence of the collision partners and is hence termed the *centrifugal barrier* to reaction [23].

$$E_T = \frac{\mu}{2}\left(\frac{dR}{dt}\right)^2 + V_{eff}(R) \tag{4.32}$$

From Equation 4.31 it is clear that as the colliding partners approach each other, the effective potential increases. As the total collision energy is conserved, the increase in V_{eff} necessarily leads to a fall in the kinetic energy term in Equation 5.32. Ultimately, the colliding particles reach their smallest

separation R_0, often known as the *distance of closest approach* or *turning point.* At R_0 the kinetic energy term is zero. Hence, the total collision energy is, at this point, equal to the effective potential, thus enabling R_0 to be determined from the implicit equation in V_{eff} [23].

$$E_T = V_{eff}(R_0) = V(R_0) + E_T\left(\frac{b^2}{R_0^2}\right) \tag{4.33}$$

4.3.5 The reaction cross-section

The reaction cross-section σ_{rxn} may be defined in terms of the reaction rate constant such that:

$$k(v) = v\sigma_{rxn} \tag{4.34}$$

This relationship can be used to give a qualitative measure of the likelihood of reaction by considering a beam of the incident reactant A of number density N_A passing through a reaction cell containing the collision partner B of number density N_B. The loss of the reactant species A in the beam is given as the rate of reduction in beam intensity I_A with distance travelled in the cell

$$-\left(\frac{dI_A}{dx}\right) = k(v)N_A N_B = I_A(x)N_B\sigma_{rxn} \tag{4.35}$$

where $I_A(x)$ is the intensity of the beam of reactant species A at position x.

In a simplified model it is possible to estimate the reaction cross-section by assuming that every collision results in reaction. This is clearly a gross over-simplification as there are many other possible outcomes of a collision such as non-reactive scattering and electron-transfer to name but two. Consequently, $\sigma_c \geq \sigma_{rxn}$.

It is possible to define the likelihood of a collision event leading to reaction as a function of the impact parameter b. We define the *opacity function P(b)* as the fraction of collisions with impact parameter b that result in reaction. Hence, $0 \leq P(b) \leq 1$.

As stated in section 4.3.4, the centrifugal barrier effectively acts to keep the reactant molecules apart, preventing reaction. Hence, ignoring possible steric effects, the reaction is favoured for small impact parameters. In other words, $P(b) \rightarrow 0$ for high values of b. It is therefore possible to define a limiting condition, that is a reaction will not take place if the impact parameter exceeds a certain magnitude b_{max}. Collisions involving reactants having impact parameters greater than b_{max} will not lead to the reaction taking place. Hence, the opacity function $P(b)$ has zero value if the impact parameter exceeds b_{max}.

The inclusion of the opacity function into the equation for the collision cross-section yields the reaction cross-section σ_{rxn}, thus:

$$d\sigma_{rxn} = 2\pi bP(b)db \tag{4.36}$$

Hence, giving:

$$\sigma_{rxn} = 2\pi \int_0^{\infty} bP(b)\mathrm{d}b \tag{4.37}$$

where the opacity function $P(b)$ is given by:

$$\begin{aligned} P(b) &= P,(b \le b_{\max}) \\ P(b) &= 0,(b > b_{\max}) \end{aligned} \tag{4.38}$$

The above derivation of the reaction cross-section σ_{rxn} may be treated quantum mechanically. With the reaction probability defined for each value of the quantum number l, this gives:

$$\sigma_{rxn} = \frac{\pi}{k_B^2} \sum_{l=0}^{\infty} (2l+1)P(l) \tag{4.39}$$

where $k_B = \mu v / \hbar$ is the *de Broglie wave number* [23] and $P(l)$ is the probability of reaction for a given value of l. In the case where many l values provide a contribution to the reaction it is possible to use the semi-classical correspondence $bk_B \approx (l + 0.5)$ to convert the summation over l to an integral over b. This treatment results in Equation 4.37.

4.3.6 Collision energy-dependence and the intermolecular potential

As mentioned in section 4.3.4 the collision energy must be of sufficient magnitude to overcome the centrifugal barrier to allow a reaction to proceed. Central to determining the kinetic energy available for reaction is the role of the intermolecular potential $V(R)$ between the reactants. A prototypical form of the intermolecular potential is given by:

$$V(R) = -\frac{C_s}{R^s} \tag{4.40}$$

As previously defined, the effective potential is given by:

$$V_{\text{eff}} = V(R) + E_T\left(\frac{b}{R}\right)^2 \tag{4.41}$$

Hence substituting Equation 4.40 into 4.41 gives:

$$V_{\text{eff}} = -\frac{C_s}{R^s} + E_T\left(\frac{b}{R}\right)^2 \tag{4.42}$$

Simple differentiation of Equation 4.42 above yields $R_{\max}$,

$$\frac{\mathrm{d}}{\mathrm{d}R}\left[V_{\text{eff}}(R)\right]_{R=R_{\max}} = 0 \tag{4.43}$$

The parameter $R_{\max}$, is simply the value of R that corresponds to the maximum of the effective potential V_{eff}. This gives a criterion for reaction, namely that the reactants have non-zero kinetic energy at $R = R_{\max}$. That is, using Equations 4.29 and 4.32:

$$\frac{\mu}{2}\left(\frac{\mathrm{d}R}{\mathrm{d}t}\right)^2_{R_{\max}} = \left(E_T - V_{\text{eff}}\right)_{R_{\max}} = \left[E_T - V(R) - E_T\frac{b^2}{R^2}\right]_{R_{\max}} > 0 \tag{4.44}$$

As can be seen from Equation 4.44, increasing the impact parameter for a given value of E_T has the effect of lowering the kinetic energy, available at $R = R_{\max}$, of the reactants. This provides the

means of defining another parameter, that is the largest value of the impact parameter, b_{max} for which the molecules may overcome the effective potential and undergo reaction. This results in the condition for reaction reverting to the form of Equation 4.45.

$$\left[E_T - V(R) - E_T \frac{b_{max}^2}{R^2}\right]_{R=R_{max}} = 0 \tag{4.45}$$

Hence, having obtained an expression for b_{max} the reaction cross-section may be obtained using Equation 4.46, which is derived from Equation 4.37 above.

$$\sigma_{rxn} = 2\pi P \int_0^{b_{max}} b \cdot db = \pi P b_{max}^2 \tag{4.46}$$

A general form of the intermolecular potential is given by Levine and Bernstein [23] as Equation 4.40. Incorporating Equation 4.40 into Equation 4.43 gives R_{max} for values of $s > 2$, in Equation 4.40.

$$R_{max}^2 = \left[\frac{sC_s}{2E_T b^2}\right]^{\frac{2}{(s-2)}} \tag{4.47}$$

Hence, using the above Equations, the reaction cross-section σ_{rxn} is given by:

$$\sigma_{rxn}(E_T) = \pi b_{max}^2 = \xi(s)\pi\left(\frac{C_s}{E_T}\right)^{2/s} \tag{4.48}$$

with a constant of proportionality $\xi(s)$ [23] given by:

$$\xi(s) = \left(\frac{s}{2}\right)\left(\frac{s-2}{2}\right)^{-(s-2)/s} \tag{4.49}$$

For the special case of reactions between ions and neutral species, the form of the reactant intermolecular potential is that of a simple polarization function. Hence, $s = 4$, and $C_s = \alpha/2$. Using these in Equation 4.48 one obtains the reaction cross-section in the form of the Langevan cross-section σ_{LGS} [24]:

$$\sigma_{LGS} = \pi q\left(\frac{2\alpha}{E_T}\right)^{0.5} \tag{4.50}$$

This theoretical collision cross-section, first postulated by Gioumousis *et al* in 1958 [24], has an energy dependence in accordance with empirical results taken at low collision energies ($E_T < 0.01$ eV). The use of theoretical reaction cross-sections such as the Langevan cross-section allows a comparison with empirically-determined reaction cross-sections. Hence, any differences in the collision energy-dependence of theoretical and experimentally-determined cross-sections may be ascertained. Such differences may provide information regarding the reaction mechanism. An example of this is the work of Armentrout *et al* [25-29], where the σ_{LGS} Langevan cross-section is compared to the observed cross-sections for the reactions between molecular cations, including the nitrogen cation, and deuterium, hydrogen and deuterium hydride neutral targets. Analysis of the collision energy-dependence of the reaction processes yields important information such as possible isotope effects, the

possible formation of a reaction complex and the form of the intermolecular potential, in addition to the nature of the reaction mechanism.

The presence of a threshold energy adds a further obstacle to reaction. In such cases, the previous kinetic energy requirement is adapted to include the threshold energy E_{th} replacing Equation 4.29 with the requirement that at some separation d the kinetic energy of the reactants is greater than the threshold energy. Hence,

$$E_T - E_{th} - E_T\left(\frac{b}{d}\right)^2 \geq 0 \tag{4.51}$$

The maximum value of b that satisfies Equation 4.51 is given by:

$$b_{max} = d\left(1 - \frac{E_{th}}{E_T}\right)^{0.5} \tag{4.52}$$

this gives the following expression for the reaction cross-section:

$$\sigma_{rxn}(E_T) = \pi b_{max}^2 = 0, (E_{th} \geq E_T) \tag{4.53}$$

$$\sigma_{rxn}(E_T) = \pi b_{max}^2 = \pi d^2\left(1 - \frac{E_{th}}{E_T}\right), (E_{th} < E_T)$$

4.4 Reaction Mechanisms

A chemical reaction necessarily requires a rearrangement of the atoms making up the reactants into the configuration of the reaction products. A chemical reaction performs the rearrangement in a specific sequence of steps, this is known as the *reaction mechanism.* Reaction mechanisms may be divided into two broad classes. Firstly, 'direct' and secondly, 'complex'. The two classes of reactive pathway differ greatly, both in the dynamics of the reaction products and their reaction cross-sections.

4.4.1 Direct Reaction Mechanism

Consider the reaction $A + B \rightarrow C + (D)$. As the name implies, the direct reaction mechanism features a straightforward transfer of part or all of reactant B to reactant A. The product formed is molecule C. If only part of reactant B is transferred, then product D is the remnant of the untransferred part of B.

The most striking feature of direct reactions is the absence of the formation of a reaction (collision) complex. A complex is, in its simplest form, a short-lived species formed from the union of the two reactants. Hence, the absence of the complex ensures that the products of the reaction are scattered with a characteristic distribution of trajectories. The scattering angle χ is defined as the angle between the scattered reaction product and the line of the original reactant trajectory.

The products of the reaction maybe scattered forwards, that is $\chi < 90$, or backscattered, $180^0 \geq \chi \geq 90^0$, as shown in Figures 4.8 and 4.9 below. Such distributions are caused by differences

in the reaction dynamics, that is the values of the impact parameter that result in reaction. For example consider the two reactions [23] given by Equations 4.54 and 4.55

$$K + I_2 \rightarrow KI + I \tag{4.54}$$

$$K + ICH_3 \rightarrow KI + CH_3 \tag{4.55}$$

In the case of Equation 4.54 the KI product is forward scattered, whereas the KI product in Equation 4.55 is largely backscattered. This may be qualitatively explained by the fact that the opacity function $P(b)$ for the reaction between K and I_2 has high values ($P(b) \rightarrow 1$) for impact parameters out to relatively large values. At these large impact parameters the K atom literally picks up the I atom and because the impact parameter is large, the deflection of the recoiling products will be small, that is the KI product is forward scattered. This type of reaction is known as an *impulsive* or *spectator-stripping mechanism.*

The reaction between K and ICH_3 is characterised by the backscattering of the KI product, in this case the reaction dynamics are such that the opacity function is only of significant value at low values of b. Hence, only near head on collisions will result in reaction. These head on collisions result in the rebound of the KI product $\chi > 90^\circ$. Reactions of this type are thus described as occurring via a *rebound mechanism.*

As discussed above in section 4.3.3 (Equation 4.22), the magnitude of the reaction cross-section is strongly dependent upon b_{max}, that is the maximum value of the impact parameter that still results in reaction. Therefore, because the spectator-stripping mechanism is characterised by large impact parameters, the cross-sections for reactions proceeding by this mechanism are relatively large. In contrast to this, the cross-sections for reactions involving a rebound mechanism are, as a result of the smaller impact parameters associated with this mechanism, very much smaller.

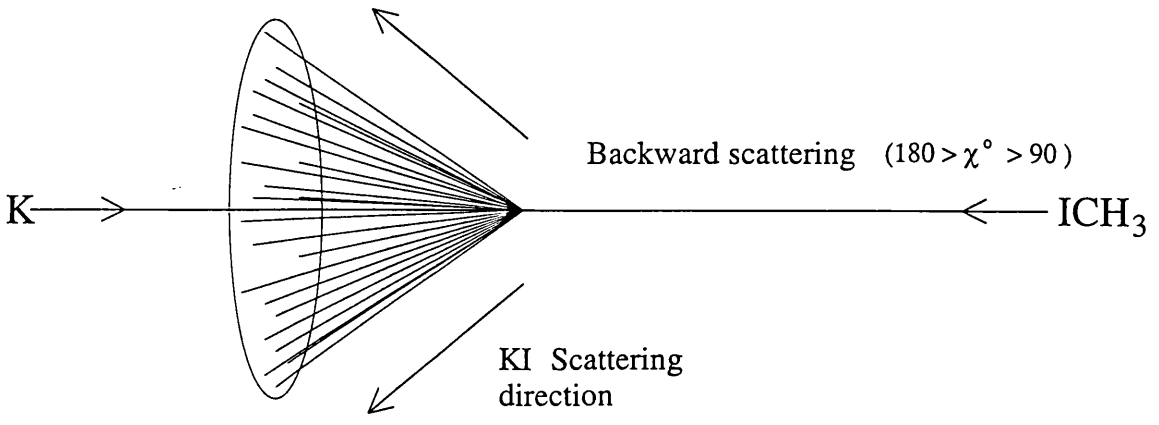

Figure 4.8 The distribution of the backscattered KI produced in the (rebound) reaction between K and ICH_3.

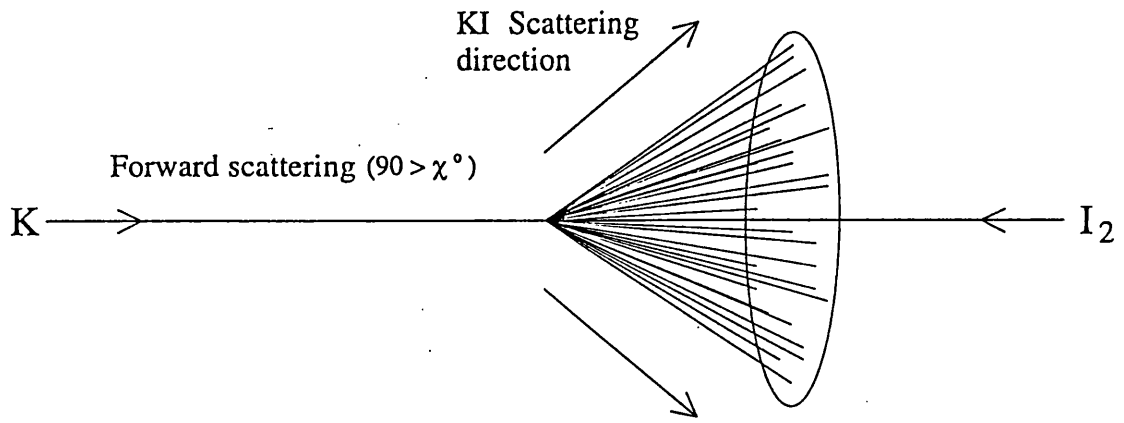

Figure 4.9 The distribution of the forward-scattered KI produced in the (spectator-stripping) reaction between K and I_2.

4.4.2 Complex formation

By contrast to the direct reaction mechanism, the complex forming mechanism, also known as the compound collision mechanism, features the formation of a reaction intermediate or complex. For example, in the reaction given by Equation 4.56 [30], the complex formed is [HOH].

$$O + H_2 \rightarrow [HOH] \rightarrow OH + H \qquad (4.56)$$

The lifetime of such an intermediate is usually of the order of $\tau > 10^{-12}$ s compared to the reaction time of $< 10^{-13}$ s for the direct type mechanism. The relatively long lifetimes of these states are of the same order as the rotation period of a typical complex. Hence, the complex may undergo several rotations before it fragments. By this time the recoiling fragments will have no 'memory' of the original trajectories and the fragments will be scattered with no particular distribution at all angles, both backwards and forwards.

4.4.3 Factors affecting the reaction mechanism

Several factors influence the nature of the reaction mechanism, that is whether the reactants form a complex or alternatively react via a direct mechanism. Key factors include the energy of the reactants, inclusive of the translational, electronic and vibrational state of the reactants, together with the potential energy surfaces and the structural complexity of the reactants.

As stated above, the electronic state of the reactants influences the reaction mechanism. For example, the reaction given in Equation 4.57 proceeds via the complex-forming mechanism at collision energies below 5 eV.

$$O_2^+(X^2\Pi_g) + H_2 \rightarrow O_2H^+ + H \qquad (4.57)$$

Whereas, the same reaction with the molecular oxygen cation in the (A $^4\Pi_u$) excited electronic state proceeds via a direct mechanism at the equivalent collision energies [31]. In common with the electronic state energy, the vibrational energy may also have a strong influence upon the reaction mechanism. For example, the same reaction between O_2^+ (X $^2\Pi_g$) and H_2 proceeds via a complex mechanism at collision energies below 5 eV for vibrational states v = 0-4. In contrast, for reactants having the same collision energy, but large amounts of vibrational energy (v > 19), the reaction proceeds via a direct mechanism [32]. These observations strongly suggest that the total energy of the reactant is of greater significance than either the internal or translational energy.

The criterion for the formation of a complex can be qualitatively explained by the presence of a well in the potential energy surface. As can be seen from Figure 4.10, reactants having insufficient total energies E_{tot}, where the total energy is the sum of the collision (translational) energy, E_{trans}, and the internal energy E_{int}, to pass through the well, will form complexes such as HOCO in the case of the reaction between atomic hydrogen and CO_2. Reactants possessing sufficient total energy will pass through the potential well and react by a direct mechanism.

$$E_{tot} = E_{trans} + E_{int} \qquad (4.58)$$

In addition to the potential energy surface, the complexity of the reactants also determines the nature of the mechanism. Highly complex reactants favour the formation of reaction complexes, as the many vibration modes associated with a complex reactant provide an efficient means of dissipating the collision energy before the energy can be localised in a fissile bond. This greatly increases the lifetime of the reaction adduct, which therefore favours the formation of a complex.

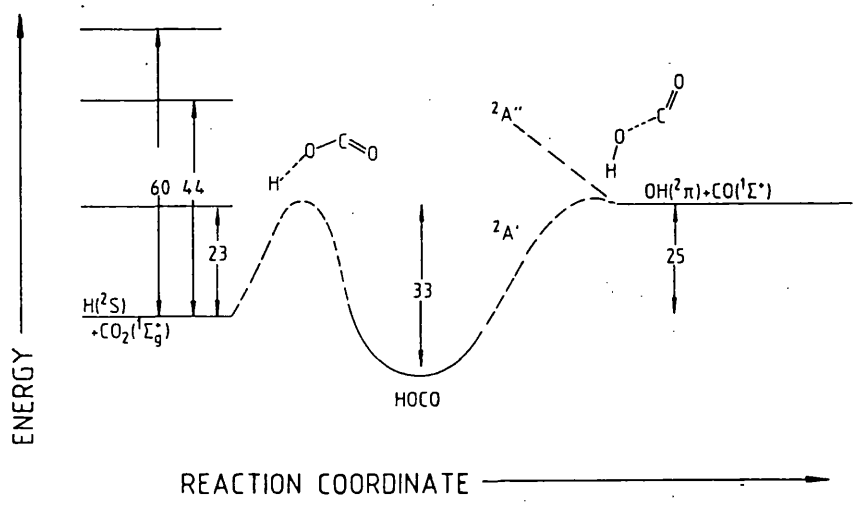

Figure 4.10 Schematic illustration of the potential well in the H + CO_2 collision system and estimated structures of the HOCO complex [33].

4.5 Isotope effects

4.5.1 Definition of an isotope effect

The course of a chemical reaction may be significantly altered as a result of a subtle difference in a physical property of the reactants. In the special case of a reaction process being altered as a result of a reactant being substituted with its isotopic analogue, this phenomenon may be described as an *isotope effect.* Isotope effects have been the subject of considerable investigation [16,19,25-29,31,32,34-43]. The primary motivation for studying isotope effects, particularly in the field of gas-phase ion-molecule reactivity, is that such effects offer the experimentalist a powerful probe with which to investigate the reaction mechanism.

A common factor causing an isotope effect is the zero-point energy (ZPE) of the reactant. The ZPE is strongly dependent upon the masses of the atoms comprising the reactant molecule. For example, the ZPE of H_2 is 26.1 kJ mol^{-1} which is 7.6 kJ mol^{-1} higher than the ZPE of D_2. As most reactions are performed at, or below, room temperature, most H_2 and D_2 molecules would be at their zero-point levels. Consequently, as the majority of H_2 molecules have 7.6 kJ mol^{-1} more ZPE than the D_2 molecules, reactions involving H_2 tend to be more rapid than equivalent reactions with D_2, and, hence, are characterised by larger reaction cross-sections [44].

4.5.2 Categories of isotope effect

Isotope effects may be divided into two main types. Firstly, the *intermolecular isotope effect.* This type of isotope effect may be observed as a change in the cross-section of a given reaction process when a reactant is substituted by its isotopic analogue. For example, consider the H atom transfer reaction between argon cations and hydrogen molecules, which is one of the most thoroughly investigated gas-phase reactions [27] (Equation 4.59). The presence of an isotope effect for this collision system may be revealed by performing the reaction with an isotopic neutral reactant, in this case deuterium molecules (Equation 4.60) and deuterium hydride (Equations 4.61 and 4.62). If an isotope effect operates in the reaction process then the cross-section of reaction 4.59 would, as discussed above, be expected to be greater than that of reaction 4.60 and the sum of the cross-sections for reactions 4.61 and 4.62.

$$Ar^+ + H_2 \rightarrow ArH^+ + H \qquad (4.59)$$

$$Ar^+ + D_2 \rightarrow ArD^+ + D \qquad (4.60)$$

$$Ar^+ + HD \rightarrow ArH^+ + D \qquad (4.61)$$

$$Ar^+ + HD \rightarrow ArD^+ + H \qquad (4.62)$$

In the above reactions, no intermolecular isotope effect is observed. However, in the analogous reactions involving a krypton ion as the charged reactant (Equations 4.63-4.66), a significant isotope effect is observed [26].

$$Kr^+ + H_2 \rightarrow KrH^+ + H \quad (4.63)$$

$$Kr^+ + D_2 \rightarrow KrD^+ + D \quad (4.64)$$

$$Kr^+ + HD \rightarrow KrH^+ + D \quad (4.65)$$

$$Kr^+ + HD \rightarrow KrD^+ + H \quad (4.66)$$

The results indicate that the ratio of the cross-sections σ (H_2): σ (HD): σ (D_2), where σ is the cross-section of the appropriate reaction (4.63 or 4.64) and σ (HD) is the sum of cross-sections for reactions 4.65 and 4.66, is approximately 1.0: 1.8: 0.8. The ordering of the cross-sections σ (HD) > σ (H_2) > σ (D_2) signifies that the intermolecular isotope effect cannot simply be ascribed as a mass (zero-point energy) effect. One possible explanation is that the anisotropic potential surface of the Kr^+-HD collision system enables the coupling of rotational and electronic degrees of freedom in the entrance channels of reactions 4.65 and 4.66, which affects the ability of the reactants to pass through the avoided crossing with the Kr + HD^+ channel. The anisotropy of the potential surfaces is caused by effects in the orientation of the heteronuclear HD [41].

Intermolecular isotope effects, or their absence, can provide much information regarding the mechanism of a reaction process. For example, consider the general reactions 4.67 and 4.68, having cross-sections σ (H_2) and σ (D_2) respectively.

$$A^+ + H_2 \rightarrow AH^+ + H \quad (4.67)$$

$$A^+ + D_2 \rightarrow AD^+ + D \quad (4.68)$$

If the values of σ (H_2) and σ (D_2) were plotted as functions of the centre-of-mass collision energy and found to be the same then this absence of an isotope effect is consistent with the operation of a direct reaction mechanism [32]. Furthermore, if the cross-sections are plotted as functions of the pairwise energy E_{pair}, given in equation 4.69, then the absence of an isotope effect indicates that the reaction proceeds via a spectator-stripping mechanism, discussed in section 4.3.1.

$$E_{pair} = E_{com} \frac{M m_{H(D)}}{(m_A + m_{H(D)})(m_{H(D)} + m_{H(D)})} \quad (4.69)$$

where $M = (m_A + m_{H(D)} + m_{H(D)})$ and E_{com} is the centre-of-mass collision energy. Additionally, the absence of an isotope effect in reactions 4.67 and 4.68, may point to the lack of an energy barrier to the transfer of $H^-(D^-)$. Isotope effects in the $H^-(D^-)$ transfer reactions are expected if a Landau-Zener style mechanism [17,18] operates. The reason for this is that the Landau-Zener theory which involves an energy barrier to $H^-(D^-)$ transfer, predicts that the lighter H^- ion tunnels through the barrier with greater efficiency than the relatively heavy D^- ion. Hence, the presence of isotope effects provides a means of determining the applicability of the Landau-Zener theory to $H^-(D^-)$ transfer reactions.

The second type of isotope effect is the *intramolecular isotope effect* [33,36-38,41,42]. This type of isotope effect is encountered in situations where a reactant molecule is, either partly or wholly, composed of a combination of different isotopic atoms. For example, the most commonly used reactant of this type is deuterium hydride (HD), which is used in place of both H_2 and D_2. Other examples include NDH_2, CDH_3 and other partly deuterated hydrocarbons. The use of a reactant like HD in place of H_2 or D_2 provides an added dimension for the reaction process. That is, reactants like HD necessarily place two isotopic reactant atoms at the reaction site, thereby offering a choice of reaction outcomes, providing an intimate probe of the reaction process. For example, consider the reaction between krypton and HD (Equations 4.65 and 4.66). An imbalance in the branching ratio of the two product ions reveals the operation of an intramolecular isotope effect [26]. In this case, the formation of the deuterated product (Equation 4.65) is marginally favoured at centre-of-mass collision energies below 0.03 eV. Between 0.03 and 0.1 eV the KrH^+ product dominates the product ion yield; at collision energies beyond 0.1 eV the isotope effect diminishes, giving a branching ratio of unity value.

At the lower collision energies (E_{com} < 0.03 eV), statistical effects favour the deuterated product. Such statistical effects are caused by the closer spacing of vibrational and rotational energy levels in the case of KrD^+. At intermediate collision energies, an attractive ion-induced dipole interaction exerts a torque on the HD molecule as it approaches the reactant ion. This torque, which arises as a result of the different positions of the centre-of-mass and the centre-of-polarization along the H-D bond, tends to rotate the HD molecule so that more collisions occur in the $[Kr\text{-}H\text{-}D]^+$ configuration rather than in $[Kr\text{-}D\text{-}H]^+$ configuration, therefore preferentially forming the hydrogenated product. At higher collision energies (E_{com} > 0.1 eV), this orientation effect becomes less significant as the increased collision energies allow insufficient time for the rearrangement of the HD molecule into the $[Kr\text{-}H\text{-}D]^+$ configuration. Hence, at such high collision energies, the orientation of HD with respect to the reactant ion is essentially random, resulting in equal yields of KrH^+ and KrD^+ product ions.

4.6 Conclusion

The experimental investigation of the gas-phase reactivity of doubly-charged molecules with neutral molecular targets is a comparatively new and expanding field of research. In general, theoretical studies play an important role in supporting experimental investigations, just as the experimental results offer a means of gauging the applicability of theoretical models. Hence, in situations where there is a paucity of comparative data, as is the case of the gas-phase reactivity of doubly-charged molecules with neutral molecular targets, the importance of related theoretical information must not be underestimated.

The subjects discussed in this Chapter are all important in gaining an understanding of reactive processes. The Landau-Zener model provides a means of gauging the likelihood of electron-transfer reactivity. Indeed, this predictive tool allows the probability of a particular channel of electron-transfer reactivity to be estimated. The dynamical calculations of ion-molecule interactions provide a theoretical rate constant, and from this the Langevan cross-section a benchmark of ion-molecule reactivity, which allows a comparison to be made with experimental results. Finally, the proposed reaction mechanisms, described above, present a physical picture of the reaction processes.

References

1 T. Chang and R. T. Poe, *Phys. Rev. A*, **12** (1975) 1432.

2 P. Millie, I. Nenner, P. Archirel, P. Lablanquie, P. Fournier and J. H. D. Eland, *J. Chem. Phys.*, **84** (1986) 1259.

3 N. Levasseur and P. Millie, *J. Chem. Phys.*, **92** (1990) 2974.

4 M. Lundqvist, D. Edvardsson, P. Baltzer, M. Larsson and B. Wannberg, *J. Phys. B At. Mol. Opt. Phys.*, **29** (1996) 499.

5 M. Kolbuszewski and J. S. Wright, *J. Phys. Chem.*, **99** (1995) 3455.

6 D. Mathur, *Phys. Reports,* **255** (1993) 195.

7 M. Larsson, B. J. Olsson and P. Sigray, *Chem. Phys.*, **139** (1989) 457.

8 G. Dujardin, L. Hellner, M. Hamdan, A. G. Brenton, B. J. Olsson and M. J. Besnard-Ramage, *J. Phys. B.*, **23** (1990) 1165.

9 G. Parlant, J. Senekowitch, S. V. O'Neil and D. R. Yarkony, *J. Chem. Phys.*, **94** (1991) 7208.

10 D. Duflot, J-M. Robbe and J-P. Flament, *J. Chem. Phys.*, **103** (1995) 10571.

11 B. F. Yates, W. J. Bouma and L. Radom, *J.American Chem. Soc.*, **108** (1986) 6545.

12 M. Manning, S. D. Price and S. R. Leone, *J. Chem. Phys.*, **99** (1993) 8695.

13 S. A. Rogers, S. D. Price and S. R. Leone, *J. Chem. Phys.*, **98** (1993) 280.

14 S. D. Price, S. A. Rogers and S.R.Leone, *J. Chem. Phys.*, **98** (1993) 9455.

15 S. D. Price, M. Manning and S. R. Leone, *J.American Chem. Soc.*, **116** (1994) 8675.

16 S. D. Price, *J. Chem. Soc., Faraday Trans.*, **93** (1997) 2451.

17 L. Landau, *Phys. Z. Sov.*, **2** (1932) 46.

18 C. Zener, *Proc. Royal Soc. London Ser. A*, **137** (1932) 696.

19 K. A. Newson and S. D. Price, *Chem. Phys. Letters*, **269** (1997) 93.

20 S. E. Butler and A. Delgardo, *Astrophys. J.*, **241** (1980) 838.

21 R. E. Olson and A. Salop, *Phys. Rev. A.*, **14** (1976) 579.

22 R. E. Olson, F. T. Smith and E. Bauer, *App. Opt.*, **10** (1971) 1848.

23 R. D. Levine and R. B. Bernstein, *Molecular reaction dynamics and chemical reactivity*, Oxford University Press Inc, New York 1987.

24 G. Gioumousis and D. P. Stevenson, *J. Chem. Phys.*, **29** (1958) 292.

25 R. H. Schultz and P. B. Armentrout, *J. Chem. Phys.*, **96** (1992) 1036.

26 K. M. Ervin and P. B. Armentrout, *J. Chem. Phys.*, **85** (1986) 6380.

27 K. M. Ervin and P. B. Armentrout, *J. Chem. Phys.*, **83** (1985) 166.

28 K. M. Ervin and P. B. Armentrout, *J. Chem. Phys.*, **86** (1987) 6240.

29 J. L. Elkind and P. B. Armentrout, *J. Chem. Phys.*, **84** (1986) 4862.

30 P. A. Whitlock, J. T. Muckerman and E. R. Fisher, *J. Chem. Phys.*, **76** (1982) 4468.

31 E. A. Gislason, B. H. Mahan, C. W. Tsao and A. S. Werner, *J. Chem. Phys.*, **50** (1969) 5418.

32 K. Tanaka, T. Kato, P. M. Guyon and I. Koyano, *J. Chem. Phys.*, **79** (1983) 4302.

33 K. Kleinermanns, E. Linnebach and J. Wolfrum, *J. Phys. Chem.*, **89** (1985) 2525.

34 K. A. Newson and S. D. Price, *Chem. Phys. Letters*, in press.

35 R. A. Dressler, R. H. Salter and E. Murad, *J. Chem. Phys.*, **99** (1993) 1159.

36 P. Tosi, O. Dmitrijev, Y. Soldo, D. Bassi, D. Cappelletti, F. Pirani and V. Aquilanti, *J. Chem. Phys.*, **99** (1993) 985.

37 F. S. Klein and I. Friedman, *J. Chem. Phys.*, **41** (1964) 1789.

38 T. F. Moran and I. Friedman, *J. Chem. Phys.*, **42** (1965) 2391.

39 R. Wolfgang, *Discus. Faraday Soc.*, **44** (1967) 179.

40 M. E. Weber, N. F. Dalleska, B. L. Tjelta, E. R. Fisher and P. B. Armentrout, *J. Chem. Phys.*, **98** (1993) 7855.

41 C. E. Dateo and D. C. Clary, *J. Chem. Soc., Faraday Trans.*, **85** (1989) 1685.

42 P. M. Hierl, *J. Chem. Phys.*, **67** (1977) 4665.

43 P. B. Armentrout, *Am. Chem. Soc. Symposium*, Series 502 (1992) 194.

44 K. J. Laidler, *Chemical Kinetics*, 1987, Harper and Row, New York.

Chapter 5

Electron-transfer and bond-forming reactions between CF_2^{2+} and H_2/D_2

5.1 Introduction

Previous investigations of the gas-phase reactivity between molecular dications and neutral molecules have, as mentioned in Chapter 1, concentrated mainly on the reaction channel involving single charge (electron) transfer from the neutral to the dicationic reactant [1-5]. However, other dication-neutral collision systems display other types of reactivity, such as collision-induced charge-separation (dissociation) [6] and collision-induced neutral-loss [7]. In addition to these reaction channels several dicationic reactants exhibit significant cross-sections for bond-forming reactivity with neutral diatomic targets [8,9].

To date, experimental investigations of the bond-forming reactivity between molecular dications and neutral species have been scarce, principally involving the identification of the product ions formed in collisions between molecular dications and neutral molecular collision partners using mass spectrometry. The bond-forming reaction that has received the most attention has been that between the CF_2^{2+} dication and D_2 [8-10]. This collision system has been shown to undergo the bond-forming reaction given by Equation 5.1:

$$CF_2^{2+} + D_2 \rightarrow DCF_2^+ + D^+ \qquad (5.1)$$

in addition to dissociative and non-dissociative electron-transfer reactions.

In the previous Chapter, isotope effects were considered from a theoretical perspective. Such isotope effects offer a powerful probe of the dynamics and mechanism of a chemical reaction. Hence, substituting H_2 in place of D_2 as the neutral collision partner in reactions with CF_2^{2+} should provide an insight into the reaction mechanism, by comparing the relative cross-sections of the electron-transfer and bond-forming reaction channels for the two collision systems. This investigation of the relative reactivity of the two collision systems may be performed simply by using mass spectrometric methods rather than measurements of the product ion scattering angle distributions.

Previous studies of electron-transfer reactivity [11] between monocations, such as Ar^+ and N_2^+ with neutrals such as H_2O and D_2O over a similar range of collision energies to those in the experiments presented in this thesis (3-13 eV in the laboratory frame), have revealed only slight isotope effects when isotopically substituted target gas reactants are used. These isotope effects are principally caused by differences between the vibrational levels of D_2 and H_2. Such differences in the vibrational energy cause subtle changes in the reaction exothermicity. As can be seen from figure 5.1, the reactant and product potential surfaces for electron-transfer between a monocationic species and a neutral are similar, as both are dominated by polarization attraction [12]. Because of this similarity between the potential surfaces, the Landau-Zener theory predicts efficient charge transfer reactivity only for

collision systems having small differences in their asymptotic energy, that is a small reaction exothermicity. Hence, although the energetic differences in the vibrational levels are small, they nevertheless may dramatically affect the electron-transfer reactivity.

The product and reactant potential surfaces for single electron-transfer in dication-neutral collision systems are fundamentally different to those of monocation-neutral collision systems. For dication-neutral systems the product potential is dominated by Coulombic repulsion, whilst the reactant potential is largely dominated by the polarization attraction [12]. The dissimilar potential surfaces result in efficient electron-transfer reactions having a significant exothermicity. Consequently, the small differences in reaction exothermicity that are caused by the differences in the vibrational energy content of the H_2 and D_2 neutral targets (< 0.15 eV) do not significantly affect the efficiency of the electron-transfer reaction. Hence, a comparison of the relative intensities of the products of bond-forming and electron-transfer reactions involving CF_2^{2+} with H_2 and D_2 collision systems will indicate if an isotope effect is in operation in the bond-forming process. This information provides a probe of the bond-forming reaction mechanism.

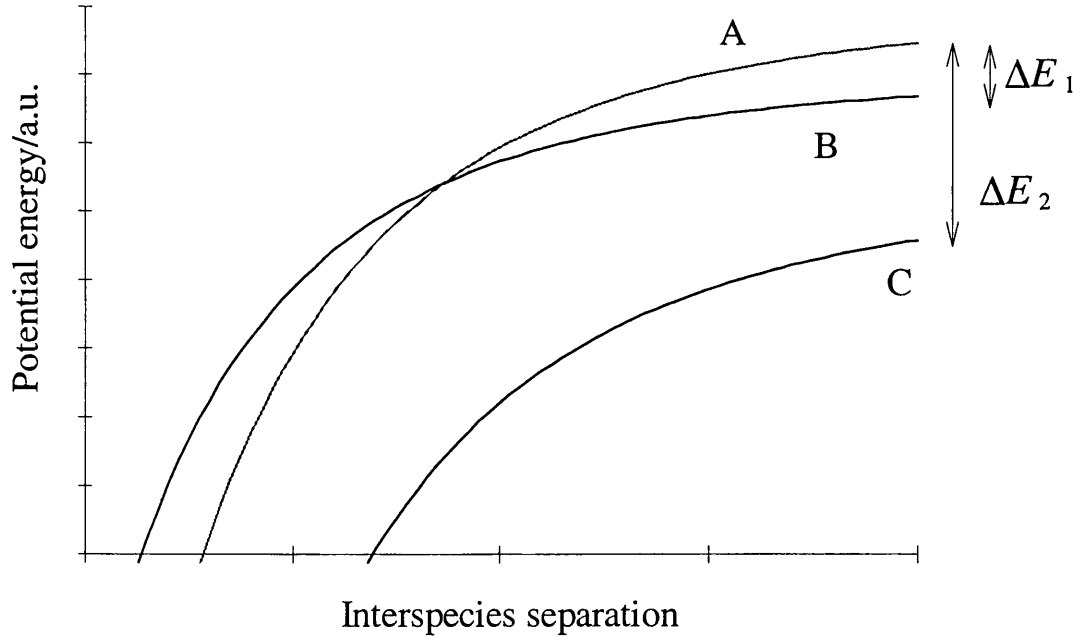

Figure 5.1a Schematic reactant and product potential energy curves for an electron-transfer reaction between a monocation and a neutral target. The relatively low reaction exothermicity (ΔE_1) allows curves A and B to cross permitting reaction. In contrast, the high value of ΔE_2 prevents the crossing of curve C with either A or B, therefore preventing reaction.

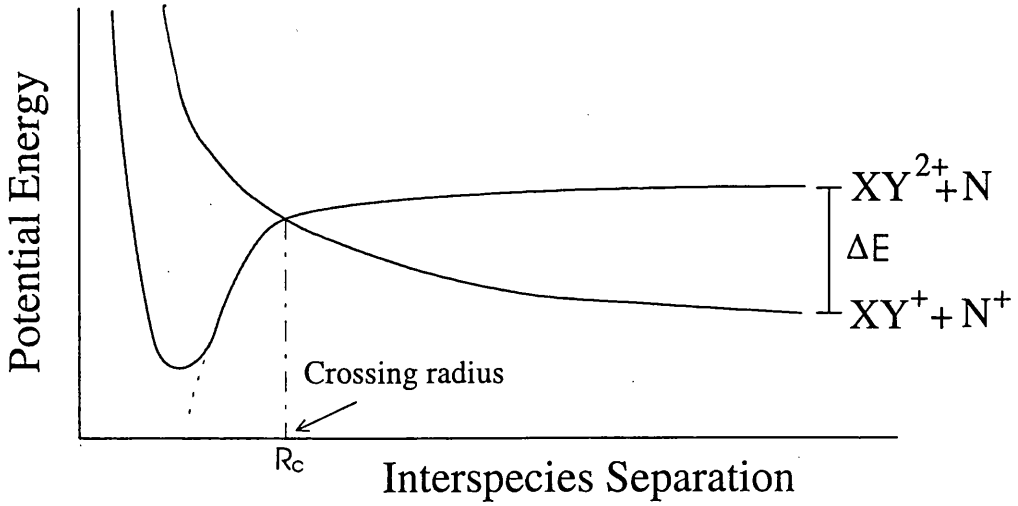

Figure 5.1b Schematic reactant and product potential energy curves for an electron-transfer reaction between a molecular dication and a neutral target.

5.2 Experimental details

A detailed account of the experimental methodology employed in the mass spectrometric measurements is given in Chapter 2. However, for this particular collision system, the pressure of the target gas was set at a gauge value of 2×10^{-6} Torr rather than the usual value of 4×10^{-6} Torr. Despite the fact that this value is half that of the usual value for non-hydrogen collision partners, the actual number densities of the target gases are in fact the same in each case. The pressures of hydrogen and deuterium gas targets are set at the lower value as a result of the insensitivity of the ion gauge to H_2/D_2 [13]. This insensitivity arises because of the higher ionization potentials of the hydrogen (and deuterium) targets relative to those of other gases such as ammonia, meaning that the gauge reads low for H_2, D_2 and HD gases.

Previous work [14] has indicated that the yield of the CF_2^+ product ion may be highly sensitive to the presence of excited electronic states of the reactant dication in the ion beam. Hence, to ensure that the electronic state distribution in the dication beam is the same throughout the course of the experiment, the operating conditions of the ion source are strictly controlled so as to be constant during the experiments [12].

5.3 Results and Analysis

Time-of-flight mass spectra were recorded following collisions between the dication and neutral reactants at laboratory frame collision energies in the range 3 to 13 eV, which corresponded to

centre-of-mass collision energies of ~0.2 to 1 eV for the dication/D_2, and ~0.1 to 0.5 eV for the dication/H_2 collision systems. The resulting TOF mass spectra indicate the presence of CF_2^+, CF^+, XCF_2^+, X_2^+ and X^+ (X = H or D) product ions in addition to that of the unreacted dications. Sections of representative time-of-flight mass spectra are shown in Figures 5.2 a and b.

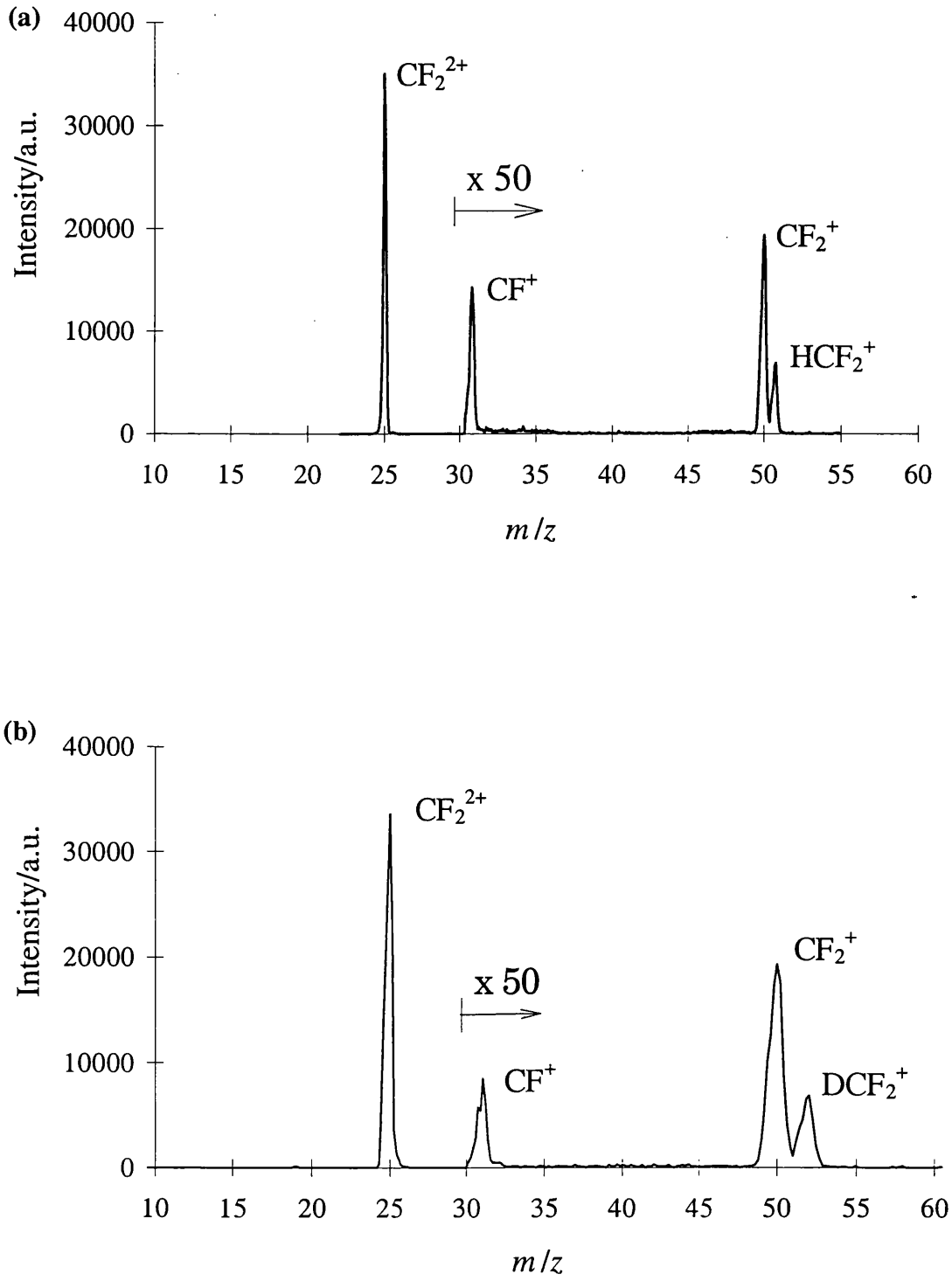

Figure 5.2 Sections of representative time-of-flight mass spectra showing the reaction products formed in collisions of the CF_2^{2+} molecular dication with (**a**) H_2, and (**b**) D_2 neutral collision partners, recorded at centre-of-mass frame collision energies of 0.50 and 0.74 eV, respectively.

5.3.1 Assignment of product ions

As mentioned above, the TOF mass spectra indicate the presence of CF_2^+, CF^+, XCF_2^+, X_2^+ and X^+ product ions. Representative values of the background-corrected product ion intensities, recorded following collisions between CF_2^{2+} and D_2, at a centre-of-mass collision energy of 2.53 eV, are given in Table 5.1. Note, the table does not include the intensity of the X_2^+ and X^+ ions. The reason for this is that the spectrometer has a low collection efficiency for ions formed from the neutral collision partner, so an accurate determination of these ion's intensities would be difficult to achieve. However, a number of mass spectra were recorded at various collision energies to determine, qualitatively, the presence of these ions. The TOF mass spectra also indicate the presence of a weak F^+ signal. However, when corrected for background ions this F^+ signal was not found to be a real product ion, and was therefore disregarded.

Table 5.1 Background-corrected intensities of product ions formed following collisions between CF_2^+ and D_2 at a collision energy of 0.741 eV.

CF^+	CF_2^+	DCF_2^+	CF_2^{2+}
356	723	192	92348

The product ion intensities, such as those in Table 5.1, indicate that three types of reactivity are observed. Firstly, the CF_2^+ product ion can only be formed as a result of non-dissociative electron-transfer (Equation 5.2). The second reaction process leads to the formation of CF^+ which may be formed either by means of dissociative electron-transfer or by collision-induced charge separation (CICS). However, the absence of a real F^+ signal in the mass spectra eliminates the possibility of the CF^+ being formed in CICS reactions. Hence, the CF^+ ion may be assigned as the product of a dissociative electron-transfer reaction (Equation 5.3).

A third type of reactive process, that leads to the formation of new chemical bonds, is also observed. This bond-forming reaction results in the generation of the XCF_2^+ product ion. The observation of an X^+ signal, together with the absence of any F^+ or XF^+, allows the formation of the XCF_2^+ product ion to be unambiguously assigned to the reaction given by Equation 5.4. Finally, the lack of any doubly-charged product ions in the mass spectra signifies that no collision-induced neutral-loss (CINL) reactivity occurs for the CF_2^{2+}/X_2 collision system at the energies employed in these experiments. This observation is in accord with the previous investigation of the gas-phase reactivity of CF_2^{2+} with D_2 [8]. The low probability of the CF_2^{2+} molecular dication undergoing a CINL reaction may be explained by the fact that the CF_2^{2+} dication, being isoelectronic with CO_2, has tightly bound F

atoms. In contrast, other perfluorinated dications, such as CF_3^{2+} and SF_4^{2+}, have some weakly bound F atoms and, hence, relatively large CINL reaction cross-sections [4,5,15].

$$CF_2^{2+} + X_2 \rightarrow CF_2^+ + [X+X]^+ \qquad (X = H, D) \qquad (5.2)$$

$$CF_2^{2+} + X_2 \rightarrow CF^+ + [X+X]^+ + F \qquad (X = H, D) \qquad (5.3)$$

$$CF_2^{2+} + X_2 \rightarrow XCF_2^+ + X^+ \qquad (X = H, D) \qquad (5.4)$$

5.3.2 Product ion intensities

The relative intensities of the XCF_2^+ ion, produced by the bond-forming reaction, and the CF_2^+ ion, produced by non-dissociative electron-transfer, are listed in Table 5.2 as a function of the centre-of-mass collision energy. This ratio is independent of the target gas number density and the incident dication beam current. In addition, this ratio should indicate whether an intermolecular isotope effect is in operation in the reaction process, as the cross-section for electron-transfer and therefore the CF_2^+ yield is, as discussed below, expected to be similar for reactions between CF_2^+ and both H_2 and D_2 [11]. As described below, this ratio is a powerful probe of the collision energy-dependence of the bond-forming reactivity of this collision system.

Tables 5.2 Background-corrected relative intensities of the bond-forming and electron-transfer product ions, as a function of the centre-of-mass collision energy (E_{com}), formed in collisions between CF_2^{2+} and H_2 (D_2). The uncertainties in the ratios are given in parentheses. Note, as will be shown later these relative intensities are a good representation of the relative cross-sections for the bond forming and electron-transfer reactions

E_{com} /eV	$\frac{I(HCF_2^+)}{I(CF_2^+)}$	E_{com} /eV	$\frac{I(DCF_2^+)}{I(CF_2^+)}$
0.115	0.503(±0.107)	0.222	0.362(±0.051)
0.192	0.339(±0.051)	0.370	0.349(±0.029)
0.269	0.350(±0.043)	0.519	0.294(±0.029)
0.346	0.380(±0.057)	0.667	0.267(±0.013)
0.423	0.342(±0.051)	0.815	0.252(±0.025)
0.500	0.291(±0.044)	0.963	0.217(±0.022)

As mentioned in Chapter 3, the effective detection efficiency of the product ions will depend upon their transverse velocity. Those ions having high transverse kinetic energies are detected less efficiently. As described above, a correction formula (Equation 5.5) may be used to obtain relative cross-section values for the bond-forming and electron-transfer reactions from ratios of the detected product ion intensities, such as those in Table 5.2.

$$\frac{\sigma_A}{\sigma_B} = \alpha \frac{I_A}{I_B} = \frac{I_A}{I_B} \frac{v_A}{v_B} \frac{L_B}{L_A} \tag{5.5}$$

where α is the correction factor applied to the relative intensities, σ is the cross-section of a given reaction process, I is the intensity of a given product ion, v is the transverse velocity of a given product ion, and L is the transverse length of a volume of the interaction region imaged onto the ion detector, for reactions A and B.

In practice the masses of the product ions CF_2^+ and XCF_2^+ (X = H or D) are very similar, as are their transverse velocities and the values of the impulse given to the ions as a result of the reaction process. Hence, as the detection efficiency for the products of electron-transfer and bond-forming reactions are very similar, the correction factor α is approximately unity. Representative values of the correction factor α for the two collision systems are given in Table 5.3. Hence, in this particular case, given the experimental uncertainties, the ratio of the relative ion signal intensities as shown in Table 5.2, effectively represents the ratio of the bond-forming and non-dissociative electron-transfer reaction cross-sections.

As described in Chapter 3, the values of the product ion and unreacted dication intensities are obtained by integration of the ion peaks of the time-of-flight mass spectra. Any contribution to the ion signals from background ions is calculated and subtracted using spectra recorded in the absence of the target gas.

Table 5.3 Relative detection efficiency correction factors (α) for the bond-forming and electron-transfer products formed in collisions between CF_2^{2+} with D_2 and H_2 at various centre-of-mass frame collision energies.

E_{com}/eV	$\alpha(D_2)$	$\alpha(H_2)$
0.1	1.050	1.080
0.2	1.045	1.067
0.3	1.047	1.061
0.4	1.055	1.057
0.5	1.088	1.055

Before the collision energy-dependence of the bond-forming reaction can be established from the ratio of the XCF_2^+ and CF_2^+ product ion intensities, such as those listed in Table 5.2, it is necessary to consider the collision energy-dependence of the electron-transfer reaction leading to the formation of CF_2^+ which is contained in the ratio of the XCF_2^+ and CF_2^+ intensities. Fortunately, the cross-section of the electron-transfer reaction that leads to the formation of CF_2^+ has been found, both by experimental observation and calculation [14], to be approximately constant over the range of collision energies used in this experiment. However, one factor that may cause an apparent isotope effect for

this reaction system concerns the relative ease of ionizing the target molecule to a particular vibration level. Hence, if it is much more likely to ionize the H_2 to a high vibrational level and D_2 to a low vibrational level or vice versa, then the resulting differences in the exothermicity of the electron-transfer reactions could be large enough to cause significant differences in the cross-sections for electron-transfer reactions between CF_2^{2+} and D_2/H_2. The possibility of an isotope effect being caused in this manner can be gauged by considering the Franck-Condon factors (FCF) for the ionization process, which is a measure of the ease of vibronic transition from a neutral to a ionic electronic state. Such an ionization process is represented in Equation 5.6.

$$X_2 (v'' = 0) \rightarrow X_2^+ (v' = 0 \rightarrow 8) + e^- \qquad (5.6)$$

The values of the FCF's were found in the literature for both gases [16]. In addition to this, approximate values of the Franck-Condon factors (FCF's) for the process of ionization of hydrogen and deuterium may be obtained from one of the many theoretical models [17-22]. One notable model that may be used to obtain approximate FCF values incorporates the Noumerov algorithm [22-24], which is used to find solutions of the one-dimensional vibrational Schrodinger equation. A detailed description of the methodology of the Noumerov algorithm, and the calculation of approximate FCF values using this method is given in Appendix 5.

The resulting calculated values of the FCF's for the transitions given by Equation 5.6, where X_2 is either H_2 or D_2, are listed in Tables 5.4a and b. The results also include values taken from the literature [16]. As may be observed from Tables 5.4a and b, there is excellent agreement between the literature and the FCF values derived from the iterative calculation described above. The similarities in the FCF values for the ionization of H_2 and D_2 suggest that the probabilities of populating a given vibrational level are approximately the same for the two target species. Hence, there should be no significant differences in the reaction exothermicities. The fact that the detected intensities of the D_2^+ and H_2^+ product ions are very similar provides evidence for the validity of the above conclusion.

Therefore, given the collision energy-independence of the electron-transfer cross-section, in addition to the similarities in the FCF values for the ionization of H_2 and D_2, the suitably corrected ratios of the XCF_2^+ and CF_2^+ product ion intensities provide a good representation of the cross-section of the bond-forming reaction. Hence, the collision energy-dependence of the bond-forming reaction for both the CF_2^{2+}-H_2 and CF_2^{2+}-D_2 collision systems may be seen in Figure 5.3, in which the background-corrected relative intensities of the XCF_2^+ and CF_2^+ products of the bond-forming and non-dissociative electron-transfer reactions are plotted as a function of the centre-of-mass collision energy.

Table 5.4a Comparison of calculated Franck-Condon factors for the ionizing transition $H_2(v = 0) \rightarrow H_2^+$ ($v = 0$ to 7), with values taken from the literature [16].

v''_{H_2}	$v'_{H_2^+}$	Calculated FCF	Literature FCF
0	0	0.0995	0.0871
0	1	0.1880	0.1555
0	2	0.2011	0.1793
0	3	0.1659	0.1515
0	4	0.1199	0.1193
0	5	0.0807	0.0879
0	6	0.0522	0.0624
0	7	0.0329	0.0434

Table 5.4b Comparison of calculated Franck-Condon factors for the ionizing transition $D_2(v = 0) \rightarrow D_2^+$ ($v = 0$ to 7), with values taken from the literature [16].

v''_{D_2}	$v'_{D_2^+}$	Calculated FCF	Literature FCF
0	0	0.0404	0.0328
0	1	0.1114	0.0829
0	2	0.1659	0.1217
0	3	0.1798	0.1370
0	4	0.1599	0.1318
0	5	0.1241	0.1147
0	6	0.0871	0.0934
0	7	0.0564	0.0728

The relative intensities of the XCF_2^+ and CF_2^+ product ions, as listed in Table 5.2 and illustrated in Figure 5.3, show that the probability of forming XCF_2^+ is independent of which hydrogen isotope is used as the collision partner, indicating the absence of an isotope effect in the bond-forming reaction. In addition, the results show that the cross-section for the bond-forming reaction increases with decreasing collision energy.

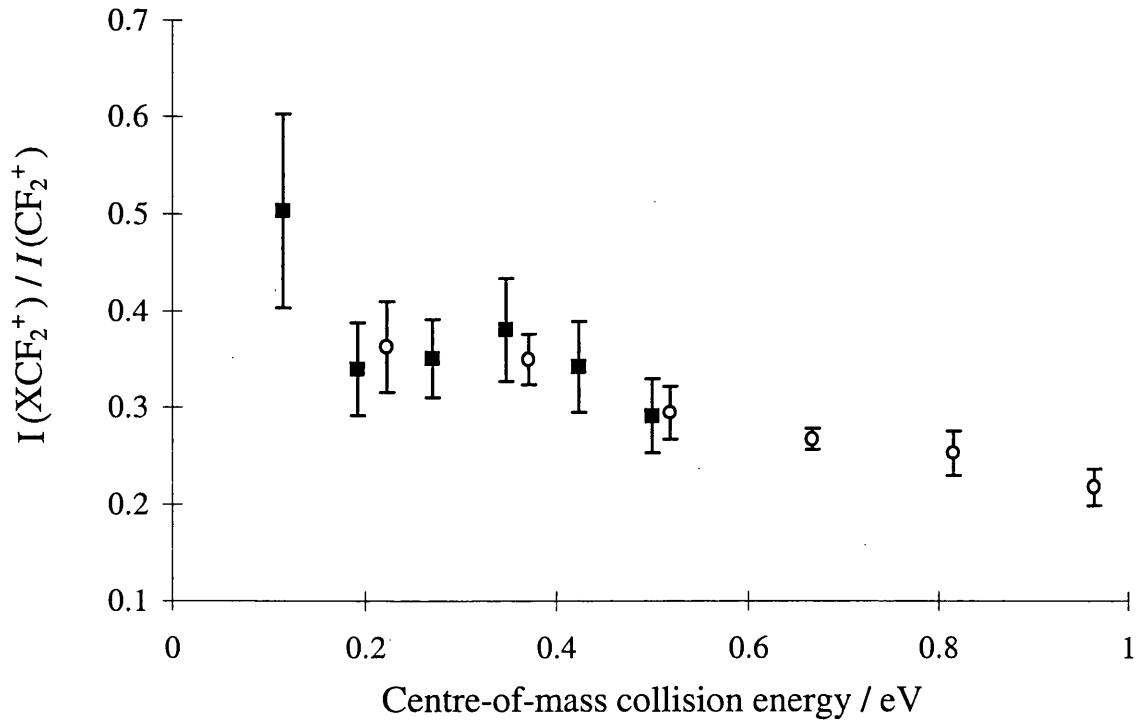

Figure 5.3 Collision energy-dependence of the ratios of the intensities of bond-forming/electron-transfer product ions generated in the reaction of CF_2^{2+} with H_2 (■) and D_2 (O)neutral targets.

5.4 Discussion

5.4.1 Analogous reactivity and the applicability of the reaction window theory

Consider the bond-forming reaction between the CF_2^{2+} dication and the neutral D_2 target

$$CF_2^{2+} + D_2 \rightarrow DCF_2^+ + D^+ \qquad (5.7)$$

This bond-forming reaction may crudely be considered as effectively arising via the transfer of a deuteride (D^-) ion from the neutral D_2 to the molecular dication. Analogous reactivity has been observed following collisions between transition-metal dications and small hydrocarbons such as C_2H_6 [25]. In these reactions the metal dications abstract hydride ions from the neutral hydrocarbon as in Equation 5.8.

$$Nb^{2+} + C_2H_6 \rightarrow NbH^+ + C_2H_5^+ \qquad (5.8)$$

In an attempt to explain the reactivity of the transition metal dication/alkane collision system, the reaction process has been rationalized using a 'curve crossing' model based on the Landau-Zener theory of electron-transfer [26,27]. A full account of this theory is given in Chapter 4. However, in the case of bond-forming reactivity, instead of electron-transfer, the model is adapted to describe the transfer of a hydride (H^-) or deuteride (D^-) ion. This adapted Landau-Zener theory therefore treats hydride transfer in exactly the same manner as electron-transfer; that is the H^-/D^- transfer is qualitatively viewed as the transfer of a heavy electron [25,28,29].

As mentioned in Chapter 4, for the H^- transfer reaction to proceed the reactant and product curves must intersect at an interspecies separation within a restricted range of values, this range is termed the *reaction window.* Analysis of the exothermicities and potential curves for reaction between transition metal dications and a variety of neutral alkane target molecules has indicated that the reaction window for the hydride-transfer reaction (bond-forming) lies in the range of 0.4 to 0.6 nm. This range is lower than that for electron-transfer. This difference was rationalized as being caused by the considerable difference in the relative masses of the transferred electron and hydride ion.

In the first investigation of bond-forming reactivity between molecular dications and neutral target molecules, Price *et al* [8] examined a number of molecular dication/neutral collision systems. It was found that many collision systems exhibited bond-forming reactivity. For those systems that exhibited bond-forming reactions the relevant crossing radii were calculated. The values of these crossing radii almost exclusively fell in the range of 0.17 to 0.69 nm, which, considering the uncertainties in the thermodynamic data used in the calculation offered good qualitative agreement with the predictions of the Landau-Zener model of the hydride-transfer reaction.

Despite the apparent similarity of the hydride-transfer reactions between transition metal dications and alkanes to that of molecular dications with neutral collision partners, a number of problems arise when the Landau-Zener model is applied to the bond-forming reactions between molecular dications and neutral targets. Firstly, not all collision systems exhibit bond-forming reactivity. For example, the reaction between the nitrogen molecular dication and hydrogen has several possible bond-forming reaction channels such as:

$$N_2^{2+} + H_2 \rightarrow HN_2^+ + H^+ \qquad (5.9)$$

However, no bond-forming reactivity is observed for this collision system, even though the exothermicities of the possible bond-forming reactions would place the curve crossing at a favourable position inside the reaction window.

The second problem with the applicability of the Landau-Zener model to bond-forming reactions concerns the dynamic effects caused by differences in the mass of the transferred reactant. The Landau-Zener model of the transfer of the hydride ion may be pictured as the tunnelling of the H^- between the potential wells of the neutral reactant and the dication at the intersection of the reactant and product potential energy surfaces. Logically, the Landau-Zener model suggests that a lighter particle, such as H^- should therefore be transferred with a greater efficiency than heavier particles such as D^-. Hence, this model of H^-/D^- transfer qualitatively predicts that the cross-section for the formation of the HCF_2^+ bond-forming product ion should be markedly greater than the corresponding cross-section for the formation of DCF_2^+ because of the greater efficiency of transferring the lighter H^- ion. However , as can be seen from the results of our investigation (Figure 5.3), this work shows that at a

given centre-of-mass collision energy, the ratio of the cross-sections of the bond-forming and the electron-transfer reactions is, within the experimental uncertainties, the same for both the CF_2^{2+}/D_2 and CF_2^{2+}/H_2 collision systems. Hence, the bond-forming reaction cross-section is independent of which isotope of hydrogen is used as the collision partner. This observation clearly indicates an absence of a measurable isotope effect, contradicting the expected behaviour predicted by the Landau-Zener model, and therefore casts doubt on the applicability of this physical model of dication reactivity.

5.4.2 Mechanistic conclusions

As stated in Chapter 4, isotope effects are a powerful probe of the reaction dynamics. The lack of an isotope effect is consistent with the operation of a direct ('spectator-stripping') reaction mechanism in which the dication strips off the hydride ion from the neutral target as it passes it during the 'collision' [30,31]. If such a stripping-direct mechanism is operating, differences in the bond-forming reaction cross-sections may still be apparent if the cross-sections are plotted against the centre-of-mass collision energy. However, as described in Chapter 4, there should be no sign of an isotope effect if the cross-sections are plotted against the pairwise energy [11,32].

Consider the general reaction:

$$A^+ + BC \rightarrow AB^+ + C \tag{5.10}$$

In the pairwise energy model the reaction is considered as occurring solely between the reactant ion (A) and the transferred part of the neutral reactant (B), the non-transferred fragment (C) of the neutral reactant is deemed as being unaffected by the reaction process. The centre-of-mass collision energy is given by:

$$E_{com} = \frac{\mu v^2}{2} = \frac{m_A(m_B + m_C)v^2}{2(m_A + m_B + m_C)} \tag{5.11}$$

where m_I is the mass of I, and v is the magnitude of the relative velocity of the reactants $|v_A - v_{BC}|$. As stated above, in the pairwise model, the untransferred fragment (C) does not affect the reaction process. Therefore, for reactions of this type the effective collision energy, the *pairwise energy* E_{pair}, is determined from the kinematics of the reactants participating in the reaction process, in this case (A) and (B). Hence the pairwise energy is given by:

$$E_{pair} = \frac{m_A m_B v^2}{2(m_A + m_B)} \tag{5.12}$$

In the pairwise model, the relative velocity v is unchanged as $v_B = v_{BC}$. Hence, the substitution of Equation 5.11 into Equation 5.12 gives the pairwise energy E_{pair} in terms of E_{com}:

$$E_{pair} = E_{com} \frac{Mm_B}{(m_A + m_B)(m_B + m_C)} \tag{5.13}$$

where $M = (m_A + m_B + m_C)$. For a reaction of this type, no isotope effect is expected if only kinematic arguments are considered. That is, the reaction isotope effect disappears when the relative cross-sections for the bond-forming reaction are plotted with respect to the pairwise energy.

As can be calculated from Equation 5.13, in the case of hydrogen/deuterium neutral targets, the pairwise energy for the reaction between the CF_2^{2+} and the neutral target, is within 2%, the same fraction of the centre-of-mass collision energy. Hence, in the case of the $CF_2^{2+}/H_2/D_2$ collision system, plotting the relative cross-sections of the bond-forming and electron-transfers reactions as a function of the centre-of-mass collision energy is effectively the same as plotting the relative cross-sections as a function of the pairwise energy.

The absence of any isotope effects in the reaction between CF_2^{2+} and both H_2 or D_2, although consistent with the operation of a 'spectator-stripping' direct type reaction mechanism, is, in itself, not definitive, as the lack of an isotope effect does not eliminate the possibility of complexation although it means it is unlikely. However, this conclusion is consistent with those of a recent crossed-beam scattering experiment [9]. In this experiment, which measured the scattering angle distribution of the products of the reaction between CF_2^{2+} and D_2, the DCF_2^+ product ion was observed to be predominantly forward scattered. This scattering distribution is a definitive indicator of the operation of a spectator-stripping direct mechanism.

As can be seen in Figure 5.3, the relative yield of the products of bond-forming (DCF_2^+ and HCF_2^+) and electron-transfer reactivity (CF_2^+) increases with decreasing collision energy. The observed collision energy-dependence may be qualitatively explained as arising because at lower collision energies the reactant's relative velocities will be correspondingly lower and therefore the reactants will be within a range of interspecies separations that are favourable for chemical reaction for longer periods of time. That is, the 'interaction time' is increased.

The fact that the yield of the bond-forming reaction increases with decreasing collision energy, down to centre-of-mass collision energies of ~0.1 eV, strongly indicates the absence of an energy barrier to reaction. This conclusion is supported by the failure of the Landau-Zener model to account for the absence of an isotope effect in the H^-/D^- transfer reaction between CF_2^{2+} and H_2/D_2, as the Landau-Zener theory, which involves a barrier to reaction, also predicts an isotope effect.

The failure of the Landau-Zener model to account for the H^-/D^- transfer reaction between CF_2^{2+} and H_2/D_2 is in contrast to H^- transfer reactivity in transition metal dication/alkane collision systems. Given the successful application of the Landau-Zener model apparent to atomic dication/neutral reactivity described above, the flawed applicability of the Landau-Zener model to H^-/D^- transfer reactivity between CF_2^{2+} and H_2/D_2 is likely to be caused by differences in the form of the charged reactant. The atomic transition metal dication is a very much closer approximation of a point

charge, which was the original form of charged species modelled by Landau and Zener, than a polyatomic dication such as CF_2^{2+}. In addition the Landau-Zener model makes no attempt to allow for the anisotropy of the electric field exerted by the molecular dication, or the many possible permutations of crossings between each of the different vibrational states of the reactants and products.

5.5 Conclusion

The intensities of the product ions generated in bond-forming (XCF_2^+) and electron-transfer (CF_2^+) reactions between CF_2^{2+} and X_2 (X = H or D), have been recorded at laboratory frame collision energies between 3 and 13 eV. The ratios of the intensities of the two categories of product ion indicate that no isotope effect occurs when H_2 is used in place of D_2. That is, the probability of forming XCF_2^+ is independent of the choice of hydrogen isotope as the neutral collision partner. The absence of an isotope effect rules out the application of the Landau-Zener model of H^-/D^- transfer reactivity to the CF_2^{2+}-H_2/D_2 collision systems. In addition, the lack of an isotope effect is consistent with the operation of a direct type spectator-stripping reaction mechanism.

The results show that the yield of the bond-forming product XCF_2^+ increases with decreasing collision energy. This collision energy dependence may be qualitatively explained as arising as a result of the increased time the (lower energy) reactants spend at interspecies separations that are suitable to allow the formation of chemical bonds. In addition, the collision energy dependence strongly indicates that there is no energy barrier to hydride/deuteride ion transfer for the CF_2^{2+}-H_2/D_2 collision systems.

References

1 D. Price, S. A. Rogers and S. R. Leone, *J. Chem. Phys.*, **98** (12) (1993) 9455.

2 S. A. Rogers, S. D. Price and S. R. Leone, *J. Chem. Phys.*, **98** (1) (1993) 280.

3 M. Manning, S. D. Price and S. R. Leone, *J. Chem. Phys.*, **98** (11) (1993) 8695.

4 C. E. Melton and G. F. Wells, *J. Chem. Phys.*, **27** (1957) 1152.

5 Z. Herman, P. Johnathon, A. G. Brenton and J. H. Beynon, *Chem. Phys. Letters,* **41** (1989) 433.

6 S. E. Kupryanov, *Soviet J. Phys. Tech. Phys.*, **9** (1964) 659.

7 S. D. Price, M. Manning and S. R. Leone, *Chem. Phys. Letters,* **214** (1993) 553.

8 S. D. Price, M. Manning and S. R. Leone, *J. American Chem. Soc.,* **116** (1994) 8675.

9 Z. Dolejsek, M. Farnik and Z. Herman, *Chem. Phys. Letters,* **235** (1995) 99.

10 K. A. Newson and S. D. Price, *Chem. Phys. letters,* **269** (1997) 93.

11 R. A. Dressler, R. H. Salter and E. Murad, *J. Chem. Phys.*, **99** (1993) 1159.

12 A. Ehbrecht, N. Mustafa, C. Ottinger and Z. Herman, *J. Chem. Phys.*, **105** (1996) 9833.

13 Manufacturers operating manual (Edwards Ltd 1995).

14 K. A. Newson and S. D. Price, *Paper in press.*

15 Y. Lee, S. R. Leone, P. Champkin, N. Kalysoyannis and S. D. Price, *J. Chem. Phys.*, **106** (1997) 7981.

16 G. H. Gunn, *J. Chem. Phys.*, **44** (1966) 2592.

17 J. W. Moore, *J. Chem. Education,* **60** (1983) 207.

18 C. Kubach, *J. Chem. Education,* **60** (1983) 212.

19 J. Lerme, *Chem. Phys.,* **145** (1990) 67.

20 F. M. Fernandez and J. F. Ogilvie, *Chem. Phys. Letters,* **169** (1990) 292.

21 R. W. Nicholls, *J. Chem. Phys.*, **74** (1981) 6980.

22 U. Blukis and J. M. Howell, *J. Chem. Education,* **60** (1983) 205.

23 R. L. Dunbrack, *J. Chem. Education,* **63** (1986) 952.

24 B. Noumerov, *Royal Astron. Soc.,* **84** (1924) 592.

25 R. Tonkyn and J. C. Weisshaar, *J.American Chem. Soc.*, 108 (1986) 7128.

26 L. Landau, *Phys. Z. Sov.*, **2** (1932) 46.

27 C. Zener, *Proc. Royal Soc. London Ser A,* **137** (1932) 696.

28 L. M. Roth, B. S. Freiser, *Mass Spectrom. Rev.,* **10** (1991) 303.

29 P. Johnathon, M. Hamdan, A. G. Brenton and G. D. Whillet, *Chem. Phys,*. **119** (1988) 159.

30 R. D. Levine and R. B. Bernstein, *Molecular reaction dynamics and chemical reactivity,* 1987 Oxford University Press, New York.

31 K. Tanaka, T. Kato, P. M. Guyon and I. Koyano, *J. Chem. Phys.*, **79** (1983) 4302.

32 J. L. Elkind and P. B. Armentrout, *J. Chem. Phys.*, **84** (1986) 4862.

Chapter 6

Electron-transfer and bond-forming reactions between CF_2^{2+} and NH_3

6.1 Introduction

Studies of bond-forming gas-phase reactivity involving molecular dications and neutral targets have been limited to the reactions of molecular dications with small diatomic molecules, notably D_2 and H_2 [1-4], at low collision energies. This Chapter reports the first observation of a bond-forming reaction between a molecular dication (CF_2^{2+}) and a polyatomic molecule, NH_3. The experimental results reveal the collision energy-dependence of both the electron (charge)-transfer and the bond-forming reaction processes. Such results provide important information regarding the mechanism of bond-formation in this collision system. In addition to this, NH_3 possesses a dipole moment, unlike the D_2 and H_2 diatomic collision partners listed above. The presence of the dipole moment, and its effects upon the bond-forming reaction, may also provide an insight into the mechanism of the bond-forming process.

6.2 Experimental details

A detailed description of the experimental apparatus and methodology is given in Chapter 2. The ammonia collision partner is obtained from a lecture bottle (Aldrich) and is stored in a low pressure (< 700 Torr) reservoir. The number density of the neutral collision partner in the interaction region is strictly maintained at a constant value; this is achieved by the careful monitoring of the target gas pressure, which is nominally set at 4×10^{-6} Torr. The stringent regulation of the target gas pressure not only ensures single collision conditions, but also attempts to avoid pressure related deviations in the intensities of the product ions. Hence, any deviations in the product ion intensities may then be attributed directly to fundamental changes in the reaction process.

Previous work [5] has indicated that the yield of the CF_2^+ product ion may be highly sensitive to the electronic state of the reactant dication. Hence, to ensure that the electronic state distribution in the dication beam is uniform during the course of the experiment, the operating conditions of the ion source are strictly controlled so as to be constant during the running of the experiments [6].

6.3 Results and analysis

Time-of-flight mass spectra were recorded following collisions between CF_2^{2+} and NH_3 at laboratory-frame collision energies between 2 and 15 eV; these correspond to centre-of-mass frame collision energies between 0.5 and 4 eV. The resulting TOF mass spectra indicate the presence of CF_2^+, CF^+, $HNCF^+$, C^+, NH_3^+, NH_2^+ and H^+ product ions in addition to unreacted dications. A section of a representative time-of-flight mass spectrum is shown in Figure 6.1.

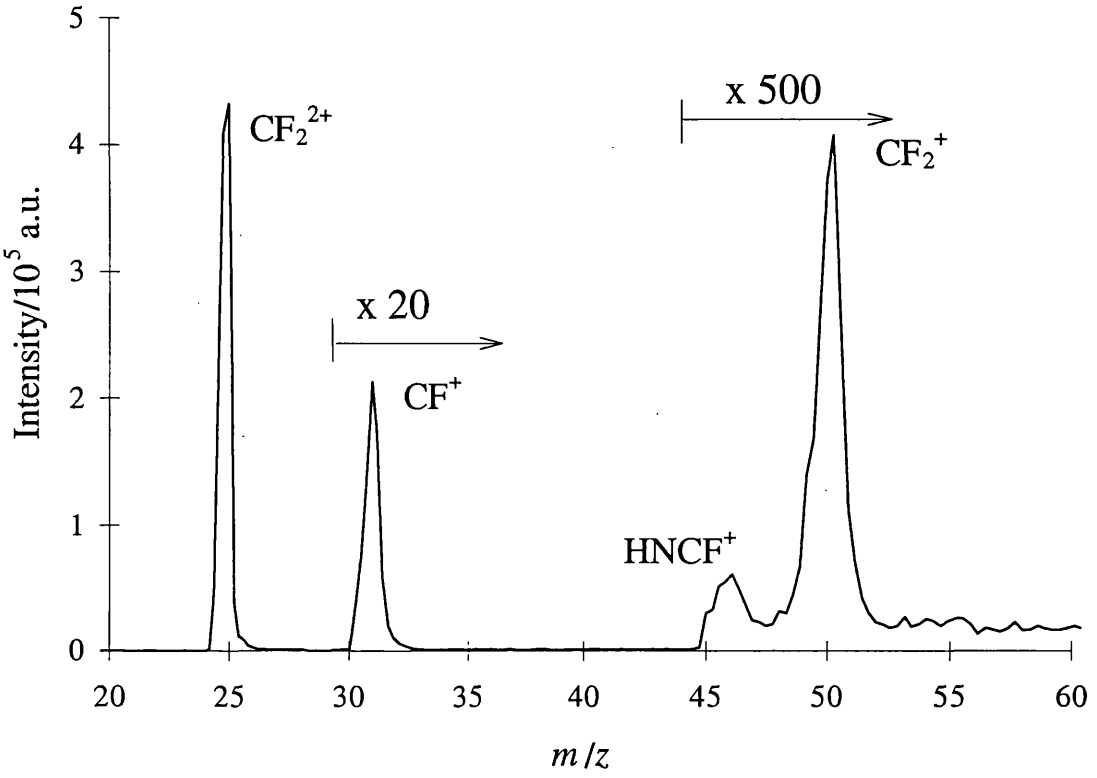

Figure 6.1 A section of a representative time-of-flight mass spectrum showing some of the product ions formed in collisions between CF_2^{2+} and NH_3 at a centre-of-mass frame collision energy of 2.03 eV.

6.3.1 Assignment of product ions

As mentioned above, the TOF mass spectra indicate the presence of CF_2^+, CF^+, $HNCF^+$, C^+, NH_3^+, NH_2^+ and H^+ product ions. Representative values of the background-corrected product ion intensities, recorded at a centre-of-mass collision energy of 2.53 eV are given in Table 6.1.

Table 6.1 Background-corrected product ion intensities, recorded at a centre-of-mass collision energy of 2.53 eV

CF_2^{2+}	CF_2^+	CF^+	$HNCF^+$	NH_3^+	NH_2^+	C^+	H^+
105581	3752	32736	327	13359	263	70	42

Of the various types of reactivity encountered in dication-neutral molecule collisions described in Chapter 1, the product ions observed following collisions between CF_2^{2+} and NH_3 indicate that three main reaction pathways occur at the collision energies used in these experiments. Firstly, the CF_2^+ product ion can only be formed as a result of the non-dissociative electron-transfer reaction given in Equation 6.1. Secondly, the CF^+ and C^+ product ions may be formed either by dissociative electron-transfer or by collision-induced charge-separation (CICS). However, the absence of any real F^+ signals in the mass spectra eliminates the possibility of the CF^+ and C^+ ions being formed in CICS reactions.

Hence, the CF^+ and C^+ products must be formed by dissociative electron-transfer reactions (Equations 6.2 and 6.3). Similarly, the NH_2^+ and NH_3^+ product ions must also be formed in electron-transfer reactions, with the NH_2^+ product being formed as a result of the NH_3 losing an electron to populate a dissociative electronic state of NH_3^+.

$$CF_2^{2+} + NH_3 \rightarrow CF_2^+ + [NH_3]^+ \quad (6.1)$$

$$CF_2^{2+} + NH_3 \rightarrow CF^+ + [NH_3]^+ + F \quad (6.2)$$

$$CF_2^{2+} + NH_3 \rightarrow C^+ + [NH_3]^+ + 2F \quad (6.3)$$

A third type of reactive process, leading to the formation of a new chemical bond, is also observed. This reaction results in the formation of the $HNCF^+$ product ion. The observation of an H^+ signal, together with the absence of F^+, H_2^+ or HF^+ strongly indicates that the $HNCF^+$ product ion is formed in the reaction given in Equation 6.4.

$$CF_2^{2+} + NH_3 \rightarrow HNCF^+ + H^+ + [F + H] \quad (6.4)$$

The lack of any doubly-charged product ions in the mass spectra signifies that no collision-induced neutral-loss (CINL) reactions occur in the CF_2^{2+}/NH_3 collision system at the collision energies employed in these experiments. This observation, which was also made in Chapter 5, indicates that the CF_2^{2+} molecular dication does not undergo CINL reactivty. The absence of CINL reactivity in CF_2^{2+}/neutral collision systems is in contrast to larger perfluorinated dications such as CF_3^{2+} and SF_4^{2+} which display relatively strong CINL reactivity [4,7]. This behaviour may be explained by the fact that the CF_2^{2+} dication, being isoelectronic with CO_2, has tightly bound F atoms. In contrast, other perfluorinated dications such as CF_3^{2+} and SF_4^{2+} have some weakly bound F atoms and, hence, relatively large CINL cross-sections [8].

6.3.2 Product ion intensities

In common with the results of all the collision experiments reported in this thesis, the intensities of the competing electron-transfer and chemical (bond-forming) reaction channels are obtained from suitably background ion-corrected measurements of the detected intensities of the product ions. In addition to the background ion contribution, the product ion intensities are also corrected for variations in the ion detection efficiency.

As stated in Chapter 3, dication reactions may result in a significant release of kinetic energy. This kinetic energy release (KER) in the centre-of-mass frame affects the product ions translational energy component in the laboratory frame [3]. Each of the reaction channels may have differing average KER values and differing distributions of the KER. Consequently, different product ions may have different transverse velocities. Therefore, due to their different transverse velocities, the product ions will travel through different distances across the spectrometer, in a plane perpendicular to its

central (longitudinal) axis, in the transit time between leaving the spectrometer's source region and reaching the MCP detector. The overall result of the differing transverse velocities of the product ions is that the length of the source region imaged onto the MCP detector varies with the transverse component of the product ion's kinetic energy. The greater the length imaged onto the detector the greater is the effective efficiency with which an ion is detected. Hence, as described in Chapter 3, the analysis procedure involves the use of a correction formula, which makes allowance for such differences in the ion detection efficiencies. A detailed discussion of the methodology behind the background ion correction and the subsequent correction for the detection efficiency variability is given in Chapter 3.

Unfortunately, no data concerning the KER values and distributions for the electron-transfer and bond-forming reactions between CF_2^{2+} and NH_3 is available in the literature. Hence, in view of this paucity of data, the analogous KER data for the CF_2^{2+}/D_2 collision system [3] is used in the correction process mentioned above. This use of the KER data for the CF_2^{2+}/D_2 collision system does not represent a major approximation as the KER will be dominated by the Coulombic repulsion between the two singly-charged product ions for both the bond-forming and electron-transfer reactions.

To examine the collision energy-dependence of the bond-forming reaction, the resulting intensity of the $HNCF^+$ ion relative to the intensities of both the unreacted dication and the CF_2^+ ion are listed as a function of the centre-of-mass frame collision energy in Table 6.2 and illustrated in Figures 6.2 and 6.3. The intensity of $HNCF^+$ relative to CF_2^+ is independent of the target gas pressure, and represents the branching ratio for the bond-forming and non-dissociative electron-transfer reactions. As stated above, the table also lists the ratio of the intensities of the $HNCF^+$ bond-forming product ion to that of the unreacted dication. Although this ratio is pressure-dependent, the experiments were performed under effectively identical conditions. Therefore, the ratio of the $HNCF^+$ ion intensity to that of the unreacted dication serves as a sound indicator of the intensity of the bond-forming reaction at a given collision energy, without the complication of possible changes in the intensity of the electron-transfer reaction that are contained in the $HNCF^+/CF_2^+$ ratio. However, as can be seen from the similarity of Figures 6.2 and 6.3, the cross-section of the electron-transfer reaction producing CF_2^+ displays little change across the range of centre-of-mass collision energies used in these experiments. The absence of any significant variation in the intensity of the CF_2^+ ion with a change in collision energy supports the conclusions of the previous Chapter. Namely, that the cross-section for the non-dissociative electron-transfer reaction leading to the formation of the CF_2^+ product ion is effectively constant across the range of collision energies used in these experiments.

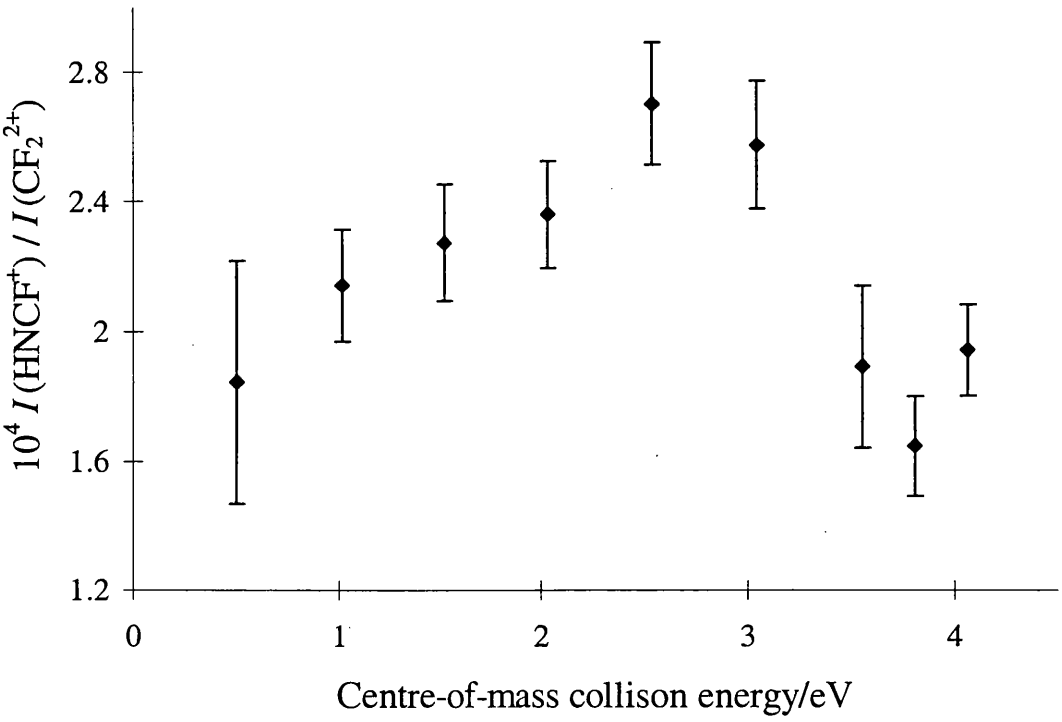

Figure 6.2 Corrected intensity of the $HNCF^+$ product ion relative to that of the unreacted CF_2^{2+} dication, as a function of the centre-of-mass collision energy.

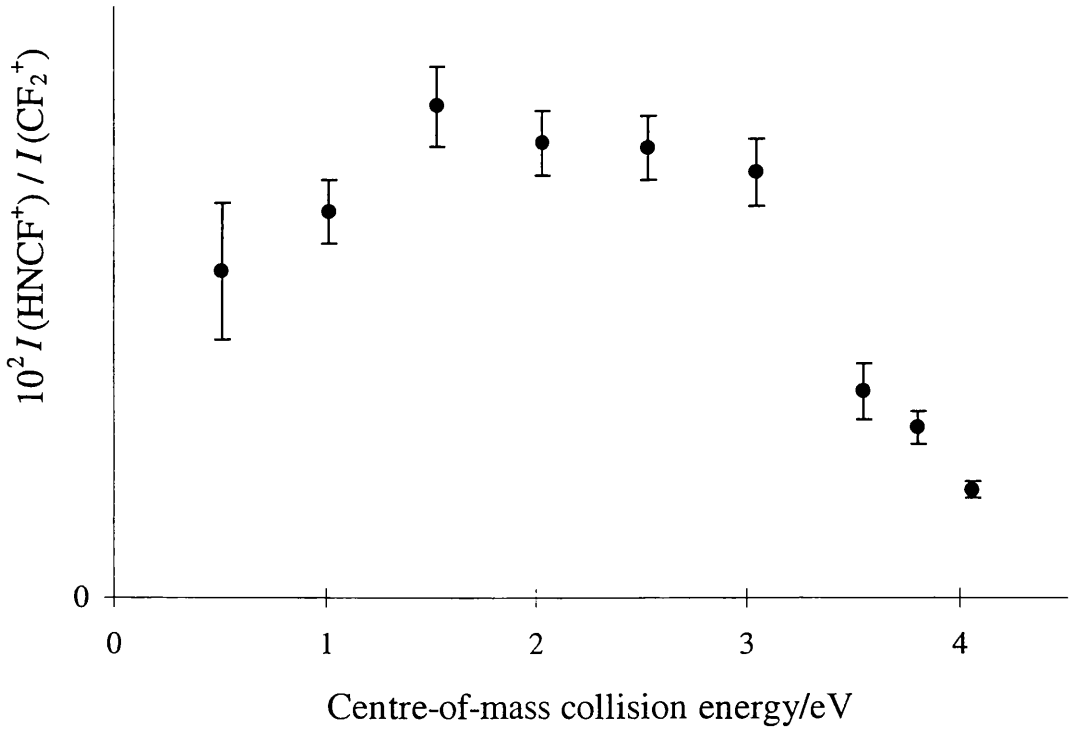

Figure 6.3 Corrected intensity of the $HNCF^+$ product ion relative to that of the CF_2^+ product ion as a function of the centre-of-mass collision energy.

Table 6.2 The variation with centre-of-mass collision energy E_{com} of the corrected relative intensities of product ions formed in collisions between CF_2^{2+} and NH_3.

E_{com}/eV	$10^4 \frac{I(HNCF^+)}{I(CF_2^{2+})}$	$10^2 \frac{I(HNCF^+)}{I(CF_2^+)}$
0.5	1.84	1.66
1.0	2.14	1.96
1.5	2.27	2.50
2.0	2.36	2.31
2.5	2.70	2.28
3.1	2.58	2.16
3.6	1.89	1.05
3.8	1.65	0.87
4.1	1.94	0.55

6.4 Discussion

6.4.1 Electron-transfer reactions

As may be seen in Table 6.1, electron-transfer reactions, both dissociative and non-dissociative, dominate the gas-phase reactivity between CF_2^{2+} and NH_3. The dominant process being the dissociative electron-transfer reaction that leads to the formation of the CF^+ product ion. The rationalization of the observed relative intensities of the products of electron-transfer has been shown to be a reliable source of information regarding the composition of the reactant beam [5]. Therefore, in an attempt to account for the observed product ion intensities, the yields of the electron-transfer processes have been calculated using a computational method based on the semi-classical Landau-Zener theory of electron-transfer [9-12]. This treatment allows the electron-transfer products that are derived from the neutral reactant to be unambiguously assigned. As can be seen from Equations 6.1-6.3, the definitive assignment of such ions is not always possible.

Although originally intended to model electron-transfer between atomic species [9-12], the Landau-Zener theory has previously been used to model electron-transfer reactivity between molecular dications and neutral rare gas targets and was found to give reliable results [4,5,13-15]. A detailed account of the Landau-Zener theory is given in Chapter 4. The computer model employing the Landau-Zener theory calculates the reaction probability as a function of the impact parameter and the electronic state energy of the principle product ion. The computer program can then be used to estimate electron-transfer cross-sections by integrating the reaction probability with respect to the impact parameter from zero to the maximum value for which the collision reaches the crossing radius.

This produces an estimate of the electron-transfer cross-section for the formation of a product ion with a particular amount of electronic excitation.

In the case of the CF_2^{2+}/NH_3 collision system, the calculated cross-section for forming a particular product ion in an electron-transfer reaction is given as the sum of the individual cross-sections for populating each electronic state of CF_2^+ that fragments to form the product ion of interest. The CF_2^+ ion has three relevant dissociation channels, (forming $CF^+ + F$, $C^+ + 2F$ and $F^+ + CF$). The energies of these dissociation asymptotes E_{ass}, relative to the ground electronic state of the CF_2^+ ion, are listed in Table 6.3. The energies of the low-lying electronic states of CF_2^+ relative to the ground state ion have been determined both experimentally, by photoelectron spectroscopy, and by *ab initio* calculation by Dyke *et al* [16] and are listed in Table 6.4. These electronic state energies are needed as in constructing this model we assume that if a CF_2^+ ion is formed in an electronic state that lies above a dissociation asymptote, it dissociates to give the products corresponding to that particular asymptote. If the CF_2^+ ion is formed in an electronic state that lies above more than one dissociation asymptote, it is assumed that the ion dissociates into the closest-lying limit. For example, as can be seen from Tables 6.3 and 6.4, CF^+ product ions are formed as a result of CF_2^+ populating the five electronic states lying at energies between 2.5 eV and 10.5 eV above the electronic ground state. Therefore, the cross-section for the dissociative electron-transfer reaction for forming CF^+ is simply the sum of the calculated cross-sections for populating each of the five electronic states lying at energies between 2.5 eV and 10.5 eV relative to the electronic ground state of CF_2^+.

Table 6.3 Dissociation channels of the CF_2^+ ion and their asymptotic energies, relative to the ground electronic state of CF_2^+ [5].

Dissociation Channel	E_{ass}/eV
$CF_2^+ \rightarrow CF^+ + F$	2.5
$CF_2^+ \rightarrow C^+ + 2F$	10.5
$CF_2^+ \rightarrow F^+ + CF$	11.0

The Landau-Zener model also requires data regarding the relative energies of the reaction products and reactants to calculate the reaction exothermicity, which in turn determines the curve crossing radius. As demonstrated above, the energies of the electronic states of CF_2^+ are reasonably well known. However, there is a paucity of analogous data concerning the CF_2^{2+} dication. A previous study of the electron-transfer of CF_2^{2+} with rare gas targets [5] has indicated that that the electronic ground state of CF_2^{2+} lies between 32 and 33 eV above the ground state of CF_2. The same study also indicated the presence of a long-lived excited state of the dication, lying between 35 and 37.5 eV above

the ground state of neutral CF_2. In the absence of more precise data, the above energetics of CF_2^{2+} are used in the Landau-Zener calculations.

Table 6.4 Relative energies of the low-lying electronic states of CF_2^+ [16].

Electron ionized	$6a_1$	$4b_2$	$1a_2$	$5a_1$	$1b_1$	$3b_2$	$4a_1$
Energy/eV	0.0	4.1	5.1	6.9	8.6	9.9	11.7

From Table 6.1 it is clear that the dissociative electron-transfer reaction leading to the formation of CF^+ is the dominant reactive process. The calculated cross-sections for forming CF^+ by dissociative electron-transfer (Equation 6.5) are listed in Table 6.5, as a function of the centre-of-mass collision energy, with the energy of the reactant dication set at 32 eV with respect to neutral CF_2. Previous work has shown that cross-section values greater than about 10^{-15} cm^2 result in large signals in the product ion mass spectra [13,14]. Conversely the intensities of product ions formed in reactions having cross-sections below ~10^{-16} cm^2 are considered as being unobservably low. Hence, the relatively large calculated values in Table 6.5 are in accord with the experimental results, which indicate that CF^+ is the dominant product ion.

$$CF_2^{2+} + NH_3 \rightarrow CF^+ + NH_3^+ + F \qquad (6.5)$$

Table 6.5 Calculated cross-sections of the dissociative electron-transfer reaction leading to the formation of CF^+ given in Equation 6.5, at various centre-of-mass frame energies.

E_{com}/eV	0.51	1.01	1.78	2.53	3.29
$10^{16}\sigma_{calc}$ /cm^2	29.75	29.89	30.39	30.95	30.83

For the electronic state of the reactant dication at 32 eV, the calculated cross-sections for the non-dissociative electron-transfer reaction (Equation 6.6), which leads to the formation of the CF_2^+ product ion, are given in Table 6.6. However, as may be observed from Table 6.6, the very low calculated cross-sections suggest that the probability of forming CF_2^+ by the non-dissociative electron-transfer given in Equation 6.6 is very small.

The calculated cross-sections for formation of CF_2^+ by means of the reaction given in Equation 6.6 are, at first, puzzling. As can be seen from Table 6.1, the experimental product ion intensities show that CF_2^+ ions are a significant component of the total product ion yield, yet the calculated cross-sections for this reaction are small. Clearly the reaction channel leading to the formation of CF_2^+ must be different to Equation 6.6.

$$CF_2^{2+} + NH_3 \rightarrow CF_2^+ + NH_3^+ \qquad (6.6)$$

Table 6.6 Calculated cross-sections of the non-dissociative electron-transfer reaction (Equation 6.6) at various centre-of-mass frame collision energies.

E_{com}/eV	0.51	1.01	1.78	2.53	3.30
$10^{16}\sigma_{calc}$ /cm^2	0.06	0.05	0.06	0.07	0.08

In order to identify the reaction channel that leads to the formation of the CF_2^+ product ion, the reaction exothermicities (ΔE) and the potential curve crossing radii (R_c) of possible reaction pathways leading to the formation of CF_2^+ were calculated and are listed in Table 6.7.

Table 6.7 Reaction exothermicities and crossing radii of possible reaction channels leading to the formation of the CF_2^+ product ion. Note, the values of the exothermicities and curve crossing radii are calculated with a dication state energy of 32 eV, with values for a dication state energy of 33 eV in parentheses.

Reaction channel	ΔE/eV	R_c/nm
$CF_2^{2+} + NH_3 \rightarrow CF_2^+ + NH_3^+$	10.41, (11.41)	0.216, (0.207)
$CF_2^{2+} + NH_3 \rightarrow CF_2^+ + NH_2^+ + H$	4.71, (5.71)	0.346, (0.305)
$CF_2^{2+} + NH_3 \rightarrow CF_2^+ + NH^+ + 2H$	endothermic	n/a

As stated in Chapter 4, the reaction window for electron-transfer lies approximately at interspecies separations of 0.3 to 0.6 nm. Hence, the curve crossing radius of the first reaction channel in the above table, having a relatively high reaction exothermicity of 10.41 (11.41) eV, lies outside the reaction window. This explains why the calculated cross-sections for the channel forming CF_2^++NH_3^+, given in Table 6.6, are close to zero. The third channel, which gives CF_2^++NH^++2H, is endothermic. Hence, there is no curve crossing and consequently the Landau-Zener theory gives a zero cross-section for this reaction.

In contrast to the Landau-Zener theory, the Demkov model of electron-transfer [4,17,18] would permit electron-transfer for such nominally endothermic channels, but as the Demkov mechanism only operates in a high collision energy regime, it can be discounted in our particular experiment. This endothermic reaction channel may therefore be discounted as a source of the CF_2^+ product ion. This conclusion is also supported by the fact that no NH^+ is observed experimentally.

In contrast to the two other reaction channels, the second pathway in the above table (CF_2^++NH_2^++H) has an exothermicity of 4.71 (5.71) eV, which corresponds to a curve crossing radius of 0.346 (0.305) nm. As discussed in Chapter 4, these values are favourable, and strongly suggest that the source of CF_2^+ is from this process (Equation 6.7). Indeed, further support for this conclusion comes from the high values of the calculated cross-section for this channel, which are listed at various

centre-of-mass collision energies in Table 6.8, where again the electronic state of the reactant dication is assumed to lie at 32 eV above the ground state of neutral CF_2.

$$CF_2^{2+} + NH_3 \rightarrow CF_2^+ + NH_2^+ + H \qquad (6.7)$$

Table 6.8 Cross-section values of the electron-transfer reaction given in Equation 6.7, at various centre-of-mass collision energies. Note, the values of the exothermicities and curve crossing radii are calculated with a dication state energy of 32 eV, with values for a dication state energy of 33 eV in parentheses.

E_{com}/eV	0.51	2.03	3.30
$10^{16}\sigma_{calc}$ /cm^2	22.22, (6.06)	19.18, (6.87)	19.04, (8.06)

As may be observed in Tables 6.5 and 6.8, the electron-transfer cross-sections for the formation of CF_2^+ and CF^+ display little dependence on the collision energy, supporting previous experimental observations [2,5]. The relatively low intensity of NH_2^+ in the product ion mass spectra (Table 6.1) is due to the low detection efficiency of our apparatus for ions produced from the neutral reactant. This arises as such ions have relatively low transverse kinetic energies in the laboratory frame, and are therefore inefficiently collected by the mass spectrometer which is specifically designed for the optimum collection and detection of product ions derived from the dication, such as CF^+ and CF_2^+.

As mentioned in section 6.3.1, the C^+ product ion may be assigned as a product of dissociative electron-transfer. From Table 6.3, the asymptote for the unimolecular dissociation, given in Equation 6.8, lies 10.5 eV above the ground state of the CF_2^+ ion [5]. However, the value of 10.5 eV is too high for this dissociative channel to be populated, via electron-transfer, by the reactive dications in their electronic ground state (32-33 eV). Hence, the obvious conclusion is that, given the relatively low intensity of the C^+ ion (Table 6.1), a small proportion of the dications in the ion beam are present in an excited electronic state.

$$\left[CF_2^+\right]^* \rightarrow C^+ + 2F \qquad (6.8)$$

The presence of CF_2^{2+} in an excited electronic state in an ion beam has been reported before [5]. As mentioned above, this earlier study identified an excited dication state lying between 35 and 37.5 eV above the ground state of neutral CF_2. Hence, if a proportion of the reactant dication beam contained CF_2^{2+} ions in this excited state, these reactants may have enough energy to populate the excited states of the CF_2^+ product ion that can dissociate to give C^+. To test this hypothesis, the reaction exothermicity (ΔE) and the corresponding value of the curve crossing radii (R_c) were calculated for the three possible reaction channels that lead to the formation of the C^+ product ion. Again, because of the uncertainty in the energy of the excited state of the dication, two values of the

exothermicity and curve crossing radii are calculated, these correspond to the upper and lower limits of the excited electronic state of the dication, 35 eV and 37.5 eV.

Table 6.9 Reaction exothermicities and crossing radii of reaction channels leading to the formation of C^+ from the $(CF_2^+)^*$ product ion. Note, the values of the exothermicities and curve crossing radii are calculated with a dication state energy of 35 eV, and 37.5 eV for the values given in parentheses.

Reaction channel	ΔE/eV	R_c/nm
$CF_2^{2+*} + NH_3 \rightarrow [CF_2^+]^* + NH_3^+ \rightarrow C^+ + 2F + NH_3^+$	2.38, (4.85)	0.62, (0.34)
$CF_2^{2+*} + NH_3 \rightarrow [CF_2^+]^* + NH_3^+ \rightarrow C^+ + 2F + NH_2^+ + H$	endothermic	n/a
$CF_2^{2+*} + NH_3 \rightarrow [CF_2^+]^* + NH_3^+ \rightarrow C^+ + 2F + NH^+ + 2H$	endothermic	n/a

From Table 6.9, we can see that the second and third reaction channels are endothermic for both the upper and lower values of the excited dication electronic state energy and, according to the Landau-Zener model of electron-transfer, have zero cross-section. However, the first reaction channel in Table 6.9, giving C^++NH_3^++2F, has a reaction exothermicity between 2.38 and 4.85 eV, which should permit electron-transfer. The asymptote for the dissociation $[CF_2^+]^* \rightarrow C^+$+$NH_3^+$+2F has an energy 10.5 eV above the ground state of CF_2^+. Therefore, from Table 6.4, we can see that C^+ can be formed only as a result of the reaction populating the $4a_1$ and higher-lying electronic states of CF_2^+. However, as can be seen from Figure 6.4, the dication in the 35 eV electronic state has not enough electronic energy to populate these excited states. Hence, in view of the inability of CF_2^+ dications in an electronic state at 35 eV to undergo the dissociative reaction given by Equation 6.9, values of the cross-section for this reaction are calculated only for the dication in the 37.5 eV electronic state. These values of the calculated cross-section are listed in Table 6.10 as a function of the centre-of-mass frame collision energy.

$$CF_2^{2+*} + NH_3 \rightarrow [CF_2^+]^* + NH_3^+ \rightarrow C^+ + 2F + NH_3^+ \qquad (6.9)$$

Table 6.10 Cross-section values of the dissociative electron-transfer reaction (Equation 6.9) as a function of centre-of-mass frame energies for the CF_2^{2+} dication in the excited electronic state 37.5 eV above the ground state of neutral CF_2^+.

E_{com}/eV	0.51	1.01	1.78	2.53	3.29
$10^{16}\sigma_{calc}$ /cm^2	5.88	7.79	10.22	12.08	13.51

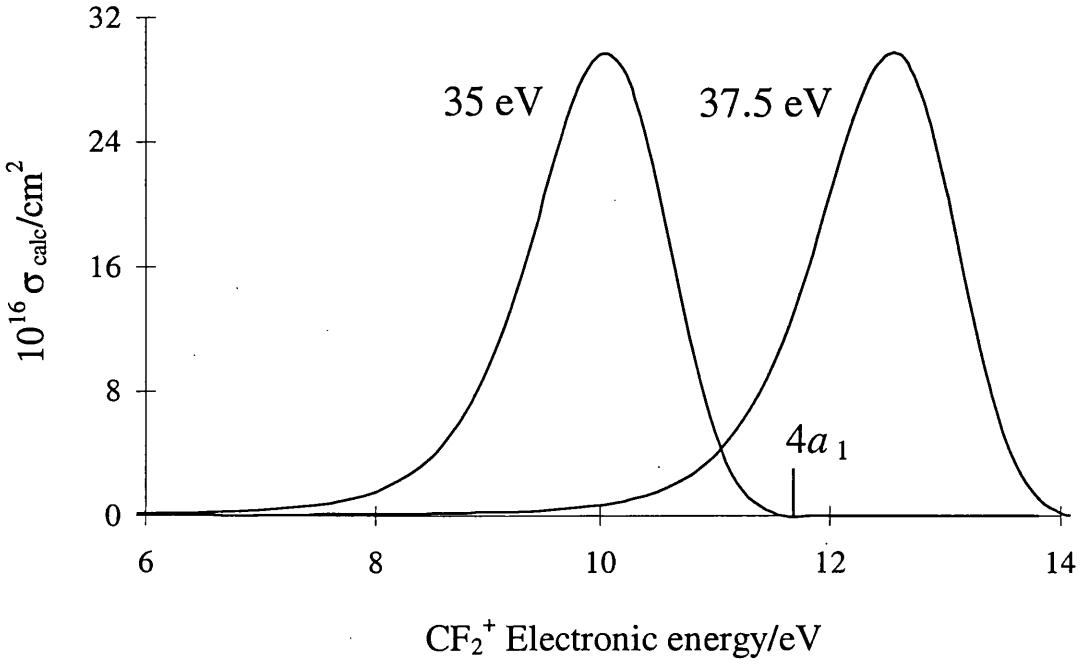

Figure 6.4 Calculated cross-sections for the electron-transfer reaction between $(CF_2^{2+})^*$ and NH_3 as a function of the electronic excitation of the resulting CF_2^+ relative to its electronic ground state. The vertical line represents the term energy of the $4a_1$ electronic state of CF_2^+ that is assumed to dissociate to C^+ and 2F. The two curves correspond to two possible energies of excited states of the reactant dication at 35 and 37.5 eV above the ground state of CF_2.

The fact that the signals for the C^+ ion are so weak is indicative of the relatively low abundance of the excited state of the reactant dication in the ion beam. A crude estimate may be made of the proportion of the dications in the excited state in the ion beam from the relative intensities of the product ions (Table 6.1). This estimate suggests that the ion beam contains ~1% of dications in the excited electronic state. As stated above, the earlier work of Manning *et al* [5] also reported the presence of an excited state of CF_2^{2+} in their dication beam. Although the earlier study made no mention of the abundance of the excited state, a consideration of the relative intensities indicates that the two beams contained similarly low abundances of the excited state.

The cross-section values listed in Table 6.10 are for the production of CF_2^+ in the $4a_1$ electronic state, which, as stated above, has an energy of 11.7 eV with respect to the CF_2^+ ground state. This state lies higher in energy than both the asymptotes for the dissociation of CF_2^+ to C^++2F and F^+ + CF which have energies of 10.5 eV and 11 eV with respect to the CF_2^+ ground state. Hence, the $4a_1$ electronic state of CF_2^+ can potentially dissociate to give either C^+ + 2F or F^+ + CF. However, no F^+ signal is observed in our experiments. So the appearance of a weak C^+ signal in our experiments perhaps indicates that the higher-lying excited electronic states of CF_2^+ preferentially dissociate to give C^+ + 2F.

6.4.2 Bond-forming reactivity

As stated in section 6.3, electron-transfer reactions dominate the product ion yield following collisions between the neutral NH_3 and the reactant dication. However, the mass spectra indicate a small but significant signal due to the $HNCF^+$ product ion at all the collision energies employed in these experiments.

The observation of $HNCF^+$ is the first detection of a bond-forming reaction following collisions between molecular dications and a polyatomic neutral target. Hence, the available data relating to the bond-forming reaction for the CF_2^{2+}/NH_3 collision system is non-existent. However, our data allows us to draw the first tentative conclusions regarding the mechanism of the bond-formation. The collision energy-dependence of the bond-forming reaction and electron-transfer cross-sections of this reaction system may be compared to other systems that have exhibited bond-forming reactivity and have been studied to a greater extent. Examination of Figure 6.2 clearly shows a very different collision energy-dependence of the bond-forming yield in this collision system than in the case of the corresponding reactions exhibited by the CF_2^{2+} and D_2/H_2 collision systems. In the case of the CF_2^{2+} and D_2/H_2 collision systems, described in Chapter 5, the relative cross-section for bond formation rises steadily with decreasing collision energy [2]. This collision energy-dependence is indicative of a reactive pathway in which there is no energy barrier [19]. However, in the case of the bond-forming reaction between CF_2^{2+} and NH_3, the yield reaches a maximum at centre-of-mass collision energies between 2 and 3 eV. Such a maximum can be considered to arise because of an energy barrier [19] which, in the absence of tunnelling, must be surmounted before the reaction can occur. Hence, at lower collision energies (< 2 eV) the yield of the $HNCF^+$ ion is low as relatively few collision partners have sufficient energy to surmount the energy barrier. At centre-of-mass collision energies in excess of 3 eV, the ratio of cross-sections decreases because of a reduction in the reaction time, that is an effective reduction in the length of time in which the reactants are sufficiently close enough for chemical rearrangement.

The fundamental differences in the collision energy-dependencies of the $CF_2^{2+}/H_2/D_2$ and CF_2^{2+}/NH_3 collision systems point to significant differences in the respective reaction mechanisms. This may also account for the much higher cross-sections for the bond-forming reaction in the $CF_2^{2+}/H_2/D_2$ collision system. The bond-forming reaction for the $CF_2^{2+}/H_2/D_2$ collision system has been found to proceed via a direct, *spectator-stripping* mechanism [2,19-23]. Hence, the bond-forming reaction for the CF_2^{2+}/NH_3 collision system would seem to proceed via a different reaction mechanism. Perhaps the $HNCF^+$ ion is formed following the formation of a collision complex, as in Equation 6.10. The generation of a complex would certainly be assisted by the presence of the dipole moment associated with NH_3, as such a dipole moment would invariably increase the interaction between the reactants leading to a 'sticky' collision and the formation of a complex.

$$CF_2^{2+} + NH_3 \rightarrow [H_3NCF_2]^{2+} \rightarrow HNCF^+ + H^+ + H + F \qquad (6.10)$$

6.5 Conclusion

Relative yields of the electron-transfer and bond-forming product ions, following collisions between CF_2^{2+} and NH_3, have been recorded as a function of the centre-of-mass collision energy. The relative cross-sections of the competing reaction processes are obtained from the recorded product ion intensities. The ion yields indicate that the two electron-transfer reactions leading to the formation of the CF^+ and CF_2^+ product ions dominate the interaction of the dication with the neutral NH_3 collision partner. However, a bond-forming reaction pathway that leads to the generation of the $HNCF^+$ product ion is a significant reaction channel. The identification of a very weak C^+ ion signal is, in the absence of a charge-separating reaction channel, thought to arise through dissociative electron-transfer. This reaction cannot proceed with the reactant dication in its ground electronic state, and hence provides evidence for the presence of electronically excited dications in the reactant dication beam.

Our results indicate that the bond-forming reaction displays a significant collision energy-dependence. In this case, the ratio of the cross-sections of the bond-forming reaction to those of the electron-transfer reaction processes reaches a maximum value at a collision energy of approximately 2-3 eV in the centre-of-mass frame. This behaviour points to the existence of a barrier to reaction. The CF_2^{2+}/NH_3 collision system displays significant differences, both in terms of its collision energy-dependence and in the magnitude of its cross-section for bond formation, to the CF_2^{2+}-H_2/D_2 collision system, which has been found to undergo bond-forming reactions via a direct reactive pathway. The differences in the behaviour of the two collision systems point to a different reaction mechanism operating in the CF_2^{2+}/NH_3 collision system. The presence of the dipole moment associated with the NH_3 reactant would tend to increase the interaction between the reactants. Such an increased interaction could lead to sticky collisions and would therefore favour complexation. The cross-sections for reactive pathways which involve complexation are usually much lower than those of reactions in which a direct mechanism operates. Hence, the operation of a complexation mechanism in the bond-forming reaction between CF_2^{2+} and NH_3 would be consistent with the observed behaviour.

References

1 S. D. Price, M. Manning and S. R. Leone, *J. Am. Chem. Soc.*, **116** (1994) 8673.

2 K. A. Newson and S. D. Price, *Chem. Phys. Letters,* **269** (1997) 93.

3 Z. Dolejsek, M. Farnik, and Z. Herman, *Chem. Phys. Letters*, **235** (1994) 99.

4 S. D. Price, *J. Chem. Soc., Faraday Trans.*, **93** (1997) 2451.

5 M. Manning, S. D. Price and S. R. Leone, *J. Chem. Phys.*, **99** (1993) 8695.

6 A. Ehbrecht, N. Mustafa, C. Ottinger and Z. Herman, *J. Chem. Phys.*, **105** (1996) 9833.

7 S. D. Price, M. Manning and S. R. Leone, *Chem. Phys. Letters*, **214** (1993) 553.

8 Y. Lee, S. R. Leone, P. Champkin, N. Kalysoyannis and S. D. Price, *J. Chem. Phys.*, **106** (1997) 7981.

9 L. Landau, *Phys. Z.*, **2** (1932) 26.

10 C. Zener, *Proc. R. Soc, London Ser. A.*, **137** (1932) 696.

11 C. Y. Ng, T. Baer and I. Powis, *Unimolecular and Bimolecular Ion-Molecule Reaction Dynamics*, 1994 John Wiley and sons Ltd Inc.

12 T. Baer and C. Y. Ng, *State Selected and State-to-State Ion-Molecule Reaction Dynamics Part 2 (Theory)* 1992 John Wiley and sons Ltd Inc.

13 S. D. Price, S. A. Rogers and S. R. Leone, *J. Chem. Phys.*, **98** (12) (1993) 9455.

14 S. A. Rogers, S. D. Price and S. R. Leone, *J. Chem. Phys.*, **98** (1) (1993) 280.

15 P. H. Champkin, N. Kaltsoyannis and S. D. Price, *Int. J. Mass Spectrom. Ion. Proc.* (1998) in press.

16 J. M. Dyke, L. Golob, N. Johnathon, J. Morris, and M. Okuda, *J. Chem. Soc., Faraday Trans.*, **70** (1974) 1828.

17 Y. U. Demkov, *Sov. Phys. JETP.*, **18** (1964) 138.

18 R. A. Dressler, S. T. Arnold and E. Murad, *J. Chem. Phys.*, **103** (1995) 9989.

19 R. D. Levine and R. B. Bernstein, *Molecular Reaction Dynamics and Chemical Reactivity* 1987 Oxford University Press, Inc.

20 R. A. Dressler, R. H. Salter and E. Murad, *J. Chem. Phys.*, **99** (1993) 1159.

21 K. Tanaka, T. Kato, P. M. Guyon and I. Koyano, *J. Chem. Phys.*, **79** (1983) 4302.

22 Z. Herman, J. Kerstetter, T. Rose and R. Wolfagang, *Discus. Faraday Soc.*, **44** (1967) 123.

23 W. R. Gentry, E. A. Gislason, Y. T. Lee, B. H. Mahan and C. W. Tsao, *Discus. Faraday Soc.*, **44** (1967) 137.

Chapter 7

Electron-transfer and bond-forming reactivity between CF_3^{2+} and H_2/D_2

7.1 Introduction

As described in Chapter 5, the gas-phase reactivity between the CF_2^{2+} molecular dication and H_2/D_2 has received the most attention of that in any molecular dication-neutral collision system [1-3]. This collision system has been shown to display bond-forming reactivity at low collision energies (3-13 eV in the laboratory frame) in addition to electron-transfer reactions. In contrast, the analogous reaction of CF_3^{2+} with D_2 has received little attention, with only a single investigation reported in the literature [1]. This initial study reported the observation of a DCF_2^+ product ion, in addition to other product ions formed in electron-transfer and collision-induced neutral-loss reactions. Interestingly, the reported yield of the DCF_2^+ ion produced in the bond-forming reaction between CF_3^{2+} and D_2 (12 %) was actually greater than that of the CF_2^{2+}/D_2 collision system (9 %).

The earlier investigation of intermolecular isotope effects in the reaction between CF_2^{2+} and H_2/D_2, discussed in Chapter 5, provided a significant amount of data regarding the mechanism of the bond-forming reaction in that particular collision system. As CF_2^{2+} and CF_3^{2+} are both perfluorinated molecular dications, it would seem likely that the two dication/neutral collision systems share similar reactive characteristics, such as their reaction mechanism. Hence, to study the mechanism and collision energy-dependence of the bond-forming reaction between the CF_3^{2+} dication and neutral hydrogen isotopic targets, collisions between CF_3^{2+} and H_2/D_2 were performed under the same conditions and collision energies as those involving the $CF_2^{2+}/H_2/D_2$ collision systems. The effects of isotopic substitution, achieved by using H_2 and D_2 as the neutral collision partner, allows the bond-forming and electron-transfer reactions to be checked for possible intermolecular isotope effects. Such isotope effects are, as outlined in Chapters 4 and 5, a powerful probe of the reaction dynamics and mechanism [3-25] operating in a given reactive encounter.

7.2 Experimental details

A full account of the experimental methodology employed in the mass spectrometric measurements is given in Chapter 2. However, for this particular collision system, the pressure of the target gas was set at a gauge value of 2×10^{-6} Torr rather than the usual value of 4×10^{-6} Torr. Despite the fact that this value is half that of the usual value for non-hydrogen collision partners, the actual number densities of the target gases are in fact the same in each case. The gauge readings of the pressures of hydrogen and deuterium gas targets are set at the lower value as a result of the insensitivity of the ion gauge to H_2/D_2. This insensitivity arises because of the higher ionization

potentials of the hydrogen (and deuterium) targets relative to those of other gases, such as ammonia, meaning that the gauge reads low for H_2, D_2 and HD.

In common with all the experimental work reported in this thesis, the careful monitoring of the target gas pressure not only ensures single collision conditions [26] but also attempts to avoid pressure-related deviations in the intensities of the product ions. Hence, any deviations in the product ion intensities may then be attributed directly to fundamental changes in the reaction process.

The change of reactant dication from CF_2^{2+} to CF_3^{2+} is achieved by simply adjusting the potential difference of the electrostatic plates of the Colutron velocity filter [27,28]. Changing the electric field strength inside the velocity filter perturbs the dication beam. This may cause the ion beam to become poorly focused. Such a deterioration in the focusing quality may also cause the ion beam to become divergent and poorly collimated, leading to a reduction in the beam current. The cross-section of the dissociative ionization of CF_4 that leads to the production of the CF_3^{2+} reactive dication is relatively small. Therefore, to form a beam of usable intensity necessitates the re-optimization of the ion optics. This optimization is a very important procedure, as in addition to increasing the dication beam current, a poorly collimated beam will lead to product ions being formed across a greater width of the source region, and hence a greater spread along the axis of the spectrometer. As described in Appendix 2, this increased spread has a detrimental effect on the mass resolution of the TOF mass-spectrometer. In the case of the $CF_3^{2+}/H_2/D_2$ (and the $CF_2^{2+}/HD/H_2/D_2$) collision systems, the mass spectral peaks of the HCF_2^+ and DCF_2^+ product ions are in close proximity to the much larger peak of the CF_2^+ ion. Therefore, good mass resolution is crucial to obtaining accurate values of the intensity of the HCF_2^+ and DCF_2^+ product ions.

7.3 Results and analysis

Time-of-flight mass spectra were recorded following collisions between CF_3^{2+} dications and the H_2/D_2 neutral collision partner at collision energies in the range of 3 to 13 eV in the laboratory frame, corresponding to a range of centre-of-mass collision energies between 0.113 to 0.423 eV for the H_2 system, and 0.219 to 0.712 eV for the D_2 system. Analyses of the mass spectra indicate that CF_3^+, CF_2^+, CF^+, CF_2^{2+}, X^+, X_2^+ and XCF_2^+, where X is H or D, ions are produced in the collisions. In addition to the product ions, the TOF mass spectra, of course, show the presence of a large number of unreacted dications. Sections of representative time-of-flight mass spectra are shown in Figures 7.1a and b of the product ions produced in reactions between CF_3^{2+} and D_2/H_2 neutral collision partners at the indicated collision energy.

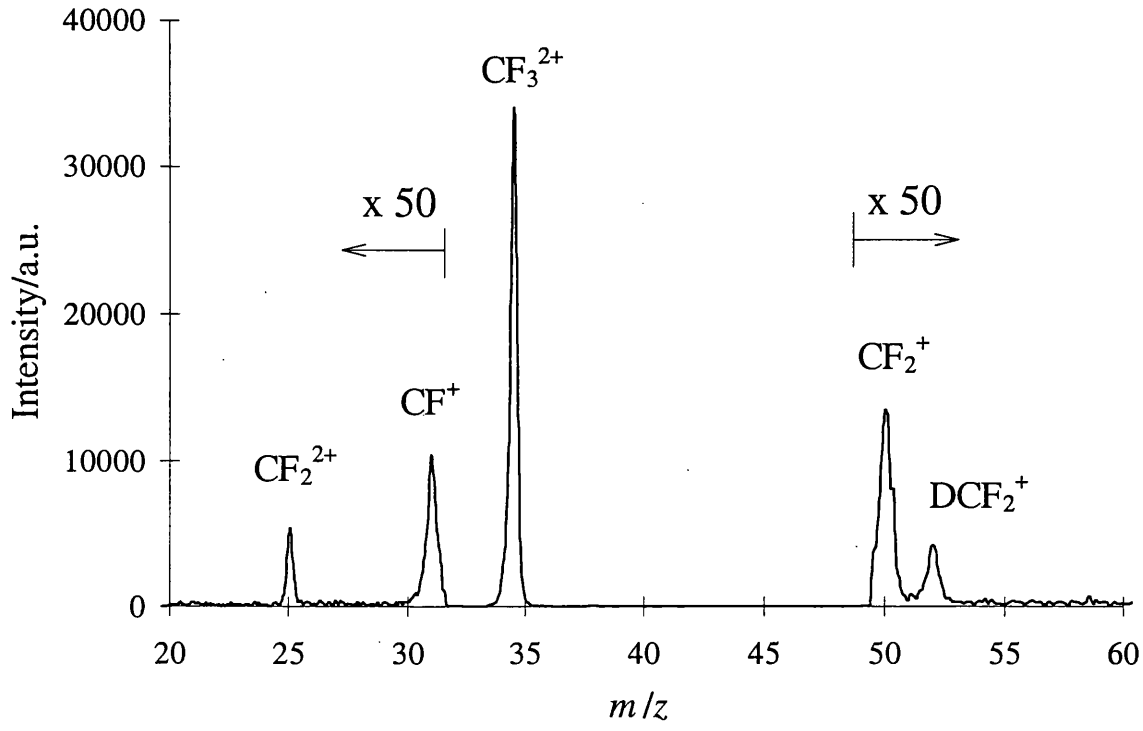

Figure 7.1a A section of a representative time-of-flight mass spectrum showing the product ions formed following collisions between CF_3^{2+} and D_2 at a centre-of-mass collision energy of 0.49 eV.

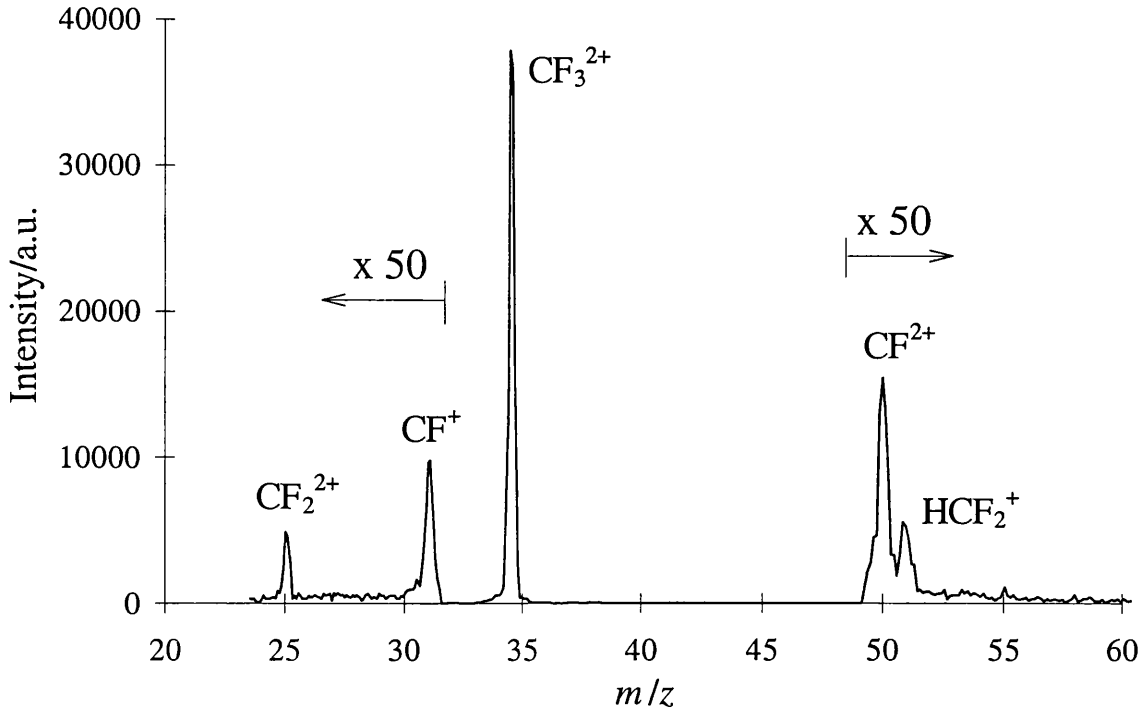

Figure 7.1b A section of a representative time-of-flight mass spectrum showing the product ions formed following collisions between CF_3^{2+} and H_2 at a centre-of-mass collision energy of 0.36 eV.

7.3.1 Assignment of product ions

As mentioned above, the TOF mass spectra show the presence of CF_3^+, CF_2^+, CF^+, CF_2^{2+}, X^+, X_2^+ and XCF_2^+ (X = H or D) product ions, in addition to the unreacted dications. To allow ready comparison of the relative intensities, typical values of the background-corrected product ion intensities are given below in Tables 7.1a and b. As discussed in Chapter 5, the data contained in Tables 7.1a and b do not include the intensities of the X^+ and X_2^+ ions. The reason for this is that the spectrometer has a low collection efficiency for ions formed from the neutral collision partner, so an accurate determination of this ion's intensity would be difficult to achieve. However, a number of mass spectra were recorded at various collision energies to confirm, qualitatively, the presence of these ions.

The product ion intensities, listed in Tables 7.1a/b, recorded following collisions between the reactant CF_3^{2+} dications and the H_2/D_2 neutral collision partner, indicate that four types of reactive processes are observed at the collision energies used in these experiments. The CF_3^+ product ion can only be formed as a result of non-dissociative electron-transfer (Equation 7.1), whereas, the CF_2^+ and CF^+ product ions may be formed either by dissociative electron-transfer or by collision-induced charge-separation (CICS). However, the absence of any real F^+ signal in the mass spectra eliminates the possibility of the CF_2^+ and CF^+ products being formed in CICS reactions. Hence, the CF_2^+ and CF^+ products may be assigned as products of dissociative electron-transfer reactions (Equations 7.2 and 7.3).

A third type of reactive process that leads to the formation of new chemical bonds is also observed. This bond-forming reaction results in the generation of the XCF_2^+ product ion. The observation of an X^+ signal, together with the absence of an XF^+ signal strongly indicates that the XCF_2^+ product ion is formed in Equation 7.4. Finally, the CF_2^{2+} product ion may be unambiguously ascribed as the product of collision-induced neutral-loss (CINL) reactivity (Equation 7.5). The relatively intense CINL reactivity of CF_3^{2+} with H_2/D_2 and other neutral targets [29-31] is in stark contrast with the behaviour of the analogous CF_2^{2+} dication, where no CINL reactivity is observed. As discussed in Chapter 5, the CINL reactivity associated with CF_3^{2+} arises as one F atom is weakly bound. Whereas the CF_2^{2+} dication, being isoelectronic with CO_2, has only strongly bound F atoms.

$$CF_3^{2+} + X_2 \rightarrow CF_3^+ + [X+X]^+ \quad (7.1)$$

$$CF_3^{2+} + X_2 \rightarrow CF_2^+ + [X+X]^+ + F \quad (7.2)$$

$$CF_3^{2+} + X_2 \rightarrow CF^+ + [X+X]^+ + 2F \quad (7.3)$$

$$CF_3^{2+} + X_2 \rightarrow XCF_2^+ + X^+ + F \quad (7.4)$$

$$CF_3^{2+} + X_2 \rightarrow CF_2^{2+} + X_2 + F \quad (7.5)$$

The product ion intensities listed in Tables 7.1a and b indicate that although electron-transfer is the dominant reactive pathway, the cross-sections for bond-forming and CINL reactivity are such that these processes make a significant contribution to the overall product ion yield of this collision system.

Table 7.1a Background-corrected intensities of ions formed in collisions between CF_3^{2+} and H_2 at a centre-of-mass collision energy of 0.366 eV.

CF_3^{2+}	CF_3^+	CF_2^+	CF^+	CF_2^{2+}	HCF_2^+
110334	124	807	279	292	238

Table 7.1b Background-corrected intensities of ions formed in collisions between CF_3^{2+} and D_2 at a centre-of-mass collision energy of 0.548 eV.

CF_3^{2+}	CF_3^+	CF_2^+	CF^+	CF_2^{2+}	DCF_2^+
81810	137	512	548	125	121

7.3.2 Product ion intensities

Having assigned the product ions to their respective reaction pathways, we now consider the relative intensities of the product ions, and the collision energy-dependence of the given reaction process. As stated in Chapters 5 and 6, the collision energy-dependence is a powerful probe of the reaction mechanism. In common with all the results of collision experiments reported in this thesis, the relative cross-sections of the competing electron-transfer and chemical (bond-forming) reaction channels are obtained from suitably background-corrected measurements of the detected intensities of the product ions.

For the reactions of CF_2^{2+} with H_2/D_2 and NH_3, as described in the preceding Chapters, the relative intensities of the products of bond-forming and electron-transfer reactions were corrected for differences in the detection efficiency of the fluxes of the respective product ions. As stated in Chapter 3, the detection efficiency variability is caused by the differences in the amount and distribution of the kinetic energy released in a given reaction process [2]. The kinetic energy release (KER) changes the ion's laboratory frame transverse velocity component, which, in turn, affects the ion's detection efficiency. Therefore, because different reaction processes may have different kinetic energy releases, ions formed in different reaction processes may be detected with differing efficiencies. Hence, to overcome the problems caused by these differences in detection efficiency, the analysis procedure incorporates a correction process which makes allowance for such differences in the ion detection

efficiencies. The detailed description of the methodology behind this correction is presented in Chapter 3.

The calculation of the correction factor α requires details of the kinetic energy released upon reaction of the dication and neutral. In the case of the reaction between CF_2^{2+} and H_2/D_2, such data was available in the literature [2]. However, no such data concerning the KER values and distributions for the electron-transfer and bond-forming reactions between CF_3^{2+} and H_2 or D_2 is available. Despite the paucity of appropriate data, the correction procedure may still be carried out by using the KER value used for the CF_2^{2+} and H_2/D_2 collision system. Using this data in the calculation of the correction factor α for the $CF_3^{2+}/H_2/D_2$ collision systems does not represent a major approximation as the KER will be dominated by the Coulombic repulsion between the singly-charged product ions, as it is in the $CF_2^{2+}/H_2/D_2$ case, for both the bond-forming and electron-transfer reactions. Representative values of the correction factor α for the two collision systems are given in Table 7.2.

Table 7.2 Relative detection efficiency correction factors (α) for the bond-forming and electron-transfer products formed in collisions between CF_3^{2+} with D_2 and H_2 at various centre-of-mass frame collision energies. The KER value used to calculate α is 6.5 eV.

E_{com}/eV	α(D_2)	α(H_2)
0.1	0.993	1.002
0.2	1.000	1.008
0.3	1.007	1.018
0.4	1.015	1.036

The ratios of the correction factors α for the ionic products of bond-forming and electron transfer reactivity are close to unity. Hence, in view of the relative values of the correction factor, which will hardly change the values of the product ion ratios, together with the additional uncertainty produced by using an approximate KER value in the correction procedure, in this case we consider that the product ion yield provides a reliable estimate of the relative cross-sections of the bond-forming process.

The relative intensities of various product ions are given as a function of the centre-of-mass frame collision energy in Tables 7.3a and 7.3b and illustrated in Figures 7.2a-d. The tables list the intensity of the bond-forming product ion XCF_2^+ relative to the CF_2^+ electron-transfer product ion for both collision systems. Additionally, the results also include the intensity of the CF_2^{2+} ion, produced in collision-induced neutral-loss reactions, relative to the intensity of the unreacted CF_3^{2+} dication. Although this ratio is dependent upon the pressure of the neutral reactant, the experiments were

performed under effectively identical conditions. Therefore, the ratio of the CF_2^{2+} ion intensity relative to the intensity of the unreacted dication serves as a sound indicator of the intensity of the CINL reaction at a given centre-of-mass collision energy. Additionally, as discussed in section 7.4, this ratio, when suitably extrapolated as a function of the collision energy, provides a means of roughly estimating the C – F bond energy.

Table 7.2 The variation of relative intensities of product ions formed following collisions between (**a**) CF_3^{2+} and H_2 and (**b**) CF_3^{2+} and D_2 with centre-of-mass collision energy E_{com}.

(a)

E_{com}/eV	$10^4 \frac{I(CF_2^{2+})}{I(CF_3^{2+})}$	$\frac{I(HCF_2^+)}{I(CF_2^+)}$
0.423	24.752	0.2858
0.394	25.427	0.2928
0.366	27.660	0.2916
0.338	26.494	0.2959
0.310	26.407	0.3019
0.282	23.847	0.3112
0.253	13.780	0.3099
0.225	13.220	0.3110
0.197	10.560	0.3301
0.141	4.060	0.3296
0.113	3.619	0.3301

(b)

E_{com}/eV	$10^4 \frac{I(CF_2^{2+})}{I(CF_3^{2+})}$	$\frac{I(DCF_2^+)}{I(CF_2^+)}$
0.712	47.435	0.233
0.658	43.545	0.240
0.603	39.754	0.228
0.548	40.170	0.256
0.493	30.105	0.249
0.438	22.306	0.284
0.384	11.953	0.292
0.329	5.589	0.288
0.274	9.469	0.343
0.219	6.122	0.351

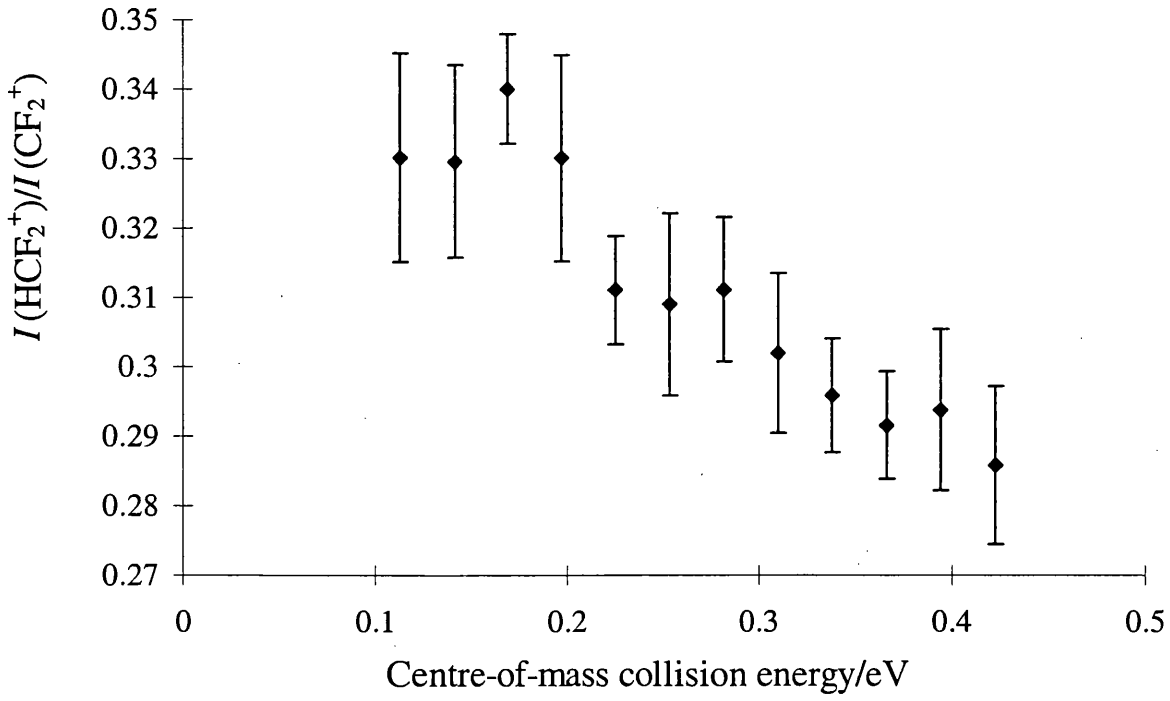

Figure 7.2a Relative intensities of the HCF_2^+ and CF_2^+ product ions as a function of the centre-of-mass collision energy, formed in collisions of CF_3^{2+} with H_2.

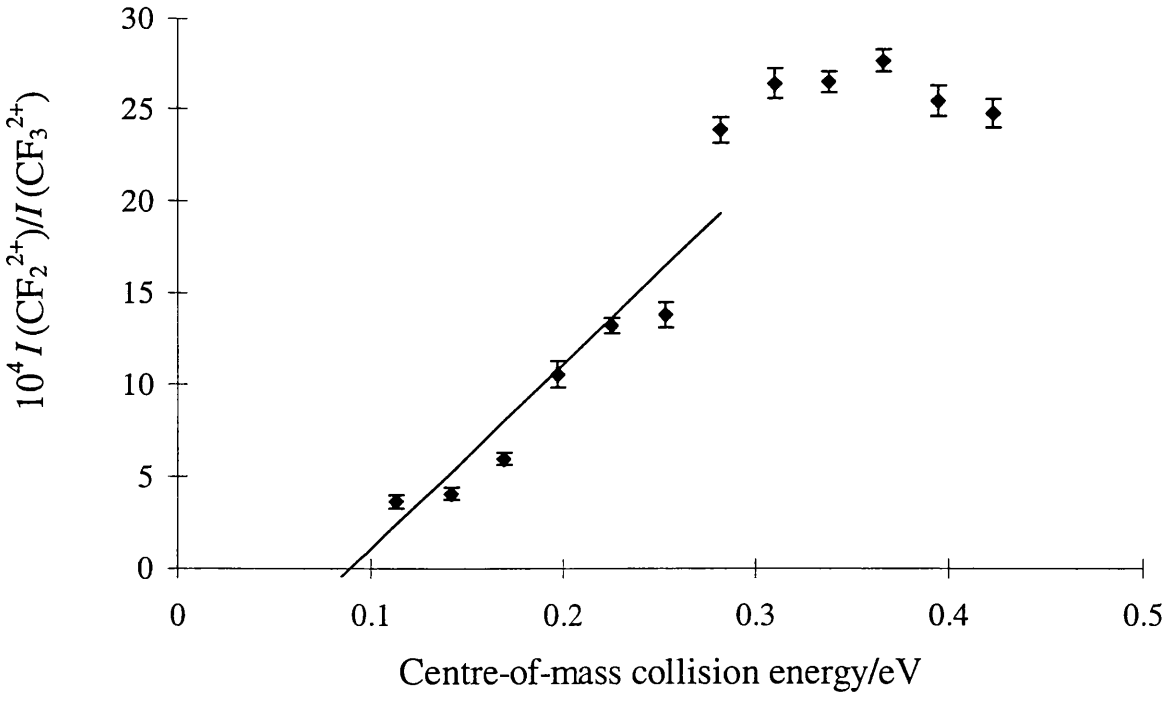

Figure 7.2b Relative intensities of the CF_2^{2+} CINL product ion and unreacted CF_3^{2+} molecular dications, as a function of the centre-of-mass collision energy, formed in collisions of CF_3^{2+} with H_2. The solid line is obtained using a least squares analysis of the experimental data and is extrapolated to indicate the intercept with the abscissa. It should be noted that as the threshold law only operates at energies just above threshold, the least squares analysis only included those data points corresponding to the lower collision energies.

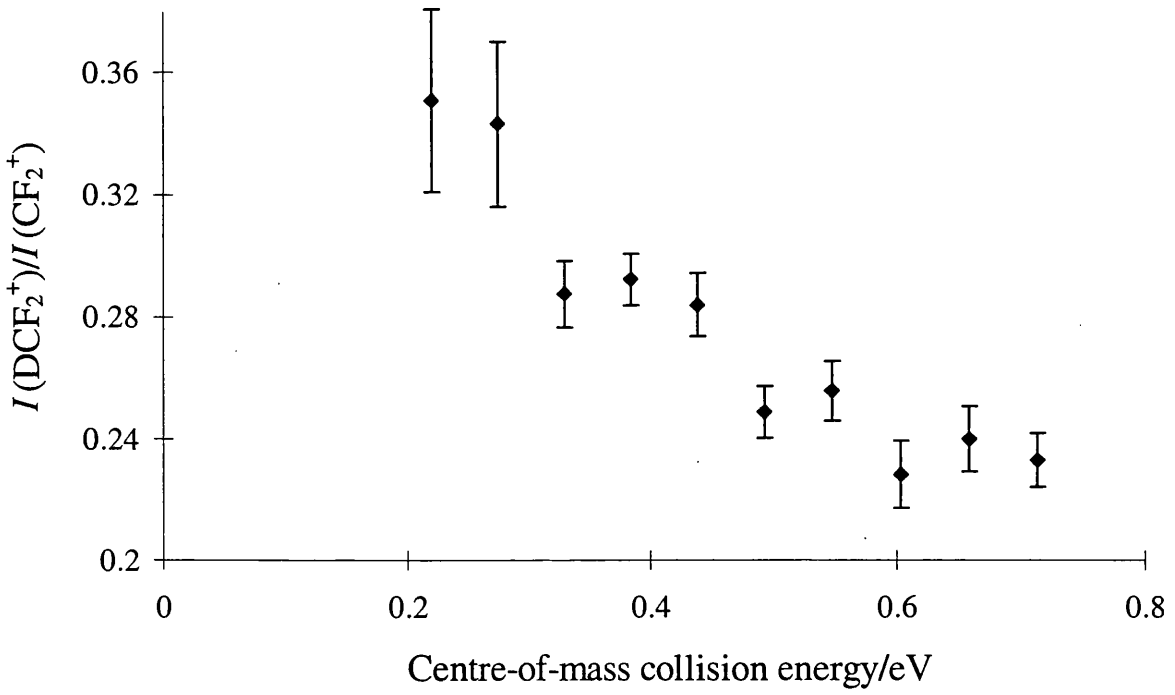

Figure 7.2c Relative intensities of the DCF_2^+ and CF_2^+ product ions as a function of the centre-of-mass collision energy, formed in collisions of CF_3^{2+} with D_2.

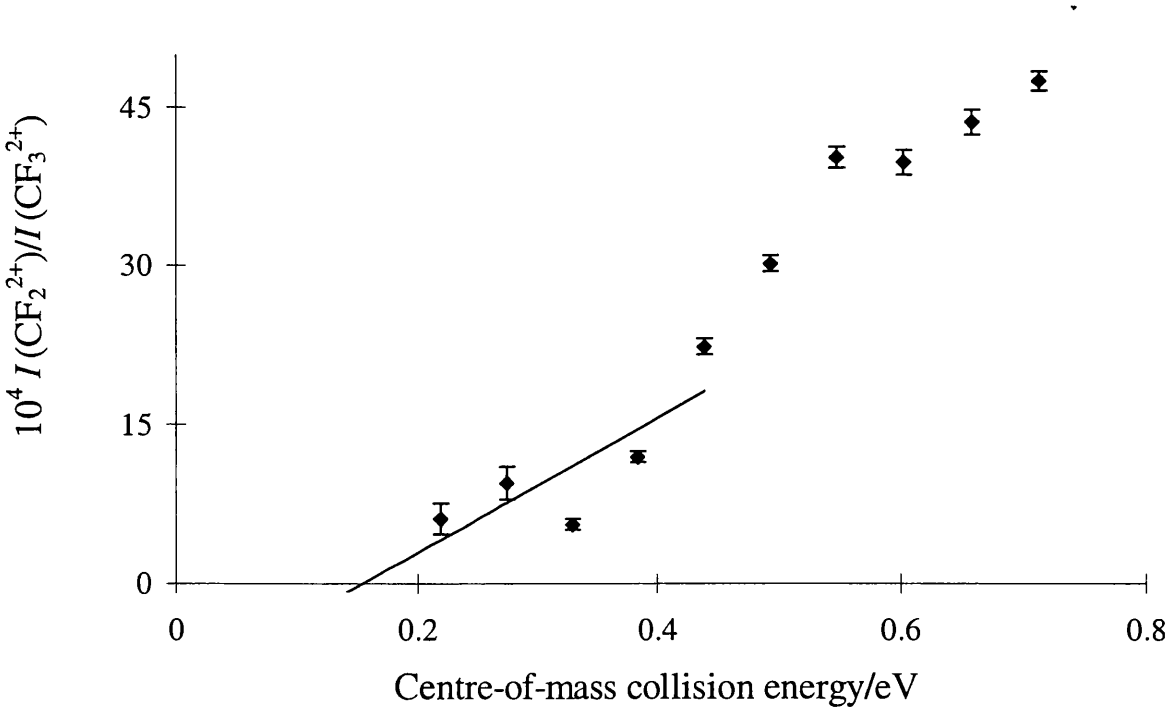

Figure 7.2d Relative intensities of the CF_2^{2+} CINL product ion and unreacted CF_3^{2+} molecular dications, as a function of the centre-of-mass collision energy, formed in collisions of CF_3^{2+} with D_2. The solid line is obtained using a least squares analysis of the experimental data and is extrapolated to indicate the intercept with the abscissa. It should be noted that as the threshold law only operates at energies just above threshold, the least squares analysis only included those data points corresponding to the lower collision energies.

7.4 Discussion

As can be observed from the data presented in Figure 7.3 below, the relative intensities of the products of bond-forming and electron-transfer reactions of CF_3^{2+} with both H_2 and D_2 neutral targets are, within experimental uncertainties, the same, for a given collision energy. Hence, the bond-forming reactivity displays no significant dependence on which isotope of hydrogen is used as the neutral collision partner. Consequently, this absence of an isotope effect matches the behaviour observed for the analogous $CF_2^{2+}/H_2/D_2$, collision system, where the absence of an isotope effect is consistent with the operation of a direct reaction mechanism. Indeed, as detailed in Chapter 5, a further investigation [2] also indicates that the bond-forming reaction between CF_2^{2+} and H_2/D_2 proceeds via a *spectator-stripping* direct reaction mechanism.

As mentioned in Chapter 4, the much larger range of reactive impact parameters associated with a spectator-stripping direct reaction mechanism results in the cross-sections for reactions proceeding via this mechanism being significantly larger than those for other reaction pathways such as the head-on *rebound* direct reaction mechanism or complexation [6]. In the cases of the CF_3^{2+}-H_2/D_2 and CF_2^{2+}-H_2/D_2 collision systems, the cross-section of the bond-forming reaction relative to that of the electron-transfer process were found to be similar. This observation points to the mechanism of the bond-forming reaction in the CF_3^{2+}-H_2/D_2 collision system being the same direct pathway as that in the CF_2^{2+}-H_2/D_2 collision system. The similarity of the cross-sections for bond-forming reactivity in these collision systems is in contrast to the analogous values for the CF_2^{2+}/NH_3 collision system, where the very much smaller values point to the operation of a different reaction mechanism for bond formation.

The cross-sections for the bond-forming reactions of the CF_3^{2+}-H_2/D_2 and CF_2^{2+}-H_2/D_2 collision systems, share very similar collision energy-dependencies. In both cases the cross-section for the bond-forming reactions rise steadily with decreasing collision energy [3]. This collision energy-dependence is indicative of a reactive pathway in which there is no energy barrier [6]. The observed increase in bond-forming reactivity with decreasing collision energy may be qualitatively explained as arising as a result of the increased time for interaction of the collision partners at lower collision energies. This apparent lack of a energy barrier casts further doubt on the applicability of the Landau-Zener model of H^-/D^- transfer to molecular dication-neutral collision systems, which was discussed in Chapter 5. Hence, given the apparent similarities in the bond-forming reactivity for the CF_2^{2+}/X_2 and CF_3^{2+}/X_2 collision systems, outlined above, it seems highly likely that the two collision systems share the same type of reaction mechanism for the bond-forming reaction. That is in both cases, the bond-forming reaction proceeds via a spectator-stripping direct reaction mechanism [6,7].

The CF_3^{2+}-H_2/D_2 collision system also exhibits collision-induced neutral-loss reactivity. The yield of the CF_2^{2+} product of CINL reactivity increases with the collision energy. This collision energy-dependence may be explained as arising because of the increase in the energy available to break the bond holding the weakly bound F atom. As mentioned above, an estimate of the C-F (weakly bound) bond energy may be made by suitable extrapolation of the data in Figure 7.2b (and 7.2d) to the abscissa. As can be seen from Figures 7.2b and 7.2d, the results of such an extrapolation indicates that the curve intercepts the abscissa at a mean energy of 0.122 eV. This corresponds to a mean value of the C-F bond enthalpy of $11.77^{+6.16}_{-2.60}$ kJ mol^{-1}. Both the extrapolated line and the uncertainty of the bond enthalpy are obtained by a least squares analysis of the experimental data.

The bond enthalpy of $11.77^{+6.16}_{-2.60}$ kJ mol^{-1} for the weak C-F bond in the case of the CF_3^{2+} molecular dication is very much lower than the literature value for a typical C-F bond (~484 kJ mol^{-1}) [32]. Therefore, the significantly lower value of the bond enthalpy for the CF_3^{2+} dication supports the model, originally applied to SiF_3^{2+} [31], in which a perfluorinated dication (CF_3^{2+} in this particular case) consists of a tightly bound 'core-dication' (CF_2^{2+}) attached to a weakly bound F atom.

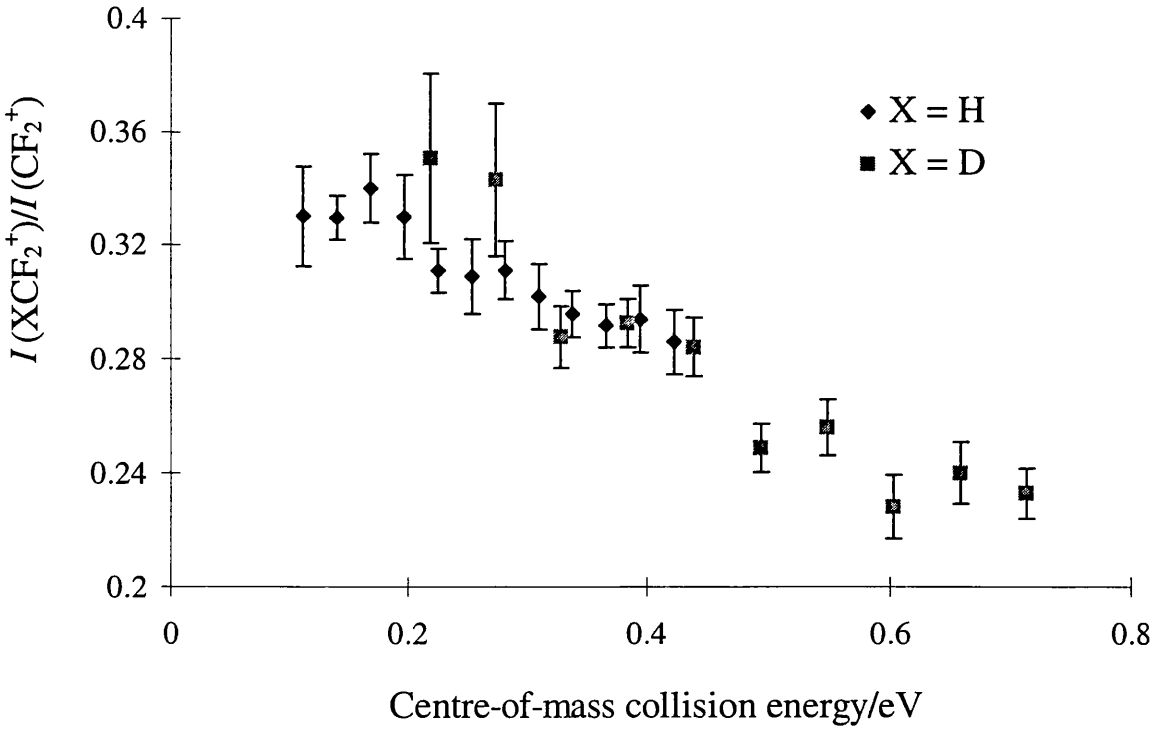

Figure 7.3 Intensities of the XCF_2^+ bond-forming product ion relative to the CF_2^+ charge-transfer product ion, as a function of the centre-of-mass collision energy, formed in collisions of CF_3^{2+} with both D_2 and H_2.

7.5 Conclusion

The relative ion yields of the products of the bond-forming reaction, electron-transfer and collision-induced neutral-loss reaction product ions have been recorded following collisions between

CF_3^{2+} and X_2 (X = D or H) at laboratory frame collision energies in the range of 3 to 13 eV. The ratios of the bond-forming product ions indicate that no isotope effect is in operation when H_2 is used in place of the D_2 neutral reactant; that is, the probability of forming the XCF_2^+ product ion is independent of the choice of hydrogen isotope used as the neutral reactant at a given collision energy. In addition, the collision energy-dependence of the bond forming reaction is indicative of a reactive pathway in which there is no energy barrier.

The similarities of both the magnitude and collision energy-dependence of the cross-sections of the bond-forming reactions, observed in the CF_3^{2+}-H_2/D_2 and CF_2^{2+}-H_2/D_2 collision systems, are such that it is probable that both collision systems share the same reactive pathway of bond formation, namely the spectator-stripping reaction mechanism.

A preliminary estimation of the enthalpy of the weak C-F bond, which is broken during CINL reactivity, indicates a bond energy of $11.77^{+6.16}_{-2.60}$ kJ mol^{-1}. This contrasts with the much higher typical value in the literature (484 kJ mol^{-1}) and supports the model in which CF_3^{2+} consists of a tightly bound 'core-dication' (CF_2^{2+}) attached to a weakly bound F atom.

References

1 S. D. Price, M. Manning and S. Leone, *J. Am. Chem. Soc.*, 116 (1994) 8673.

2 Z. Dolejsek, M. Farnik and Z. Herman, *Chem. Phys. Letters.*, 235 (1995) 99.

3 K. A. Newson and S. D. Price, *Chem. Phys. Letters.*, 269 (1997) 93.

4 K. Tanaka, T. Kato, P. M. Guyon and I. Koyano, *J. Chem. Phys.*, **79** (1983) 4302.

5 J. L. Elkind and P. B. Armentrout, *J. Chem. Phys.*, **84** (1986) 4862.

6 R. D. Levine and R. B. Bernstein, *Molecular Reaction Dynamics and Chemical Reactivity.*, Oxford University Press, New York 1987.

7 K. Tanaka, T. Kato, P. M. Guyon and I. Koyano, *J. Chem. Phys.*, **79** (1983) 4302.

8 K. A. Newson and S. D. Price, *Chem. Phys. Letters.*, in press.

9 R. A. Dressler, R. H. Salter and E. Murad, *J. Chem. Phys.*, **99** (1993) 1159.

10 P. Tosi, O. Dmitrijev, Y. Soldo, D. Bassi, D. Cappelletti, F. Pirani and V. Aquilanti, *J. Chem. Phys.*, **99** (1993) 985.

11 F. S. Klein and I. Friedman, *J. Chem. Phys.*, **41** (1964) 1789.

12 T. F. Moran and I. Friedman, *J. Chem. Phys.*, **42** (1965) 2391.

13 R. Wolfgang, *Discus. Faraday Soc.*, **44** (1967) 179.

14 M. E. Weber, N. F. Dalleska, B. L. Tjelta, E. R. Fisher and P. B. Armentrout, *J. Chem. Phys.*, **98** (1993) 7855.

15 C. E. Dateo and D. C. Clary, *J. Chem. Soc., Faraday Trans.*, **85** (1989) 1685.

17 P. M. Hierl, *J. Chem. Phys.*, **67** (1977) 4665.

18 R. H. Schultz and P. B. Armentrout, *J. Chem. Phys.*, **96** (1992) 1036.

19 K. M. Ervin and P. B. Armentrout, *J. Chem. Phys.*, **85** (1986) 6380.

20 K. M. Ervin and P. B. Armentrout, *J. Chem. Phys.*, **83** (1985) 166.

21 K. M. Ervin and P. B. Armentrout, *J. Chem. Phys.*, **86** (1987) 6240.

22 J. L. Elkind and P. B. Armentrout, *J. Chem. Phys.*, **84** (1986) 4862.

23 P. B. Armentrout, *Am. Chem. Soc. Symposium*, Series 502 (1992) 194.

24 K. M. Ervin and P. B. Armentrout, *J. Chem. Phys.*, **84** (1986) 6750.

25 K. M. Ervin and P. B. Armentrout, *J. Chem. Phys.*, **86** (1987) 2659.

26 K. Yamasaki and S. R. Leone, *J. Chem. Phys.*, **90** (1989) 964.

27 L. Wahlin, *Nuc Instrum. and Methods.*, **27** (1964) 55.

28 W. Wien, *Ann. Physik.*, **65** (1898) 440.

29 S. D. Price, M. Manning and S. R. Leone, *Chem. Phys. letters.*, **214** (1993) 553.

30 S. D. Price, *J. Chem. Soc., Faraday Trans.*, **93** (1997) 2451.

31 Y. Lee, S. R. Leone, P. Champkin, N. Kalysoyannis and S. D. Price, *J. Chem. Phys.*, **106** (1997) 7981.

32 R. C. Weast, *Handbook of Chemistry and Physics*. CRC Press (1984) Boca Raton

Chapter 8

Intramolecular isotope effects in the bond-forming reaction of CF_2^{2+} with HD

8.1 Introduction

Studies of the gas-phase reactivity between molecular dications and neutral molecules [1-4] have indicated that, although being a relatively minor process in comparison to the much more intense electron (charge)-transfer reactivity [1-3], bond-forming reactivity is nevertheless a significant reaction channel. The molecular dication/neutral collision systems exhibiting the greatest propensity for bond formation are those systems in which the neutral reactant is either molecular hydrogen or its isotope. These earlier studies of bond-forming reactivity in molecular dication/neutral collision systems have indicated that the bond-forming reaction process is favoured by low centre-of-mass collision energies. The centre-of-mass collision energy E_{com} is given by Equation 8.1. Therefore, as can be seen from this equation, the centre-of-mass collision energy at a given laboratory frame energy E_{lab} is dependent upon the masses of the reactive dication M_d and the neutral collision partner M_n. Hence, in order to achieve low centre-of-mass collision energies, investigations of the bond-forming reaction processes, such as those contained in this thesis, have concentrated on collision systems having relatively light neutral reactants such as HD. Additionally, the use of a heteronuclear neutral reactant such as HD offers the possibility of the detection of intramolecular isotope effects. Such intramolecular isotope effects are much more powerful probes of the reaction mechanism than the intermolecular isotope effects investigated in Chapters 5 and 7.

$$E_{com} = \frac{M_n}{M_n + M_d} E_{lab} \tag{8.1}$$

As discussed in Chapter 4, isotope effects (or their absence) in gas-phase reactions can provide a probe of the reaction mechanism. In Chapters 5 and 7, the various reactions of the CF_2^{2+} and CF_3^{2+} molecular dications with H_2 and D_2 were examined for signs of intermolecular isotope effects, in an attempt to gain information regarding the nature of the mechanism for bond-formation. The analysis of the experimental results revealed the absence of any detectable intermolecular isotope effects. This observation is consistent with the operation of a direct reaction mechanism and is in strong accord with the results of a previous crossed-beam scattering experiment, which measured the scattering angle distribution of the products of the reaction between CF_2^{2+} and D_2 [4]. In these investigations the DCF_2^+ product ion was observed to be predominantly forward scattered; such a scattering distribution is a definitive indicator of the operation of a spectator-stripping mechanism.

The use of HD as the neutral collision partner should therefore provide a means of determining the presence of an intramolecular isotope effect: the propensity for preferentially forming either of the HCF_2^+ or DCF_2^+ bond-forming product ions (Equations 8.2a and 8.2b).

Hence, the operation of such an isotope effect may be verified by measuring the relative intensities of the two bond-forming products, formed in collisions between the CF_2^{2+} and HD collision partners.

$$CF_2^{2+} + HD \rightarrow DCF_2^+ + H^+ \quad (8.2a)$$

$$CF_2^{2+} + HD \rightarrow HCF_2^+ + D^+ \quad (8.2b)$$

8.2 Experimental details

A detailed account of the experimental methodology employed in the mass spectrometric measurements is given in Chapter 2. However, for this particular collision system, the pressure of the target gas was set at a gauge value of 2×10^{-6} Torr rather than the usual value of 4×10^{-6} Torr. Despite the fact that this value is half that of the usual value for non-hydrogen collision partners, the actual number densities of the target gases are in fact the same in each case. The gauge readings of the pressures of HD neutral collision partner is set at the lower value as a result of the insensitivity of the ion gauge to HD. This insensitivity arises because of the higher ionization potentials of the HD (in common with H_2 and D_2) targets relative to those of other gases, such as ammonia, meaning that the gauge reads low for H_2, D_2 and HD gases.

The HD neutral collision partner is obtained from a commercial source. The purity of the HD is greater than 94%, the major contaminants being H_2 and D_2. This purity is sufficiently high for the purposes of these experiments as the uncertainties obtained in determining the relative product ion intensities are greater than those arising from the impurities in the HD reactant. As stated in Chapter 5, previous work [6] has indicated that the yield of the CF_2^+ product ion may be highly sensitive to the presence of excited electronic states of the reactant dication in the ion beam. Hence, to ensure that the electronic state distribution in the dication beam is uniform throughout the experiment, the operating conditions of the ion source are strictly controlled so to be constant during the duration of the experiments [7]. In addition, the pressure of the neutral collision partner is rigidly monitored to ensure a constant value. This careful supervision avoids potential deviations in the product ion intensities caused by fluctuations in the respective gas pressures. Hence, any deviations in the recorded product ion intensities can be directly attributed to fundamental changes in the reaction process.

8.3 Results and analysis

Time-of-flight mass spectra were recorded following collisions between CF_2^{2+} and HD at collision energies in the laboratory frame between 3 and 11 eV. These energies correspond to centre-of-mass collision energies between 0.17 and 0.63 eV. The mass spectra indicate, in common

with the analogous reactions of CF_2^{2+} with D_2 and H_2, that CF^+, CF_2^+, H^+, D^+, HD^+, HCF_2^+ and DCF_2^+ product ions are produced. A section of a representative time-of-flight mass spectrum showing the product ions formed at a centre-of-mass collision energy of 0.396 eV is displayed in Figure 8.1.

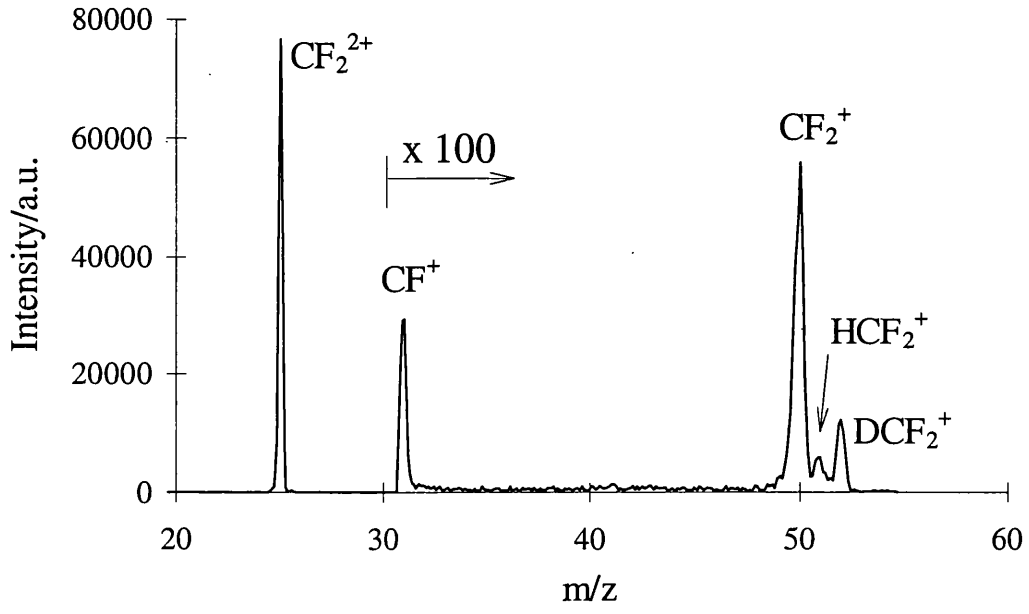

Figure 8.1 A section of a representative time-of-flight mass spectrum showing some of the charged products of the reaction between CF_2^{2+} and HD recorded at a centre-of-mass collision energy of 0.396 eV.

8.3.1 Assignment of product ions

As stated above, analysis of the mass spectra reveals that CF^+, CF_2^+, H^+, D^+, HD^+, HCF_2^+ and DCF_2^+ ions are produced in the reactions between CF_2^{2+} and HD. Representative values of the background-corrected product ion intensities, recorded following collisions between CF_2^{2+} and HD at a centre-of-mass collision energy of 0.62 eV, are given in Table 8.1. As discussed in Chapter 5, Table 8.1 does not include the intensities of the HD^+, H^+ and D^+ ions. The reason for this is that the spectrometer has a low collection efficiency for ions formed from the neutral collision partner, so an accurate determination of the intensity of these ions would be difficult to achieve. However, a number of mass spectra were recorded at various collision energies to determine, qualitatively, the presence of these ions.

In common with the reaction of CF_2^{2+} with H_2/D_2, the product ion intensities indicate that three types of reactivity are observed. Firstly, the CF_2^+ product ion can only be formed as a result of non-dissociative electron-transfer(Equation 8.3). The second reaction process leads to the formation of CF^+, which may be formed either by means of dissociative electron-transfer or by collision-induced charge-separation (CICS). However, the absence of any F^+ signal in the mass spectra eliminates the possibility of the CF^+ being formed in CICS reactions. Hence, the CF^+ ion may be assigned as the product of a

dissociative electron-transfer reaction (Equation 8.4). Additionally, a third type of reactive process that leads to the formation of new chemical bonds is also observed. This bond-forming reaction results in the generation of the HCF_2^+ and DCF_2^+ product ions. The observation of H^+ and D^+ signals, together with the absence of any F^+ or $D(H)F^+$ signals allows the formation of the HCF_2^+ and DCF_2^+ product ions to be unambiguously assigned to the reactions given by Equation 8.5 a and b.

$$CF_2^{2+} + HD \rightarrow CF_2^+ + [H + D]^+ \quad (8.3)$$

$$CF_2^{2+} + HD \rightarrow CF^+ + [H + D]^+ + F \quad (8.4)$$

$$CF_2^{2+} + HD \rightarrow DCF_2^+ + H^+ \quad (8.5a)$$

$$CF_2^2 + HD \rightarrow HCF_2^+ + D^+ \quad (8.5b)$$

The lack of any doubly-charged product ions in the mass spectra signifies that no collision-induced neutral-loss (CINL) reactivity occurs for the CF_2^{2+}/HD collision system at the collision energies employed in these experiments. This observation is in accord with previous investigations of the gas-phase reactivity of CF_2^{2+} with D_2 [1,2]. As discussed in Chapter 5, the low probability of the CF_2^{2+} molecular dication undergoing a CINL reaction is in contrast to other perfluorinated dications such as CF_3^{2+} and SF_4^{2+} which have relatively large CINL reaction cross-sections [8]. The intensities of the product ions, such as those in Table 8.1, indicate that whilst the cross-section for the bond-forming reaction is significant, the electron-transfer channels dominate.

Table 8.1 Background-corrected intensities of product ions formed following collisions between CF_2^+ and HD at a centre-of-mass collision energy of 0.622 eV.

CF_2^{2+}	CF^+	CF_2^+	HCF_2^+	DCF_2^+
184176	973	1107	154	212

8.3.2 Product ion intensities

The intensities of the HCF_2^+ and DCF_2^+ ions relative to the signal intensity of the CF_2^+ ion are listed in Table 8.2. These ratios, unlike the product ion/dication intensity ratio, are independent of both the target gas number density and the incident dication beam current. In addition, as mentioned in Chapters 5-7, the yield of the CF_2^+ ion is approximately constant with collision energy. Hence, the intensities of the HCF_2^+ and DCF_2^+ ions relative to the intensity of the CF_2^+ ion provide sound representations of the collision energy-dependence of the bond-forming processes. Table 8.2 also includes the ratio of the intensities of the two products of bond-forming reactivity, HCF_2^+ and DCF_2^+. This branching ratio should indicate whether an intramolecular isotope effect is in operation in the bond-forming reactive pathway, and is, hence, an intimate probe of the reaction mechanism of the bond-forming process.

In all cases the ion intensities are background-corrected and the values given in Table 8.1 are the mean values of at least three data sets. The error bars in Figures 8.2 and 8.3 are obtained by considering the uncertainty in the measured ion peak areas. The mass spectral peaks corresponding to the two bond-forming ion products HCF_2^+ and DCF_2^+, having masses of 51 and 52 a.m.u. respectively, are very close together and, in spite of the efforts to maximize the mass resolution of the TOFMS, are not resolved at the baseline level. Consequently, such overlapping peaks are difficult to analyse accurately using the conventional method of channel summation. To overcome this problem, the peak areas of the two bond-forming ion products are determined using a peak fitting procedure. This procedure uses a computer program to generate two (or more) Gaussian curves representing ion peaks of variable height, width and profile. These simulated peaks may then be partially superimposed to mimic the mass spectral peak overlap. These peaks can be matched against the actual spectral peaks for inspection, and if necessary adjusted, to determine the peak areas.

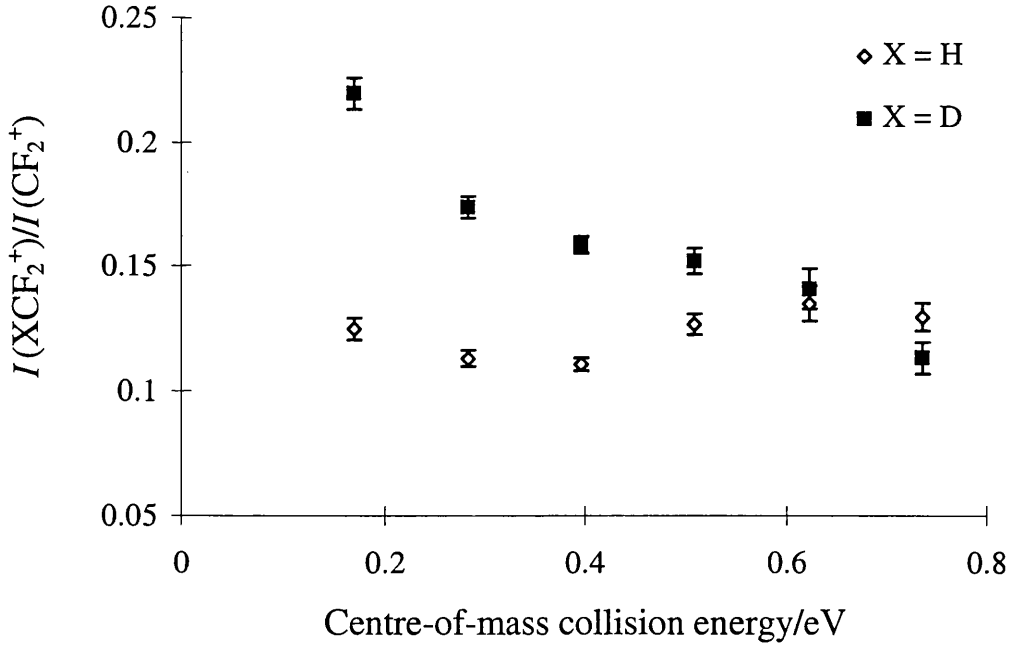

Figure 8.2 Intensities of the DCF_2^+ and HCF_2^+ product ions relative to the CF_2^+ electron-transfer product ions, as a function of the centre-of-mass collision energy.

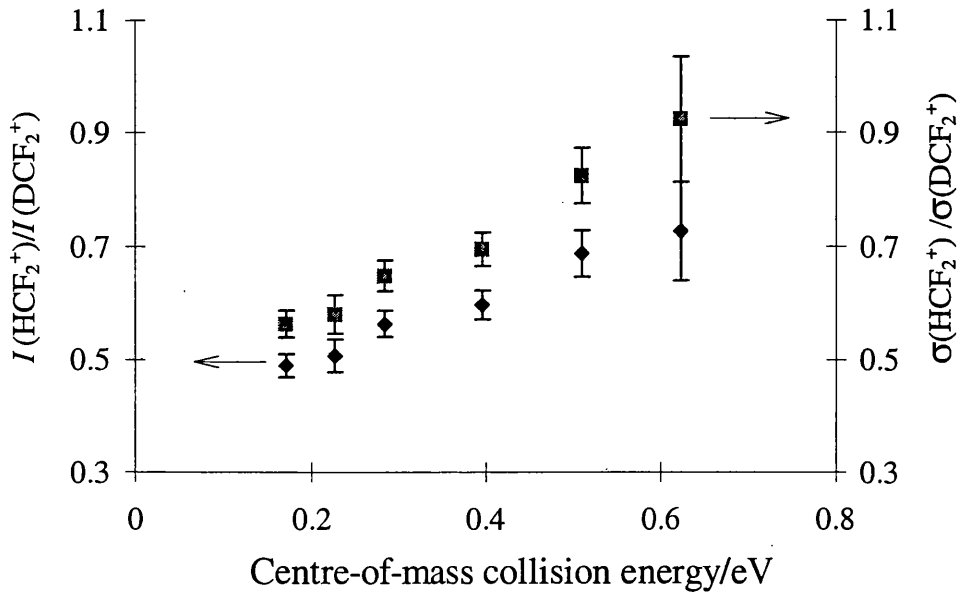

Figure 8.3 Relative cross-sections σ (■) and intensities *I* (◆) of the HCF_2^+ and DCF_2^+ product ions (branching ratio) as a function of the centre-of-mass collision energy.

Table 8.2 Relative intensities of the bond-forming and electron-transfer product ions as a function of the centre-of-mass collision energy E_{com}

E_{com}/eV	$\frac{I(HCF_2^+)}{I(CF_2^+)}$	$\frac{I(DCF_2^+)}{I(CF_2^+)}$	$\frac{I(HCF_2^+)}{I(DCF_2^+)}$
0.74	0.1363	0.1779	0.7661
0.68	0.1324	0.1749	0.7565
0.63	0.1386	0.1842	0.7531
0.57	0.1335	0.1892	0.7060
0.51	0.1287	0.1853	0.6947
0.45	0.1191	0.1877	0.6349
0.40	0.1121	0.1872	0.5989
0.34	0.1134	0.1947	0.5827
0.28	0.1142	0.2024	0.5641
0.23	0.1172	0.2232	0.5254
0.17	0.1259	0.2562	0.4916

The data in Figure 8.3 and Table 8.2 indicates that at a given collision energy we observe significantly more of the DCF_2^+ than the HCF_2^+ product ion. However, as described in Chapters 3 and 5, the effective detection efficiency of the product ions will depend upon the product ions

transverse velocity. Those ions having high transverse kinetic energies are detected less efficiently. Consequently, ions formed in different reactive processes may have different transverse kinetic energies and hence, different detection efficiencies. To overcome this problem, a correction formula (Equation 8.6) is used to amend the ion intensities I for the discriminatory effects of the variable detection efficiency, and give the relative cross-section value:

$$\frac{\sigma_A}{\sigma_B} = \alpha \frac{I_A}{I_B} = \frac{I_A}{I_B} \frac{v_A}{v_B} \frac{L_B}{L_A} \tag{8.6}$$

In Equation 8.6, σ is the cross-section of a given reaction process, v is the transverse velocity of the product ion and L is the transverse length of a volume of the interaction region imaged onto the ion detector, for reactions A and B. A detailed discussion of the methodology behind the correction formula and the origin of the variability of the detection efficiency is given in Chapter 3. As can be seen from Figure 8.3, the correction procedure results in the ratio of the cross-sections being slightly higher than the equivalent intensity ratio, indicating, as expected, that the slightly heavier deuterated product has a marginally higher detection efficiency. However, the qualitative trend is unchanged, pointing to a marked intramolecular isotope effect that favours the formation of DCF_2^+.

8.4 Discussion

Intramolecular isotope effects in ion-neutral reactions have been the motivation for a comprehensive series of experimental and theoretical investigations [9-21]. These investigations have concentrated on the reactions of singly-charged positive ions with HD employed as the neutral reactant. The relatively large ratio in the masses of H and D will emphasize any intramolecular isotope effect, making HD an excellent choice of reactant to study intramolecular isotope effects. In addition, HD is readily available commercially or, unlike many isotopic targets, HD may be prepared with relative ease in the laboratory [22].

The results of prior investigations of the reactions between monocations and HD, at collision energies comparable with those employed in our work, indicate a marked intramolecular isotope effect which usually favours the production of the hydrogenated product. The greater probability for the production of the hydrogenated product is usually explained as arising as the result of an orientation effect [10]. This orientation effect is caused by the attractive ion-induced dipole interaction exerting a torque on the HD molecule as the reactants converge.

As can be seen from Figure 8.4, the torque arises because the centre-of-polarizability of the HD molecule lies at the centre of the H-D bond, whilst the centre-of-mass of HD is located somewhat closer to the D end of the H-D bond. The attractive ion-induced dipole interaction exerts a force on the centre-of-polarizability. The resulting torque causes a rotation of the HD

molecule about its centre-of-mass, directing the H end of the HD molecule towards the reactant ion. Hence, the overall result of this effect is that more collisions occur in the $[M\text{-}H\text{-}D]^+$ configuration than the $[M\text{-}D\text{-}H]^+$ configuration, thus accounting for the preferential formation of the hydrogenated product. This qualitative reasoning is supported by both quantitative classical and quantum mechanical analysis [9,10].

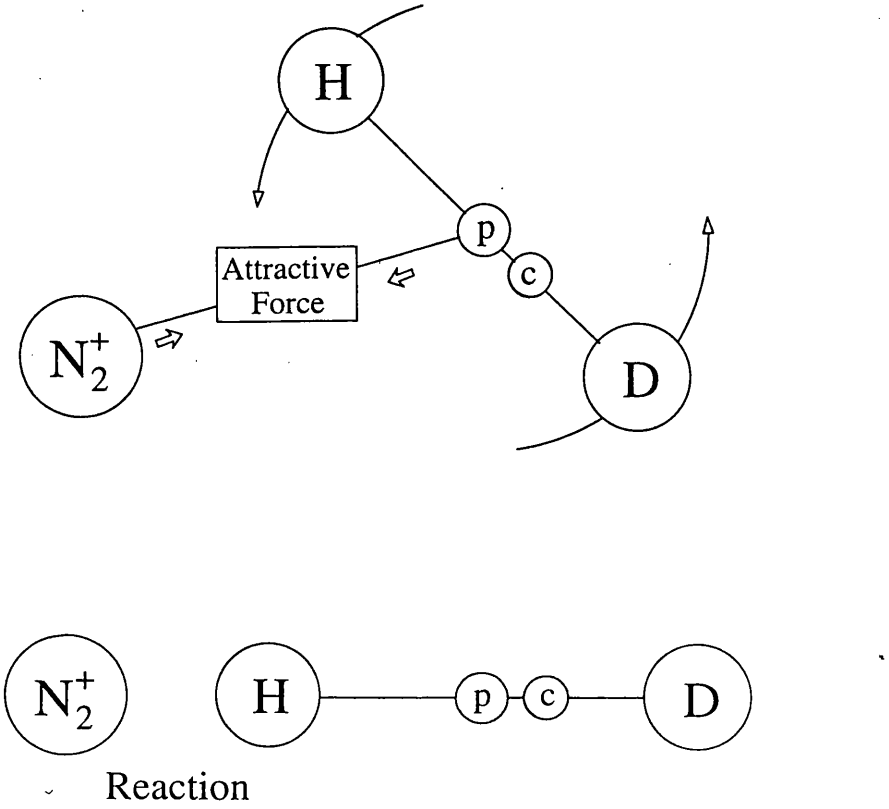

Figure 8.4 Schematic representation of the N_2^+ /HD [16] collision system. The intermolecular potential produces a force that acts at the centre-of-polarizability (P). This force exerts a torque on the HD bond, acting about the centre-of-mass (C), which tends to turn the HD bond so that the H is directed at the reactant ion.

With a doubly-charged reactant ion, as is the case in the CF_2^{2+}-HD collision system, one would expect an even stronger orientation effect favouring the hydrogenated product, due to an increase in the torque acting on the HD molecule, caused by the greater charge on the reactant ion. However, as can be seen in Figure 8.3 the reaction between HD and CF_2^{2+} exhibits a strong inverse isotope effect. That is, a preferential formation of the deuterated product. Clearly, in the case of the reaction between CF_2^{2+} and HD, the orientation effect described above is not able to account for the preponderance of the deuterated product, evidently other effects determine the reaction dynamics.

Isotope effects that favour the formation of the deuterated product in ion-molecule reactions have been observed. Such isotope effects arise because of statistical effects [12,13,18,19]. In the absence of other complications, such as the differences in reaction endothermicities for forming the deuterated and hydrogenated products in endothermic ion-neutral reactions, these statistical effects are usually very small. For example, in the reaction between N_2^+ monocations and HD at collision energies $<10^{-2}$ eV, the statistical effects result in a branching ratio of 52:48 in the N_2D^+/N_2H^+ products. Such statistical effects require the formation of an intermediate species, which has a lifetime of sufficient length to permit energy randomization.

In the case of the reaction between CF_2^{2+} and HD the intermediate species would be $[CF_2HD]^{2+}$. However, the mechanism of the bond-forming reaction between CF_2^{2+} and D_2 has been found to be direct, with no evidence of a long-lived complex [2,4]. In addition, the branching ratio of DCF_2^+/HCF_2^+ in the reaction of CF_2^{2+} with HD is between 1.32 and 2.03 depending upon the collision energy; such values of the branching ratio are markedly higher than those observed for statistical effects in exothermic reactions. Hence, statistical effects may be disregarded as the cause of the propensity for the formation of the deuterated product.

The observed reactivity of the CF_2^{2+}/HD collision system may be qualitatively rationalized if the chemical reaction is preceded by the electron-transfer reaction given by Equation 8.7.

$$CF_2^{2+} + HD \rightarrow CF_2^+ + HD^+ \qquad (8.7)$$

As can be seen from Table 8.1 and the other tables of product ion intensity in this thesis, electron-transfer is the major reaction channel in dication-neutral collision systems at laboratory frame collision energies between 2 and 15 eV. As stated in Chapter 4, electron-transfer reactivity has been modelled using an adapted form of the Landau-Zener theory. In this model, electron-transfer occurs at the crossing of reactant and product potential curves.

If, in the case of the CF_2^{2+}/HD collision system, electron-transfer occurs as the reactants converge, then the repulsion between the CF_2^+ and HD^+ reactants will exert a torque on the HD^+ ion. However, because the force between the two singly-charged reactants is repulsive, the torque will be in the opposite sense to the torque exerted in the case of monocation/HD collision systems discussed above. Therefore, for the CF_2^{2+}/HD collision system, as illustrated in Figure 8.5, electron-transfer will result in the preferential orientation of the reactants into the $[CF_2\text{-}D\text{-}H]^{2+}$ configuration, which favours the formation of the deuterated product. This effect is the exact opposite of the behaviour observed in monocation/HD collision systems.

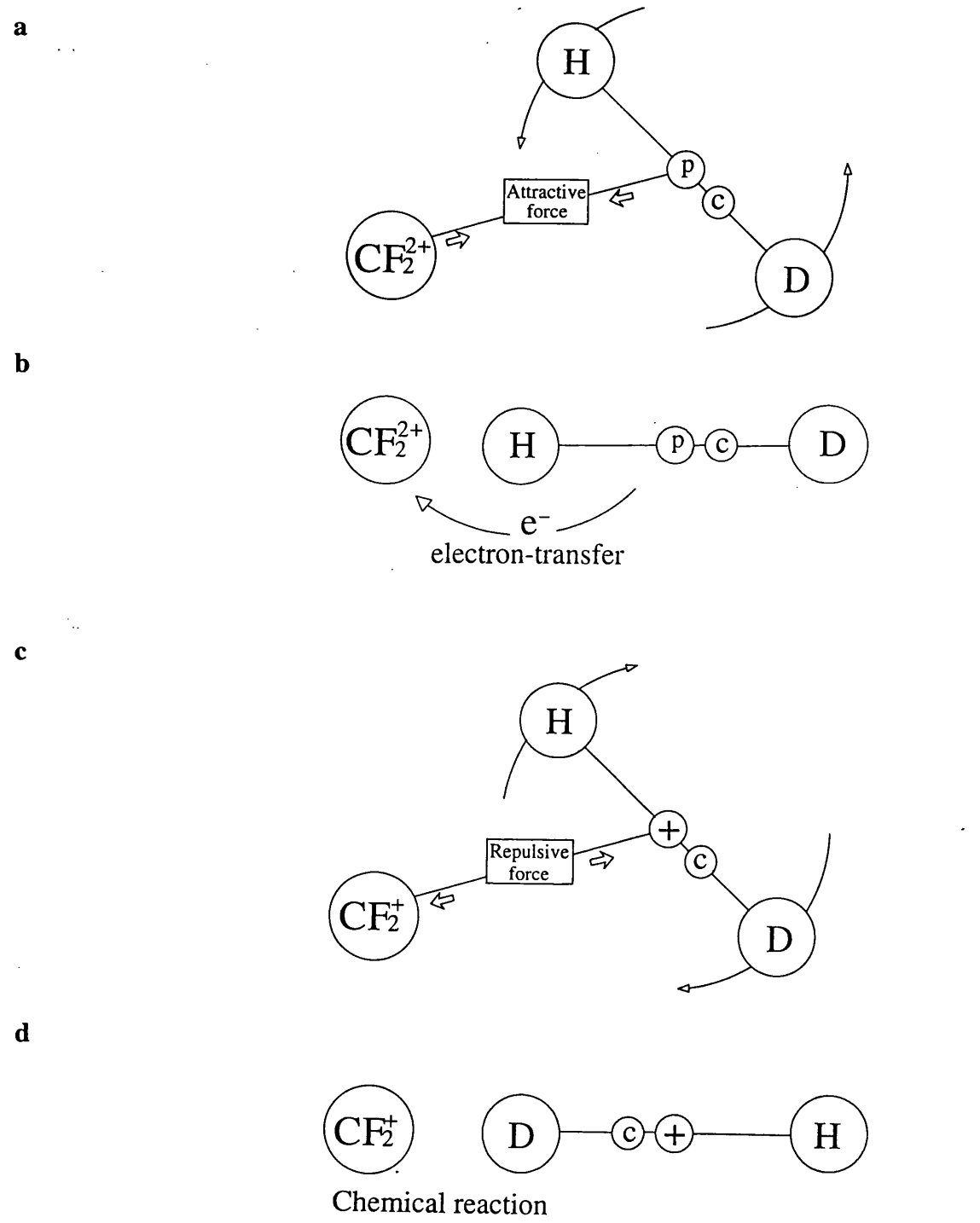

Figure 8.5 Schematic representation of the bond-forming reaction between CF_2^{2+} and HD. (**a**) As the collision partners approach one another, the intermolecular potential produces a force that acts at the centre-of-polarizability (CP), this force generates a torque on the HD bond, acting about the centre-of-mass (CM), which tends to turn the HD bond so that the H end is directed towards the reactant ion. (**b**) With the reactants in a $[CF_2\text{-H-D}]^{2+}$ orientation, an electron-transfer reaction results in the formation of CF_2^+ and HD^+ intermediates.(**c**) Following the electron-transfer reaction, repulsion between the like charges rotates the HD^+ intermediate so that the D end is now adjacent to the CF_2^+ intermediate. (**d**) With the intermediates now in a $[CF_2\text{-D-H}]^{2+}$ configuration, a bond-forming reaction takes place. The orientation of the reactants favours the preferential formation of the DCF_2^+ product ion.

The above hypothesis assumes that electron-transfer occurs at interspecies separations where the resulting singly-charged ions can still, by virtue of their kinetic energy, approach each other to within separations that permit chemical reactivity to occur. Therefore, the above model, in which chemical (bond-forming) reactivity is preceded by electron-transfer, is favoured if the electron-transfer is favoured at relatively small interspecies separations. A recent test of the above hypothesis of electron-transfer preceding chemical reactivity, modelled the reaction between a dication and HD using simple classical trajectory simulations of the approach of an HD molecule to a dicationic point charge. In this model, electron-transfer occurs at an interspecies separation of 0.3 nm. The resulting distribution of the HD^+ orientations are monitored at the closest approach. The results from this approximate model of the reaction process are in accord with the above hypothesis, namely a favouring of the $[M\text{-}D\text{-}H]^{2+}$ orientation in the dication/HD collision systems, compared to the preponderance of the $[M\text{-}H\text{-}D]^+$ orientation in the monocation/HD collision system. Interestingly, the closest approach separation between two point charges having a centre-of-mass collision energy of 0.57 eV is calculated to be approximately 0.28 nm, this compares to a separation of 0.3 nm for electron transfer. Consequently, bond-forming reactivity could, in principle, closely follow electron transfer.

The cross-sections for the bond-forming reaction in the CF_2^{2+}/HD (and H_2/D_2) collision systems are relatively large compared to those for other dication/neutral collision systems. The propensity for bond-forming reactivity in the CF_2^{2+}/X_2 (X = H or D) systems may be explained by this model: if electron-transfer precedes the chemical reaction, then the relatively high efficiency of the electron-transfer process may result in the intensity of the bond-forming reactivity being high in comparison with other dication/neutral reactants [3]. Bond-forming reactions in other collision systems such as the CF_2^{2+}/NH_3 collision system, may involve a 'sticky collision', and react with the formation of a complex intermediate. The cross-section for such a reaction pathway is likely to be significantly smaller. It is pleasing to note that the cross-section of the bond-forming reaction in the CF_2^{2+}/NH_3 collision system was, as reported in Chapter 6, significantly smaller than in the case of the $CF_2^{2+}/HD/H_2/D_2$ collision systems.

A comparison of the XCF_2^+/CF_2^+ ratio, where X = H or D, for the three neutral targets (H_2, D_2 and HD) reveals that the values of the ratio are much lower when HD is used as the neutral target. This is not unexpected since, in the case of the HD collision partner, there are two channels of bond-forming reactivity, leading to the formation of either DCF_2^+ or HCF_2^+. However, it is reassuring to note that if the ratio of the combined intensities of both bond-forming products (DCF_2^+ and HCF_2^+) to that of the CF_2^+ ion in the CF_2^{2+}/HD collision system, is plotted as a function of the centre-of-mass collision energy, the resulting ratio shows very close agreement to

the analogous ratio obtained using H_2 or D_2 targets. The collision energy-dependencies of the ratios of the bond-forming/electron-transfer product ion intensities, for the three collision systems, are displayed in Figure 8.6. The close agreement of the ratios in the above figure indicates that, at a given collision energy, the total yield of the products of bond-forming reactivity is independent of the choice of which isotope of hydrogen is employed as the neutral collision partner. In common with the results of Chapter 5, the collision energy-dependence of the combined intensities of both bond-forming products in the CF_2^{2+}/HD collision system indicates, the absence of a barrier to H^-/D^- transfer reactivity.

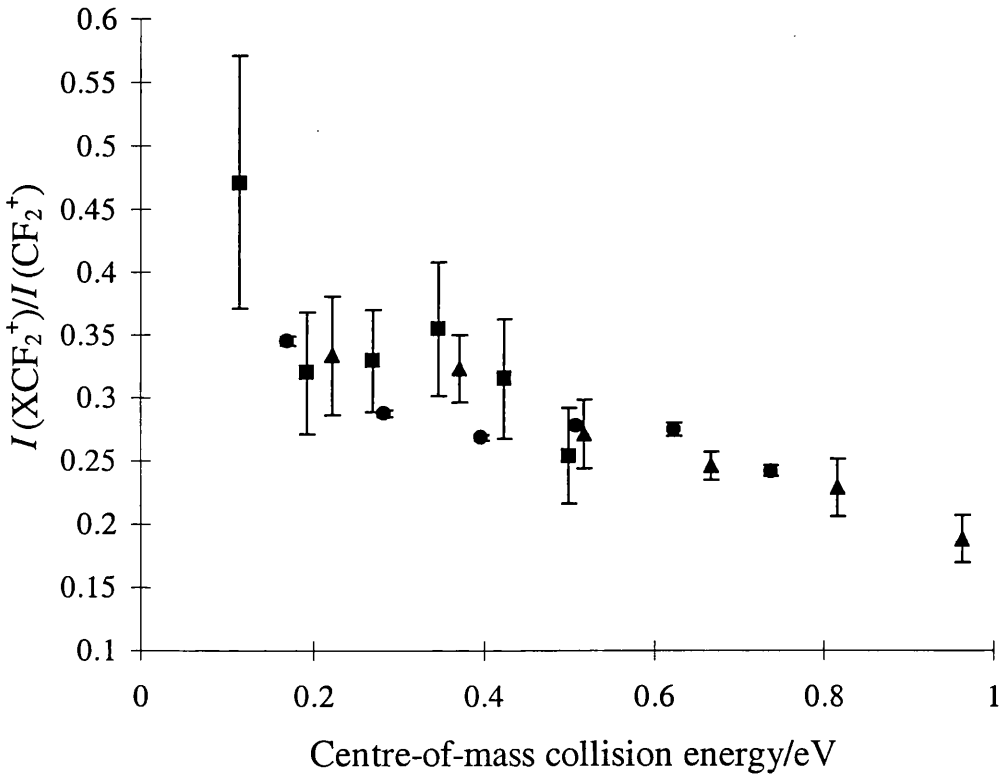

Figure 8.6 Collision energy-dependence of the ratios of the intensities of bond-forming/electron-transfer products ions generated in the reaction of CF_2^{2+} with H_2 (■), D_2 (▲) and HD (●) neutral targets.

8.5 Conclusion

An analysis of the products of bond-forming reactions following collisions between the CF_2^{2+} reactant molecular dication and HD, at centre-of-mass collision energies in the range 0.17-0.62 eV, has revealed the operation of a strong intramolecular isotope effect. This isotope effect leads to the preferential formation of the deuterated product ion (DCF_2^+) and increases with decreasing collision energy. This observation is in stark contrast to previous studies of the exothermic reactions of HD with singly-charged ions (M^+), which exhibit the opposite behaviour: the preferential formation of the hydrogenated product. The singly-charged ion behaviour has

been explained as arising because of an isotope effect that favours the alignment of the reactants into a $[M\text{-}H\text{-}D]^+$ orientation.

The cause of the anomalous reactivity of the dication/neutral collision system may be qualitatively rationalized as arising as a result of the dication's double charge. The double charge enables the reaction to proceed in two stages. Firstly, the transfer of an electron from the neutral to the dication (Equation 8.8a), resulting in the formation of two singly-charged ions. In the second stage, following the electron-transfer, the two singly-charged ions repel one-another. This repulsion exerts a torque on the H-D bond, which rotates the HD^+ ion, leading to a favouring of a $[CF\text{-}D\text{-}H]^{2+}$ orientation. The reactants may now undergo a bond-forming reaction (Equation 8.8b) which, because of the favourable $[CF\text{-}D\text{-}H]^{2+}$ orientation, leads to a preponderance of the DCF_2^+ product.

$$CF_2^{2+} + HD \rightarrow CF_2^+ + HD^+ \qquad (8.8a)$$

$$CF_2^+ + HD^+ \rightarrow D(H)CF_2^+ + H^+(D^+) \qquad (8.8b)$$

The results also suggest that the total intensity of the bond-forming reaction is, within the limits of uncertainty, the same as that observed when H_2 or D_2 molecules are used as the neutral collision partner. This observation supports the conclusion of Chapter 5. That is, the bond-forming reactivity of the CF_2^{2+}/X_2 collision system is independent of the identity of X, where X is either H or D. Consequently, the same reaction mechanism operates in all three CF_2^{2+}/X_2 collision systems: namely the spectator-stripping variety of the direct mechanism.

References

1 S. D. Price, M. Manning and S. R. Leone, *J. Am. Chem. Soc.*, **116** (1994) 8673.

2 K. A. Newson and S. D. Price, *Chem. Phys Letters.*, **269** (1997) 93.

3 K. A. Newson and S. D. Price, *J. Chem. Soc. Faraday Trans.*, in press.

4 Z. Dolejsek, M. Farnik and Z. Herman, *Chem. Phys Letters.*, **235** (1995) 99.

5 Manufacturers operating manual, (Edwards Ltd).

6 M. Manning, S. D. Price and S. R. Leone, *J. Chem. Phys.*, **98** (11) (1993) 8695.

7 A. Ehbrecht, N. Mustafa, C. Ottinger and Z. Herman, *J. Chem. Phys.*, **105** (1996) 9833.

8 S. D. Price, M. Manning and S. R. Leone, *Chem. Phys. letters,* **214** (1993) 553.

9 C. E. Dateo and D. C. Clary, *J. Chem. Soc. Faraday Trans.*, **85** (1989) 1685.

10 P. M. Hierl, *J. Chem. Phys.*, **67** (1977) 4665.

11 R. Wolfgang, *Discussion Faraday Soc.,* **44** (1967) 179.

12 M. E. Weber, N. F. Dalleska, B. L. Tjelta, E. R. Fisher and P. B. Armentrout, *J. Chem. Phys.*, **98** (1993) 7855.

13 P. B. Armentrout, *Am. Chem. Soc. Symposium*, Series 502 (1992) 194.

14 J. L. Elkind and P. B. Armentrout, *J. Chem. Phys.*, **84** (1986) 4862.

15 K. M. Ervin and P. B. Armentrout, *J. Chem. Phys.*, **83** (1985) 166.

16 R. H. Schultz and P. B. Armentrout, *J. Chem. Phys.*, **96** (1992) 1036.

17 K. M. Ervin and P. B. Armentrout, *J. Chem. Phys.*, **85** (1986) 6380.

18 K. M. Ervin and P. B. Armentrout, *J. Chem. Phys.*, **84** (1986) 6750.

19 K. M. Ervin and P. B. Armentrout, *J. Chem. Phys.*, **86** (1987) 2659.

20 R. A. Dressler, R. H. Salter and E. Murad. *J. Chem. Phys.*, **99** (1993) 1159.

21 K. Tanaka, T. Kato, P. M. Guyon and I. Koyano. *J. Chem. Phys.*, **79** (1983) 4302.

22 I. Wender, R. A. Friedel and M. Orchin, *J. M.Chem. Soc.*, **71** (1949) 1140.

Chapter 9

Future developments

The experimental results contained in this thesis demonstrate the power of time-of-flight mass spectrometry as a means of quantifying the intensity of a given channel of reaction between molecular dications and neutral collision partners. Such experimental data provides important information as to the fundamental dynamics of the reaction mechanism.

Not surprisingly, given the comparatively recent construction of the experimental apparatus, the research is in its infancy and the scope for future work is considerable. A large number of collision systems remain to be investigated, including the CO_2^{2+}, CO^{2+} and OCS^{2+} molecular dications with a variety of neutral collision partners. In addition to previously untried collision systems, much of the work undertaken so far indicates further avenues of research. For example, the CF_2^{2+}/NH_3 collision system exhibits bond-forming reactivity [1]. However, the intrinsic characteristics of the bond-forming process display marked differences to those of the other collision systems that exhibit bond-formation. Such behaviour points to a fundamentally different mechanism of the bond-forming reaction. The use of isotopic collision partners has been demonstrated to be a useful probe of the reaction dynamics [2-15]. Therefore, a comparative investigation of the bond-forming reactivity of the analogous CF_2^{2+}/ND_3 collision system may provide information regarding the bond-forming reaction mechanism exhibited by this collision system.

Another prime candidate for investigation is the CF_3^{2+}/HD collision system. Such work would serve two purposes: firstly, the bond-forming reactivity observed in the $CF_2^{2+}/H_2/D_2$ and the $CF_3^{2+}/H_2/D_2$ collision systems have many similar characteristics. Therefore, for the sake of completeness, a comparison of the bond-forming reactivity of the CF_3^{2+}/HD and the analogous CF_2^{2+}/HD collision systems would provide a further guide to the similarities of the bond-forming reactivity of the CF_2^{2+} and the CF_3^{2+} molecular dications. The second motivation for the investigation of the CF_3^{2+}/HD collision system is that the HCF_2^+/DCF_2^+ branching ratio, obtained from this study, would provide a strenuous test of the mechanism of bond formation proposed in Chapter 8.

As discussed in Chapter 1, the use of coincidence techniques provides an effective means of determining the value of the kinetic energy released upon the unimolecular dissociation of a molecular dication formed in a repulsive electronic state [16-20]. The same experimental methodology may also be employed to probe the energetics of the reactions between a doubly-charged reactant ion and a neutral collision partner that result in the formation of two singly-charged ions. Using coincidence methods, the kinetic energy released in the reaction is determined

by measuring the difference in the times-of-flight of the two singly-charged ions formed in the reaction. The experimental apparatus is readily converted from time-of-flight mass-spectrometer mode to coincidence mode by simply changing the timing electronics so that the arrival of successive ions at the detector triggers the START/STOP timing signals. As described in Chapter 1, ion-ion coincidence techniques are characterized by the use of a static source field. However, the use of a static source field with our experimental apparatus would only lead to the deflection of the reactant ion beam, thus preventing reaction with the neutral collision partner. Consequently, the extraction of the product ions produced in coincidence may be achieved by using the same pulsed source field as used in TOFMS mode. This demonstrates the versatility of the experimental apparatus used in this investigation of dication reactivity.

Finally, the fitting of a position-sensitive detector to our experimental apparatus would enable the product ion intensities to be measured at a given scattering angle. As demonstrated by the work of Dolejsek *et al* [21], the angular (scattering) distribution obtained from such an experiment would be of immense use in acquiring additional information pertaining to the dynamics of a given reactive process.

References

1 K. A. Newson and S. D. Price, *J. Chem. Soc., Faraday Trans.*, in press.

2 K. A. Newson and S. D. Price, *Chem. Phys. letters,* **269** (1997) 93.

3 K. A. Newson and S. D. Price, *Chem. Phys. Letters*, in press.

4 C. E. Date and D. C. Clary, *J. Chem. Soc. Faraday Trans.*, **85** (1989) 1685.

5 P. M. Hierl, *J. Chem. Phys.*, **67** (1977) 4665.

6 R. Wolfgang, *Discussion Faraday Soc.,* **44** (1967) 179.

7 P. B. Armentrout, *Am. Chem. Soc. Symposium*, Series 502 (1992) 194.

8 J. L. Elkind and P. B. Armentrout, *J. Chem. Phys.*, **84** (1986) 4862.

9 K. M. Ervin and P. B. Armentrout, *J. Chem. Phys.*, **83** (1985) 166.

10 R. H. Schultz and P. B. Armentrout, *J. Chem. Phys.*, **96** (1992) 1036.

11 K. M. Ervin and P. B. Armentrout, *J. Chem. Phys.*, **85** (1986) 6380.

12 K. M. Ervin and P. B. Armentrout, *J. Chem. Phys.*, **84** (1986) 6750.

13 K. M. Ervin and P. B. Armentrout, *J. Chem. Phys.*, **86** (1987) 2659.

14 R. A. Dressler, R. H. Salter and E. Murad. *J. Chem. Phys.*, **99** (1993) 1159.

15 K. Tanaka, T. Kato, P. M. Guyon and I. Koyano. *J. Chem. Phys.*, **79** (1983) 4302.

16 M. Lundqvist, D. Edvardsson, P. Baltzer, M. Larsson and B. Wannberg, *J. Phys. B: At. Mol. Opt. Phys.*, **29** (1996) 499.

17 D. M. Curtis and J. H. D. Eland, *Int. J. Mass Spec. Ion Proc.*, **63** (1985) 241.

18 S. Leach, J. H. D. Eland and S. D. Price, *J. Chem. Phys.*, **93** (1989) 7575.

19 K. A. Newson and S. D. Price, *Int. J. Mass Spec. Ion Proc.*, **153** (1996) 151.

20 K. E. McCulloh, T. E. Sharp and H. M. Rosenstock, *J. Chem. Phys.*, **42** (1965) 3501.

21 Z. Dolejsek, M. Farnik and Z. Herman, *Chem. Phys. letters,* **235** (1995) 99.

Appendix 1

Ion time-of-flight calculation

As stated in Chapter 2, the methodology behind time-of-flight mass spectrometry is founded on simple electrostatic equations and Newtonian mechanics. From these basic equations it can be shown that when two ions pass through a distance S in identical electric fields, the time-of-flight of each of the ions will be proportional to the square root of its mass. For example, consider an ion of mass m, charge q, and initial kinetic energy U_0 in an electric field of strength E. The field accelerates the ion and the time T taken for the ion to traverse a distance S is given by:

$$T = \left(\left[U_0 + EqS \right]^{1/2} \pm U_0^{1/2} \right) \frac{(2m)^{1/2}}{Eq} \tag{A1.1}$$

The ± signs in Equation A1.1 correspond to the extreme initial orientations of the ion's velocity, '+' if the ion is moving directly away from the ion detector, '-' if the ion is initially directed towards the ion detector.

A practical spectrometer, such as that used in these investigations, will usually have two electric fields, one across the ion source region and the second field accelerating the ions after they have left the source region, these fields are followed by a field-free drift region. A representative schematic diagram of such a spectrometer is given in Figure 2.5 in Chapter 2. The time-of-flight T, in terms of the ion's initial kinetic energy U_0, the final energy U_t, the two electric fields E_S (source) and E_d (acceleration), and the internal dimensions S and drift tube of length D, is simply the sum of the flight times of the ion in each region of the spectrometer.

$$T_{(U_0,S)} = T_S + T_d + T_D \tag{A1.2}$$

where:

$$U_t = U_0 + qSE_S + qdE_d \tag{A1.3}$$

giving:

$$T_S = \frac{(2m)^{1/2}}{qE_S} \left[\left(U_0 + qSE_S \right)^{1/2} \pm \left(U_0 \right)^{1/2} \right] \tag{A1.4}$$

$$T_d = \frac{(2m)^{1/2}}{qE_d} \left[\left(U_t \right)^{1/2} - \left(U_0 + qSE_S \right)^{1/2} \right] \tag{A1.5}$$

$$T_D = D \frac{m^{1/2}}{\left(2U_t \right)^{1/2}} \tag{A1.6}$$

where T_s is the time an ion takes to exit the source region, T_d is the time taken for the ion to pass through the second (acceleration) electric field, and T_D is the time an ion spends in the (field-free) drift tube.

The most striking conclusion to be gained from the above time-of-flight calculation, is the fact that in each region of the spectrometer the time-of-flight of an ion is proportional to the square root of it's mass. Hence, by summing together Equations A1.4-A1.6 one obtains the total time-of-flight of an ion. The total time-of-flight can be more conveniently expressed (Equation A1.7) as:

$$T = k(m)^{1/2} + c \tag{A1.7}$$

where k and c are mass-independent parameters used in the full time-of-flight equations (Equations A1.4-A1.6) above. As described in Chapter 2, the values of k and c are obtained by measuring the flight times of ions of two known mass/charge ratios, usually Ar^+ and Ar^{2+}, and solving the above equation for k and c. The k parameter is dependent upon the electrostatics, whilst the c parameter arises from the delays in the TOF electrics. Having obtained values of the k and c parameters, the mass of any ion is easily calculated by rearranging Equation A1.7 to give:

$$m_{ion} = \left(\frac{T_{ion} - c}{k} \right)^2 \tag{A1.8}$$

Appendix 2
Mass resolution and focusing in a time-of-flight mass spectrometer

A2.1 Mass resolution

The *mass resolution* of a mass spectrometer is a measure of a spectrometer's ability to reduce the spread of the flight times of identical ions. If the ions in a spectrometers source region were formed in a plane parallel to the repeller plate and had zero initial velocity, then the flight time would be the same for all ions of a given mass to charge ratio. In practice however, real ions will have distributions of both initial position and kinetic energy. These will cause a spread in the flight times of ions and hence lower the spectrometers resolution.

The mass resolution of a spectrometer can be considered as being the mass for which adjacent masses are essentially separated [1]. That is, the highest mass spectral peak after which the overlap between adjacent mass peaks is above the half-maximum of the peaks. For example, a spectrometer with a resolution of 100 can distinguish between an ion of mass 99 and mass 100, but cannot distinguish between an ion of mass 100 and mass 101. Mathematically, the difference ΔT in the times-of-flight of ions of mass m and mass $m+1$ is given by:

$$\Delta T = T_{m+1} - T_m = T_m\left[\left(1+\frac{1}{m}\right)^{\frac{1}{2}} - 1\right] \tag{A2.1}$$

The bracketed term of the above equation can be simplified using a binomial expansion to obtain the following approximation:

$$\Delta T \approx \frac{T_m}{2m} \tag{A2.2}$$

If, as discussed above, we define the mass resolution R, of the TOF mass spectrometer, as the mass corresponding to the value of the highest mass m of an ion that can be adequately differentiated from its neighbouring ion peaks, ΔT_M may therefore be considered as the time difference between the mass spectral peaks of the heaviest pair of ions. Hence, if the overlap of the heaviest resolvable mass spectral peaks is defined as occurring at, or just below, the half maximum of the peak then the value of ΔT_M for such a situation must be equal to the full width at half maximum (FWHM) of the upper mass peak. Therefore, rearranging Equation A2.2 and substituting R for m gives:

$$R = \frac{T_M}{2\Delta T_M} \tag{A2.3}$$

where T_M is the time-of-flight (ns) and ΔT_M is the FWHM of a given mass spectral peak (ns).

The resolving power of a TOF mass spectrometer is governed by its space and energy focusing characteristics. The focusing of the ions in the spectrometer is simply an attempt to

ensure that the time spread of a mass spectral peak is as small as possible. That is, that ions of a given mass will have, within a small range, essentially the same times of flight. The fact that ions are formed with a distribution of kinetic energies and initial source positions, increases the time-of-flight spread and, hence, causes a reduction in the resolution of the mass spectrometer.

Wiley and McLaren [1] developed a twin electric field design of TOF mass spectrometer in an attempt to improve its energy and space focusing abilities. Wiley and McLaren introduced a new parameter k_0 and made the simplifications that the ion's initial kinetic energy (U_0) is zero, and that the ion of charge q is formed at a point in the centre of the source region hence $S = S_0$. This gives:

$$U_t = qS_0E_S + qdE_d \tag{A2.4}$$

$$k_0 = \frac{(S_0E_S + dE_d)}{S_0E_S} \tag{A2.5}$$

where E is the strength of a given electric field, and d is the length of the second electric field region. These definitions (Equations A2.4 and A2.5), when substituted into the equations for the time-of-flight of an ion presented in Appendix 1 (Equations A1.4-6), gives the ion time-of-flight $T(0,S_0)$ in terms of k_0.

$$T(0,S_0) = \left(\frac{m}{2U_t}\right)^{1/2}\left(2k_0^{1/2}S_0 + \frac{2k_0^{1/2}}{k_0^{1/2}+1}d + D\right) \tag{A2.6}$$

The substitution of the k_0 parameter simplifies the time-of-flight equation and allows for easier mathematical manipulation.

Space focusing

The initial position of an ion influences the resolution of a spectrometer, as ions that are formed initially closer to the ion detector (smaller S values), will acquire less energy in the source field than those ions formed further away from the detector (larger S values). Hence, the ions with larger S values will eventually overtake the slower moving (small S value) ions. Consequently, there exists a position along the central axis of the spectrometer that the ions with large S and small S values reach simultaneously. At this point we have a space focus.

One method of optimizing a mass spectrometers space focusing capabilities is to calculate the parameters that result in first order space focusing conditions. The first order space focus may be found using elementary mathematics. That is, by obtaining the first differential of the ions time-of-flight with respect to the source position dt/dS and finding the parameter values giving dt/dS = 0.

Wiley and McLaren found the position at which the ions with initial source positions $S = S_0 \pm \frac{1}{2}\delta S$ pass each other and set $dt/dS = 0$ and, using the above equation, obtained an expression for the first order focus requirements:

$$D = 2S_0 k_0^{3/2}\left(1 - \frac{1}{k_0 + k_0^{1/2}}\frac{d}{S_0}\right) \qquad \text{(A2.7)}$$

This focus condition is the same for all ions, regardless of their mass. If the parameters d, S_0 and D are fixed, the ratio E_d/E_S is uniquely determined by the above equation. In practical terms this means that for the twin electric field TOF mass spectrometer, with fixed values of d, S_0 and D, a first order focus is obtained by adjusting the value of E_d/E_S. This adjustment is made, by changing the potentials on the various spectrometer grids/repeller plate, and contrasts with the single electric field design TOF mass spectrometer, where the focus condition is purely geometrical ($D = 2S_0$).

Energy focusing

Consider two ions, ion 1 and ion 2, of the same mass and initial source position, with initial velocity of equal magnitude v but of opposing direction, ion 1 being directed towards the ion detector, along the spectrometers central axis, and ion 2 directed along the same central axis but in the opposite direction, away from the detector. Ion 2 will initially move in its original direction, being decelerated by the source field E_S until its speed is zero. E_S then accelerates ion 2 back towards the detector at the point ion 2 reaches its initial source position S it will have the same speed as it started off with, however this speed will now be in the opposite direction. Hence, at this point, it will have the same initial velocity as ion 1. The significance of ion 2 having this same velocity at this point is that the difference in the time-of-flight of the two ions is simply the time taken for ion 2 to initially set off in the opposite direction and subsequently return to its original position. This time lag is called the *'turn around'* time.

The time spread ΔT_0, due to the turn around time, is hence simply twice the time taken for the ion having the highest initial velocity away from the detector to be decelerated to zero velocity by the source field. For example, an ion of mass m and maximum initial kinetic energy U_0 has a turn around time ΔT_0 given by:

$$\Delta T_0 = \frac{2mv}{qE_S} = \frac{2}{qE_S}(2mU_0)^{1/2} \qquad \text{(A2.8)}$$

Substituting this equation for ΔT_0 in the mass resolution equation, and using equation (A2.6) for the time-of-flight T(0,S_0), together with the focus condition of Equation (A2.7), the maximum resolvable mass M_0 is given by:

$$M_0 = 0.25\left(\frac{U_t}{U_0}\right)^{1/2}\left(\frac{k_0+1}{k_0^{3/2}} - \frac{k_0^{1/2}-1}{k_0^{3/2}+k_0}\frac{d}{S_0}\right) \qquad \text{(A2.9)}$$

In general, M_0 may be increased by increasing D or by decreasing d or S_0.

References

1 W. C. Wiley and I. H. McLaren, *Rev. Scientific instruments*, **26** (1955) 1150.

Appendix 3

Single collision conditions

To avoid the possibility of multiple ion-ion or ion-neutral collisions in the interaction region of the mass spectrometer, the target gas pressure is rigorously controlled and maintained at such a level that almost all the ions in the beam of the reactant dications do not collide with anything, and those that actually do undergo a collision event will only do so once. These single collision conditions are determined using the following analysis [1].

Probability of an ion undergoing a single collision

The fraction of species not undergoing collision with a target gas molecule within a flight path of length x is given by:

$$\frac{N}{N_0} = \exp\left(-\frac{x}{\lambda}\right) \tag{A3.1}$$

where N is the intensity of the transmitted dications, N_0 is the intensity of incident dications and λ is the mean free path. The probability that a dication collides with a target molecule between x and $x + dx$ is obtained from the exponential probability density:

$$f(x)dx = \frac{1}{\lambda}\exp\left(\frac{-x}{\lambda}dx\right) \tag{A3.2}$$

where $f(x)$ represents the probability density of the free path, defined as the distance travelled by the dicationic species between collision events.

The probability ($P_{(L-x)}$) that the dication passes through the remaining length (L-x) without a further collision event is given by:

$$P_{(L-x)} = \exp\left[\frac{-(L-x)}{\lambda}\right] \tag{A3.3}$$

Hence, the probability (P) that a molecule undergoes a collision at x and then passes through the remaining part of its path of length (L-x) without further collisions is given by:

$$P = \frac{1}{\lambda}\exp\left(-\frac{x}{\lambda}dx\right)\exp\left[-\frac{(L-x)}{\lambda}\right] \tag{A3.4}$$

Hence, the probability that the dication only experiences one collision in traversing a distance L may be obtained by integrating the above equation for all values of x between $x = 0$ and $x = L$

$$P = \int_0^L \frac{1}{\lambda}\exp\left(-\frac{x}{\lambda}\right)\exp\left[-\frac{(L-x)}{\lambda}\right]dx \tag{A3.5}$$

which gives:

$$P = \frac{L}{\lambda}\exp\left(-\frac{L}{\lambda}\right) \tag{A3.6}$$

In general, the probability of n collisions in traversing distance L is given by Equation A3.7. Using this equation, it is possible to find appropriate values of (L/λ) that will result in conditions allowing a reasonable number of single collisions without significant numbers of multiple collisions. The value of L is a constant value determined by the spectrometer's design, and so, with an optimum value of (L/λ) and a set value of L, the above may be used to calculate an optimum value of λ, the mean free path of the dication. The ambient optimum pressure conditions required to ensure against the possibility of multiple collisions (P_{SCC}) inside the spectrometers interaction region may then be obtained from the calculated value of λ using Equation A3.8.

$$P_n = \left(\frac{1}{n!}\right)\left(\frac{L}{\lambda}\right)^n \exp\left(-\frac{L}{\lambda}\right) \tag{A3.7}$$

$$P_{SCC} = \frac{k_B T}{2^{1/2}\sigma_C \lambda} \tag{A3.8}$$

Where k_B is the Boltzmann constant, T is the temperature and σ_C is the collision cross-section.

In practice, the above equation is used a starting point and a series of mass spectra are taken with internal pressures lower than this value until a desired product ion intensity is obtained. The necessity for this procedure results from the need for single collision conditions, which in addition to ensuring that the ion signal is not so high as to damage the very sensitive plates of the ion detector, also prevents multiple collision events. Such multiple collision events could make the elucidation of the reaction channels unnecessarily difficult. As shown in Figure 2.7 in Chapter 2, the presence of single collision conditions is confirmed by a linear relationship between the product ion intensity and the pressure inside the collision region of the mass spectrometer.

References

1 K. Yamasaki and S. R. Leone, *J. Chem. Phys.*, **90** (1989) 964.

Appendix 4

The impact parameter and angular momentum

The force between two structureless particles of masses m_1 and m_2 acts along the particles line of centres, and is given by:

$$m_1 \frac{d^2 R_1}{dt^2} = F(R)\,\hat{R} \tag{A4.1}$$

where $\hat{R}$ is a unit vector along the line of centres of m_1 and m_2. From Newton's third law of motion it follows that the force on the second particle is equal in magnitude and opposite in direction to the above force:

$$m_2 \frac{d^2 R_2}{dt^2} = -F(R)\,\hat{R} \tag{A4.2}$$

The equations of force (Equations A4.1 and 2) may be expressed in terms of the relative separation $\boldsymbol{R}$, where $\boldsymbol{R} = R_1 - R_2$, and the reduced mass μ. Thus:

$$\mu \frac{d^2}{dt^2} \boldsymbol{R} = F(R)\,\hat{R} \tag{A4.3}$$

The angular momentum $\boldsymbol{L}$ of the relative motion of the masses m_1 and m_2 is given by the vector product: $\boldsymbol{L} = \boldsymbol{R} \times \mu \dot{\boldsymbol{R}}$. Differentiation of the angular momentum with respect to time gives [1,2]:

$$\dot{\boldsymbol{L}} = (\dot{\boldsymbol{R}} \times \mu \dot{\boldsymbol{R}}) + (\boldsymbol{R} \times \mu \ddot{\boldsymbol{R}}) = 0 \tag{A4.4}$$

However, the value of $\dot{\boldsymbol{L}}$ is zero because $\boldsymbol{L}$ is the vector product of two parallel vectors. Hence, if $\dot{\boldsymbol{L}}$ has zero value it follows that $\boldsymbol{L}$ must have constant value, this supports the conclusion of Newton, namely the conservation of angular momentum.

The conservation of angular momentum and therefore the direction of $\boldsymbol{L}$, implies that the collision trajectory is limited to one plane. Consider a plane normal to the direction of $\boldsymbol{L}$. If the plane is defined by the vectors $\boldsymbol{R}(t)$ and $\boldsymbol{R}(t+dt)$ such that $\boldsymbol{R}(t+dt) = \boldsymbol{R}(t) + \dot{\boldsymbol{R}}\,dt$. As the direction of $\boldsymbol{L}$ is constant, it follows that $\boldsymbol{R}(t)$ and $\boldsymbol{R}(t+dt)$ are always in the same plane. Hence, the trajectory may be specified by the variables of R and ψ, where ψ is the orientation angle. This enables a relationship to be made between the impact parameter $\boldsymbol{b}$ and the angular momentum.

The impact parameter is defined as the distance of closest approach of two particles in the absence of an interparticle force, and is related to the interparticle separation vector $\boldsymbol{R}$ such that:

$$\boldsymbol{R} = \boldsymbol{R}_1 - \boldsymbol{R}_2 = \boldsymbol{v}t + \boldsymbol{b} \tag{A4.5}$$

Where $\boldsymbol{v}$ is the relative velocity of the two particles

Before the collision, as $\boldsymbol{b}$ is normal to the initial velocity and hence $\boldsymbol{L}$, the magnitude of the vector product $\boldsymbol{L} = \mu \boldsymbol{v} \times \boldsymbol{b}$ is given by:

$$L = \mu v b = I\omega \tag{A4.6}$$

Therefore, from Equation A4.6 we obtain:

$$\omega = \frac{L}{I} = \frac{\mu v b}{\mu R^2} = \frac{v b}{R^2} \tag{A4.7}$$

which is used to give Equation 4.30 in Chapter 4.

References

1 R. D. Levine and R. B. Bernstein, *Molecular Reaction Dynamics and Chemical Reactivity* Oxford University Press, New York 1987.

2 A. P. French, *Newtonian Mechanics* M.I.T introductory physics series, W. W. Norton & company, New York 1971.

Appendix 5

Numerical calculation of Franck-Condon factors.

Franck-Condon factors (FCF) provide a measure of the probability of a vibronic transition, such as the general ionization process (Equation A5.1) below.

$$X_2(v''=0) \rightarrow X_2^+(v'=0 \rightarrow 8) + e^- \tag{A5.1}$$

One notable model that may be used to obtain approximate FCF values incorporates the Noumerov algorithm [1-3], which is used to find solutions of the one-dimensional Schrodinger equation., the reduced form of which is given by:

$$-\frac{d^2 f}{dX^2} + (V_{(X)} - E)f = 0 \tag{A5.2}$$

The numerical solution of Equation A5.2 gives the wave function. The Franck-Condon factors are then given by the square of the overlap integral of two such wave functions. In the Noumerov algorithm the solution of Equation A5.2 is calculated for equally-spaced values of X, where the separation h is given by:

$$X_{n+1} - X_n = X_n - X_{n-1} = \cdots = h \tag{A5.3}$$

Taylor expansion to order h^5 gives:

$$f_{n+1} + f_{n-1} = 2f_n + h^2 f_n'' + \frac{h^4}{12} f_n^4 \tag{A5.4}$$

differentiating Equation A5.4 twice gives:

$$h^2(f_{n+1}'' + f_{n-1}'') = 2h^2 f_n'' + h^4 f_n'' + h^4 f_n^4 \tag{A5.5}$$

therefore, from equation A5.5:

$$f_k'' = (V_{(x)} - E)f_k = Y_k f_k \tag{A5.6}$$

where $f_{(k)} = f_{(x=k)}$. This gives:

$$f_{n+1} = \left[1 - \left(\frac{h^2}{12}\right)Y_{n+1}\right]^{-1}\left[(2 + \frac{5h^2}{6})Y_n f_n - (1 - \left(\frac{h^2}{12}\right)Y_{n-1} f_{n-1})\right] \tag{A5.7}$$

Therefore, values of the wave function f_{n+1} may be determined using Equation A5.7 if the two previous values, f_n and f_{n-1}, of the wave function are known. In practice, the wave function values are calculated using Equation A5.7 in an iterative process. The values of f_n and f_{n-1} used in the above equation are found by starting the iteration at an initial point where f_{n-1} has zero value, and f_n has a very small value.

The numerical solution to Equation A5.2 requires the use of reduced equations; these greatly simplify the calculation as the number of parameters is reduced to a minimum. In the iteration calculation Equation A5.2 is transformed into its reduced form:

$$\frac{d^2 f}{dx^2} = f_{(x)}Y = (2V_{(x)} - 2E_r)f \tag{A5.8}$$

The model potential used in the calculations was the Morse potential [4]. However, this potential, together with the eigenvalues E associated with the Morse potential, have to be transformed into their reduced forms $V_{(x)}$ and E_r respectively. These reduced forms are given below in Table A5.1. Also included in the table is the reduced spatial co-ordinate x.

Table A5.1 Reduced and unreduced Morse potentials and the ratio of the reduced and unreduced eigenvalues.

Morse $V_{(X)}$	**reduced $V_{(x)}$**	$\frac{x}{X}$	**constant γ**	$\frac{E_r}{E}$
$D_e\left[1-\exp^{-\beta X}\right]^2$	$\frac{1}{2}\gamma^2\left[1-\exp^{-x/\gamma}\right]^2$	$\left[\frac{(2\mu D_e)^{1/2}\beta}{\hbar}\right]^{1/2}$	$\left[\frac{(2\mu D_e)^{1/2}}{\hbar\beta}\right]^{1/2}$	$\frac{\left(\mu/2D_e\right)^{1/2}}{\hbar\beta}$

Having reduced the parameters to the form given in Table A5.1 the wave function values for a given vibrational energy level may be calculated. The iterative calculation is both lengthy and laborious to calculate manually. However, such a task is ideally suited to a spreadsheet program where, in addition to being a highly efficient calculator of the wave function, the use of such a spreadsheet also allows the wave functions corresponding to other vibrational levels or molecules to be calculated simply by changing the various spectroscopic data values in the spreadsheet program.

Having calculated the wave function values $\Psi_{v''}$ for a given ground vibronic state of hydrogen or deuterium, the values of the wave function $\Psi_{v'}$ corresponding to the ionized parent molecule in a given vibrational state are calculated in exactly the same manner. The two wave functions are then overlapped with themselves and normalized. The Franck-Condon factors (FCF's) are then given by squaring the overlap integral of the two wave functions:

$$\text{FCF} = \left[\int \Psi_{v'}\Psi_{v''}dx\right]^2 \qquad \text{(A5.9)}$$

The resulting FCF values for the ionization of H_2 and D_2 obtained using the above method are listed in Tables 5.4a and b (Chapter 5), together with values taken from the literature [5].

References

1 B. Noumerov, *Royal Astron. Soc.,* **84** (1924) 592.

2 C. Kubach, *J. Chem. Education,* **60** (1983) 212.

3 U. Blukis and J. M. Howell, *J. Chem. Education,* **60** (1983) 205.

4 P. M. Morse, *Phys. Rev.,* **34** (1929) 57.

5 G. H. Gunn, *J. Chem. Phys.*, **44** (1966) 2592.